Nanotopography of PS/PMMA Polymer Demixed Surfaces for Dynamic Platelet Assay Applications

Joanna Ward BSc (Hons)

Faculty of Computing & Engineering

Ulster University

Thesis submitted for the degree of Doctor of Philosophy

July 2020

I can confirm that the word count of this thesis is less than 100,000 words.

Table of Contents

1. Introduction 1

1.1 Overview 1

1.2 Aim and Objectives 7

2. Literature Review 9

2.1 Cell and Protein Interaction with Biomaterial Surfaces 9

2.2 Blood 11

2.3 Platelets and Haemostasis 14

2.4 von Willebrand Factor (vWF) 16

2.5 Relationship between Bleeding Disorders and vWF 20

2.6 Screening Tests for vWD Identification 24

2.7 The Dynamic Platelet Function Assay 28

2.8 Polymer Demixed Nanotopographies for Platelet Assay Testing 31

3. Materials and Methods 37

3.1 Polymer Demixed Spin Coating Solution Preparation 37

3.2 Substrate preparation 38

3.3 Fabrication of spin coated PS/PMMA thin films 38

3.4 Substrate Nomenclature 39

3.5 Hot Embossing-Fabrication of Nanoscale Features on PMMA 41

3.6 Substrate Nomenclature 45

3.7 Characterisation of Substrate Surfaces 45

3.7.1. Optical analysis 46

3.7.2. Atomic Force Microscopy (AFM) 47

3.7.3. X-ray Photoelectron Spectroscopy (XPS) 48

3.7.4. Contact angle 50

3.8 Biological Assessment of Substrates – Dynamic Platelet Function Assay (DPFA) 51

3.8.1. Blood collection 52

3.8.2. Dynamic Platelet Flow Assay (DPFA) Measurements 53

3.8.3. Calculation of the platelet surface coverage 54

3.8.4. Analysis of dynamic platelet tracking parameters 56

3.9 Statistics 59

4. Surface Properties to Induce a Direct Thrombogenic Response within a Dynamic Platelet Function Assay 60

4.1 Introduction 60

4.2 Properties of 25PS75PMMA Polymer Demixed Surfaces 62

4.3 Biological Assessment of 25PS75PMMA Polymer Demixed Surfaces 70

4.4 Properties of Augmented Polymer Demixed Surfaces 76

4.5 Biological Assessment of Augmented Polymer Demixed Surfaces 83

4.6 Dynamic Evaluation of Platelet Behaviour 90

4.7 Discussion 93

5. Influence of an Ambient Atmospheric Pressure During Spin Coating on Polymer Demixed Surface Features 104

5.1 Introduction 104

5.2 Properties of 25PS75PMMA_air Polymer Demixed Surfaces 104

5.3 Biological Assessment of 25PS75PMMA_air Surfaces 108

5.4 Properties of 25PS75PMMA_750_air Polymer Demixed Surfaces 112

5.5 Biological Assessment of 25PS75PMMA_750_air Surfaces 116

5.6 Dynamic Evaluation of Platelet Behaviour 118

5.7 Multiple Donor Study on 25PS75PMMA_750_air Substrates 120

5.8 Discussion 125

6. Platelet Interactions on Nanoscale Embossed Poly (methyl methacrylate) Surfaces 134

6.1 Introduction 134

6.2 Properties of Poly (methyl methacrylate) Pre- and Post-Embossing 135

6.3 Biological Assessment of Embossed PMMA Substrates 146

6.4 Discussion 148

7. Conclusion and Recommendations for Future Study 153

7.1 Conclusions 153

7.2 Recommendations for future study 161

8. References 163

Acknowledgements

First and foremost, I would like to express my gratitude to my supervisors, Professor Brian Meenan and Dr Adrian Boyd for their continued guidance and support throughout this journey.

This work would not have been possible without the help of Royal College of Surgeons in Ireland (RCSI), Dublin, Ireland. I would like to thank Professor Dermot Kenny and Dr Eimear Dunne for the haematological experimentation carried out within Beaumont Hospital and to Dr Ingmar Schoen for facilitating the data analysis behind my work. Thanks to all of you for putting up with my never-ending emails.

Within NIBEC there are many people, both staff and students, I would like to thank. Staff members Dr Acheson, and Dr Morton; thank you for always lending an ear to listen to my problems. Thank you to my fellow PhD students; Chris, Kieran, Shannon and Stephen who kept me sane with copious amounts of tea and crosswords, daily.

Most importantly, I would like to acknowledge my family unit whom without I would not have been able to get through the last four years. Firstly, my parents, Annette and Richard who provided unwavering support and reassurance. It is because of you both, that I believed I was able to complete this degree. To my nanny, Imelda, who gave me strength when I needed it most. I could not have got here without the constant support from my siblings, Cerri-Louise, Nathan and Catherine who always knew how to put a smile on my face when the going got tough.

Finally, to Scott McCullough who provided me with love, support and encouragement daily. I could not have got through the last 7 years of university without you by my side.

Abstract

Platelets are small but critical constituents of blood; whose role is to promote coagulation and form clots that stop bleeding after damage to blood vessels. The protein von Willebrand Factor (vWF) facilitates the attachment of platelets to the site of injury by binding to exposed collagen in the vessel wall and its availability and function are essential. Conditions such as von Willebrand Disease (vWD) affect 1 in 100 people and occurs when vWF function is compromised. Unfortunately, many who have the condition are unaware of the associated bleeding risk and so there is a need for diagnostic tests that reflect the *in vivo* physiology of vWF-platelet interactions.

A recent advancement in this regard, has been the development of a Dynamic Platelet Function Assay (DPFA) by the Royal College of Surgeons in Ireland (RSCI). This device comprises a simple microfluidic flow chamber in which a surface doped with immobilised vWF is used to challenge fluorescently labelled platelets in whole blood perfused over it at arterial shear rates (1500 s^{-1}). However, as this surface uses endogenous vWF it does not truly represent the *in vivo* circumstances.

Hence, the research presented here addresses refinement of the properties of a synthetic surface that can directly entrap vWF from flowing blood in a way that supports the requirement for it to uncoil under adequate shear force to make available platelet sites. Results obtained demonstrate how substrates designed show positive platelet interaction across all blood groups and dynamic analysis shows similar values for polymer surfaces in comparison to the endogenous surface. That created with +750 PS microspheres/ml in air has been shown to produce the highest platelet coverage (40.20 ± 13.30%) and is found to have a topography comprising nanoscale features (height: ±130 nm, FWHM <1 μm). Consequently, understanding of autologous

vWF/platelet interactions on synthetic surfaces has been significantly advanced by this work and moves DPFA testing closer to a simple and accurate diagnosis of vWD and related blood disorders.

Abbreviations

%	Percentage
µL	Microlitre
µm	Micrometre
µsphere	Microsphere
3D	Three-dimensional
5D2	Anti-Lipoprotein Lipase Antibody
A	Amps
ABO	Blood group system
ADAMTS13	A Disintegrin And Metalloproteinase with a Thrombospondin type 1 motif; member 13
ADP	Adenosine Diphosphate
AFM	Atomic Force Microscopy
AK2	Adenylate Kinase 2
Å	Angstrom
ASL	Anti-stick Layer
BE	Binding energy
C 1s	Carbon
Ca^{2+}	Calcium ion
DCM	Dichloromethane
DIOC6	3,3′-dihexyloxacarbocyanine iodide
DPFA	Dynamic Platelet Function Assay
ECM	Extracellular Membrane
ELISA	Enzyme-linked Immunosorbent Assay.

eV	Electron Volts
FITC	Fluorescein Iosthiocyanate
Fps	Frames per second
FWHM	Full Width at Half Maximum
GP	Glycoprotein
HCT	Haematocrit
IPA	Isopropyl Alcohol
ISTH	International Society on Thrombosis and Haemostasis
IU/ml	International Units Per Millilitre
kN	Kilonewton
LTA	Light Transmission Aggregometry
mbar	Millibar
Mm	Millimetre
MPV	Mean Platelet Volume
Mw	Molecular Weight
NIH	National Institute of Health
nm	Nanometre
˚	Degree
˚C	Degrees Celsius
OM	Optical Microscopy
PBS	Phosphate buffered saline
PCL	Polycaprolactone
PEI	Polyethyleneimine
PFT	Platelet Function Test
pH	Power of Hydrogen

P-LCR	Platelet-Large Cell Ratio
PLT	Platelet Count
PMMA	Poly (methyl methacrylate)
POC	Point-of-care
PS	Polystyrene
PVC	Polyvinyl Chloride
R_a	Mean Surface Roughness
RBC	Red Blood Cell
RPM	Revolutions Per Minute
R_q	Root Mean Square Roughness
s	Second
s^{-1}	Inverse Second
SSC	Scientific and Standardization Committee
V	Volts
vWD	von Willebrand Disease
vWF	von Willebrand Factor
w/v	Weight by Volume
w/w	Weight by Weight
WCA	Water Contact Angle
WESS	Wide Energy Survey Scan
WPB	Weibel-Palade Bodies
x10	Magnification objective of x10
x20	Magnification objective of x20
XPS	X-ray Photoelectron Spectroscopy

Declaration

"I hereby declare that with effect from the date on which this thesis is deposited in the Research Student ~Administration Office of Ulster University, I permit;

1. The Librarian of the University to allow the thesis to be copied in whole or part without reference to me on the understanding that such authority applies to the provision of single copies made for study purposes or for inclusion within the stock of another library.
2. The thesis to be made available through the Ulster Institutional Repository and/or EThOS under the terms of the Ulster ETheses Deposit Agreement which I have signed.

IT IS A CONDITION OF USE OF THIS THESIS THAT ANYONE WHO CONSULTS IT MUST RECOGNISE THAT THE COPYRIGHT RESTS WITH THE AUTHOR AND THAT NO QUOTATION FROM THE THESIS AND NO INFORMATION DERIVED FROM IT MAY BE PUBLISHED UNLESS THE SOURCE IS PROPERLY ACKNOWLEDGED."

Publications

Ward, J.; Dunne, E.; Bishop, D.; Boyd, A.; Kenny, D.; Meenan, B.J. Entrapment of Autologous von Willebrand Factor on Polystyrene/Poly(methyl methacrylate) Demixed Surfaces. Polymers **2017**, 9, 700.

1. Introduction

1.1 Overview

Blood is a non-Newtonian fluid that plays an essential role in regulating the body's internal systems by providing nutrients and oxygen to its cells, whilst also helping to remove the waste products associated with metabolism and digestive processes[1]. It primarily comprises red blood cells (erythrocytes), white blood cells (leukocytes) and platelets (thrombocytes) suspended in an aqueous fluid called plasma[1]. Other important components of blood are albumin, clotting factors such as von Willebrand Factor (vWF), antibodies and electrolytes.

Platelets are small cells with dimensions spanning 2-4 μm in diameter[2] and constitute a very small contribution to the cells in blood. Platelets are present in the range of 150,000 to 450,000 per microlitre of blood[3]. These important constituents of blood are essential for haemostasis, i.e. the body's response to the injury of blood vessels and subsequent bleeding, whereby a vascular thrombus or blood clot is formed to halt bleeding from a site of injury. In a damaged vessel wall, the endothelial cells are compromised and the subendothelial matrix is exposed[4]. Components such as collagen and fibrous tissue are recognised by vWF in flowing blood, which as indicated above, is the key plasma protein associated with clotting. Once vWF has adhered to the exposed matrix, primarily collagen, it uncoils under the shear conditions associated with arterial blood flow to expose domains that can bind to a protein complex made up of glycoprotein (GP) Ib, IX and V on the surface of circulating platelets. When in close contact with vWF, the platelets bound are activated to release adhesive lipoproteins and growth factors and that leads to aggregation which causes a clot, or thrombus, to form. Subsequently, a series of coagulation substances are

released by the agglomerated platelets which facilitate the stabilisation of the blood clot and the arrest of bleeding.

Clearly, the presence of an adequate amount of vWF is essential for the effective outcomes of haemostasis to the accomplished. This important glycoprotein circulates in low concentrations in blood plasma having been formed by bone marrow cells and by the endothelial cells on the inner lumen of blood vessels[5]. Its function is regulated by the enzyme ADAMTS13 such that when the protein unfolds, cleavage sites for the enzyme are also exposed which leads to its being cut into fragments that do not bind and/or activate platelets.

Von Willebrand Disease (vWD) is a condition whereby there is a deficiency in vWF; be that quantitative or qualitative[6]. This causes a malfunction in the haemostatic mechanism which can lead to excessive bleeding. vWD is known to affect 1% of the population and thus defines the motivation for this research[7]. There are more than 300 mutations in the gene that codes for vWF and that can then lead to vWD. Although many gene mutations cause only slightly reduced levels of vWF, some cause major reductions that can result in severe forms of the disease. Given the critical role of vWF in mediating thrombosis and the occurrence of conditions such as vWD, there is a clear need for a blood-based diagnostic test platform. Although, molecular genetic testing for vWD and its type (Type 2, Type 3, etc.) can be carried out, it is only indicated when the condition is confirmed via vWF and/or platelet activity assays.

There are two main approaches to vWF testing, (1) vWF-antigen expression which measures the amount of the protein in a blood sample and (2) vWF activity determination, also referred to as Ristocetin Cofactor (vWF:RCo), which determines the scale of protein-platelet interactions as a function of vWF availability. Several

other tests may be associated with vWF diagnosis including factor VIII binding assay; collagen binding activity assay; vWF propeptide to antigen ratio or multimeric analysis (determination of vWF multimer size distribution).

Platelet function testing (PFT) is commonly carried out by light transmission aggregometry (LTA), whereby light transmission is measured through a platelet suspension whilst an agonist, such as the antibiotic Ristocetin, is added to deliberately activate them. This approach to platelet function analysis is also the basis of the vWF:RCo assay for vWF. A major limitation of such PFT assays is that they occur under static blood conditions which means that they are not physiologically accurate. Specifically, they do not take account of vWF interactions occurring in flowing blow under the conditions of arterial shear stress, i.e. the force created by the tangential drag that is produced when blood moves across the inner lumen wall of a blood vessel. The magnitude of this force is proportional to blood viscosity and inversely proportional to the vessel radius cubed[8] with arterial blood flow, normally taken as 1500 s^{-1}.

As a response to providing a more physiologically representative platelet assay and by association, measuring the value of available vWF, there has been much interest in assays involving dynamic blood flow. Creation of microfluidic flow chambers that can mimic the environment of a blood vessel wall have provided an opportunity to enhance platelet (and vWF) assays, by introduction of conditions that are closer to the *in vivo* situation. Other potential advantages of this approach include the use of low sample volumes and the ability to monitor platelet behaviour in real time[9]. In particular, parallel-plate flow chambers are highly attractive for the application of platelet testing, as studies of blood fluid dynamics show that under arterial shear conditions, the red blood cells migrate to the centre of the vessel while platelets are pushed to the outer perimeter, as is the case in normal blood vessels.

Therefore, if blood is perfused across the surface of the sensor component of such a device under arterial shear conditions such that vWF adheres to the features thereon and uncoils, platelets should then recognise the protein such that their interactions can be measured in real time using a suitable high resolution microscopy measurement system. The dynamic platelet function assay (DPFA) developed by researchers at the Royal College of Surgeons in Ireland (RSCI), Dublin, Ireland is an example of such a parallel-plate flow chamber assembly whereby the contacting diagnostic sensor surface is coated with immobilised human endogenous vWF protein[10–12]. Fluorescently labelled platelets in whole blood can be perfused over this surface under arterial flow conditions and platelet interactions with the protein measured by fluorescent microscopy. Therefore, this form of platelet function assay takes into consideration the flow conditions and real time monitoring, advancing physiological relevance. However, in this configuration there is still a lack of patient specificity in relation to vWF-platelet interaction from the same patient blood sample.

Hence, the work presented in this thesis addresses the development of a synthetic diagnostic sensor surface that can entrap autologous vWF and measure the activity of fluorescently labelled platelets from the same single, whole blood sample using the DPFA assembly. In this way, it advances the delivery of a truly physiologically *in vivo* relevant assay of platelet and vWF function. In doing so, it seeks to align with the current state of the art for the DPFA by adhering as closely as possible to the standardisation of the use of microfluidic flow chambers as determined by the International Society on Thrombosis (ISTH)[13], whereby the type of perfusion chamber, type of blood used and coating on the surfaces are kept constant to avoid as far as possible these being sources of variation. The guidelines note that an optimum flow chamber for platelet function assessment should take into consideration;

- Multiple shear rates
- Use of untreated whole blood
- Real-time monitoring of platelet activity
- Single-pass, small-capacity flow device
- Controlled collagen coating

The RSCI-DPFA system used in this work provides for the first four of the ISTH requirements as noted above, when used with the immobilised human endogenous vWF protein sensor surface. The use of the synthetic surface that entraps vWF and allows for the measurement of platelet function thereon, then substitutes for a controlled collagen coating. This replacement surface is created by spin coating a polystyrene (PS) / poly (methyl methacrylate) (PMMA) solution onto a glass substrate. The polymer demixed film that results is capable of producing a surface chemistry and microstructure that is known to interact with platelets. It is the topographical features that are caused by the partially immiscible PS moving through the highly soluble PMMA during the spin coating procedure that are associated with these events. Whereas, studies to date have confirmed that PS/PMMA polymer demixed surfaces have potential as a synthetic DPFA sensor[14,15], there are still many issues (such as repeatability) with its clinical utility, particularly as a test for vWD. It is therefore the refinement of these types of biomaterial surfaces that forms the basis of the work presented here and more specifically the provision of a reproducible surface that allows for the reliable quantification of physiologically relevant platelet function.

Synthetic polymers are a class of biomaterials that are used extensively for biomedical applications due to a well-defined composition and the possibility to tailor their chemical properties. Spin coating of the PS/PMMA polymer demixed thin films onto glass substrates offers a fast, low cost means for the fabrication[16] of a DPFA

sensor surface to monitor real time entrapment of vWF and platelet interactions. As indicated, it is expected that these polymeric thin films will meet most of the ISTH guidelines mentioned above, including the use of their surface topography as alternative to the inclusion of collagen as part of the substrate. This approach avoids issues associated with the quality of many types of collagen and need for relatively aggressive acid-based preparation which is needed to create a suitable coating on the DPFA sensor surface. Previous studies have shown that an acid suspension of collagen may cause deterioration of the substrate on which it is coated[17].

The interactions which take place between a polymeric biomaterial and a biological system such as blood, are known to be influenced by a combination of surface chemistry and topography. Hence, a detailed understanding of how these characteristics influence vWF and subsequent platelet adhesion is crucial. Moreover, there is a requirement for these interactions to accurately reflect clinically relevant changes in these key blood components which requires that the sensor surface be stable and highly reproducible. In this regard, a stable PMMA surface chemistry and PS/PMMA topography that is predominantly made up of well-defined nanoscale features are needed to attain a test environment that most effectively represents physiological *in vivo* conditions. Previous research has gone some way to achieving these conditions and has delivered a well-defined PMMA only surface chemistry[14].

However, the topographies produced to date have tended to be a mixture of non-optimal micro- and nanoscale features that are difficult to reproduce. The work presented in this thesis primarily focuses on attaining a DPFA sensor surface with a much better defined nano-scale topography. In addition, it also applies for the first time an advanced analytical technique developed for the standard immobilised vWF

sensor to the data obtained from the measurement of platelet activity on autologous vWF entrapped on the synthetic PS/PMMA demixed surface.

1.2 Aim and Objectives

Existing tests for measuring platelet function are significantly limited due to the static blood contact conditions under which the assay is carried out. The development of a dynamic assay (DPFA) device has sought to overcome this issue but currently employs a surface with immobilised endogenous vWF on which platelets interact when it is perfused with blood under arterial flow conditions. The aim of this thesis is to further the knowledge of how a surface created by spin coating PS/PMMA can be used to directly entrap vWF from flowing whole blood at arterial shear (1500 s^{-1}) without the need for any biochemical factors. The successful entrapment of vWF should then facilitate platelet adhesion and aggregation in a manner that is physiologically relevant and clinically beneficial. To realise this aim, the following objectives have been identified:

1. Evaluate the effect of introducing uniform PS microspheres into the polymer blend to enable refinement of the current 25PS75PMMA mixed micro- and nano-scale topography.
2. Investigate the effect of an ambient (air) pressure environment on nanotopography of PS/PMMA thin films.
3. Specifically compare both the physical and chemical properties of each polymer surface by way of analytical techniques.
4. Complete testing using whole blood from healthy donors, to quantitatively determine the level of platelet interaction with each surface, using the DPFA.
5. Determine any nuances in the platelet behaviour regarding their dynamic characteristics by way of a novel autologous platelet algorithm.

The outcome of this research will therefore facilitate both quantification of platelet adhesion and a detailed assessment of key dynamic parameters by use of a well-defined (reproducible) surface, capable of assessing autologous vWF-platelet interactions. In this way, it advances the opportunity to better detect vWD in patients who are currently difficult to diagnose.

2. Literature Review

By way of providing an appropriate context for the new research provided in this thesis key aspects of the prior knowledge in the respective subject area have been reviewed. As such, this review of the published literature addresses the following topics:

- Cell and protein interaction with biomaterial surfaces
- Blood function and components;
- Platelets and haemostasis;
- Von Willebrand Factor (vWF);
- Laboratory tests for von Willebrand Disease (vWD) identification
- Polymer demixed nanotopographies for platelet testing

2.1 Cell and Protein Interaction with Biomaterial Surfaces

The National Institute of Health (NIH) in the USA defines a biomaterial as "*a substance (other than a drug) or combination of substances, synthetic or natural in origin, which can be used for any length of time to treat, replace or augment any tissue, organ or function of the body*"[18]. Hence, such materials need to have properties that allow for their interaction with biological systems. Although the main categories of materials; metals and metal alloys, ceramics and glasses, polymers and composites can be considered as biomaterials under the correct conditions, it is only polymers and their surface properties that are relevant to this review. Carbon-based polymers are substances with a molecular structure that consists of a large number of basic monomer units that are linked together as a result of addition or condensation polymerisation. Like all biomaterials, the key functional properties of polymers necessary for their use

in medical applications are biocompatibility and the capability of being sterilised in an appropriate manner.

When a biomaterial is placed in contact with a biological system, protein spontaneously adsorbs onto the surface[19] with the adhesion of molecules and their attendant conformation dependent on the inherent chemistry and microstructure. Hence, the resulting protein-surface interface is influenced by the surface properties of polymeric biomaterial[20], and this then governs any further interactions that may occur on the surface. Correct conformation and orientation of the adsorbed proteins is essential for other biological species, such as cell integrins, to recognise specific binding and/or signalling sites. It has been shown previously that nanoscale surface topography can significant influence protein adsorption and hence cellular adhesion[21,22].

As long ago as 1964, it was proposed that biological cells reacted directly to the surface topography of their contacting environment[23]. Subsequent research has been undertaken to understand why and how cells interact with surface features on the micro- and the nanoscale that are inherently present or that can be created on a substrate surface[19,24]. The cell is the most basic unit of a biological system and all living organisms are composed of one or more types of cells[25]. Mammalian cells have dimensions that lie in the micrometre to tens of micron (μm) size range, however, their components and interaction with the surrounding environment often occur at the nanometre (nm) scale[19]. In this context, fibroblasts, macrophages, epithelial and endothelial cells have all demonstrated a reproducible response to surface topography at the micro- and nanoscale[26–28]. For example, Dalby *et al.* have demonstrated that endothelial cells can sense and interact with features as small as 10 – 30 nm[28]. Cells react to nanometre scale surface features due to events associated with their natural

extracellular matrix (ECM) environment which contains nanoscale components such as collagen, fibrils and nucleic acids. Therefore, it is understood that a cell's interactions with these various biological components and any surrounding topography is crucial in the performance of a variety of its functions such as proliferation, migration and differentiation[29]. The adsorption of proteins that precedes cell interaction is also dependent on the attendant surface chemistry and the nature and scale of the nanotopography[30]. These properties then dictate the wettability of the surface, i.e. the degree of hydrophobicity or hydrophilicity and thereby the degree to which proteins can be adsorbed[31]. At the microscale, the probability of specific forms of cell alignment occurring can be directed by adjusting both the depth and width of topographical features. Whereas, at the nanoscale level, it appears that there is a finite limit for feature size and the degree of order with respect to influencing protein and associated cell interactions[5]. Generally, it is understood that protein and cell interactions with features are dependent on the scale at which they are occurring[32].

2.2 Blood

Blood is a major contributor to human function and delivers essential substances such as nutrients and oxygen to cells, and also acts as a means to remove metabolic waste from these same cells[1]. There are four main components of blood, namely: plasma, red blood cells (RBCs), white blood cells and platelets. Blood plasma is the fluid constituent of blood and consists of 92% water, with soluble sugar, fats, proteins and salts. The function of this plasma is to transport blood cells throughout the body along with proteins, chemical signalling agents and antibodies to help maintain the required balance to sustain life. RBCs or erythrocytes are the most abundant cell in blood, occupying between 40% and 45% of its volume[33]. The physical structure of these cells is vital for their function. RBCs are biconcave and anucleate, i.e. unlike other cells

they do not have a nucleus, which allows them to have the increased flexibility needed for moving through the smallest of blood vessels with ease. Within these cells is a protein called haemoglobin, which specifically enables the transport of oxygen from the lungs to the rest of the body, and the return of carbon dioxide from cells to the lungs for exhalation. White blood cells, or leukocytes are responsible for protection of the body against infection and make up about 1% of the blood volume[33]. Two major types of white blood cells have been distinguished; neutrophils which form the immediate response to infection and lymphocytes – comprising B and T cells – which produce antibodies complimentary to specific bacteria and directly attack infected cells, respectively. The remainder of blood is made up of platelets, or thrombocytes, which are regarded as fragments of cells as opposed to whole cells, with a diameter of approximately 3-4 μm[34] and like RBCs, are anucleate. The two main functions associated with platelets are; the initial arrest of bleeding through formation of a thrombus and the further stabilisation of a thrombus through catalysing further coagulation reactions[35]. An increased amount of these platelets in an individual's blood can result in unnecessary or abnormal clotting which may lead to a heart attack or stroke[36]. On the other hand, abnormally low levels of platelets (<150,000 per μl of blood) can cause excessive bleeding and therefore platelet function testing is a crucial requirement in cardiology.

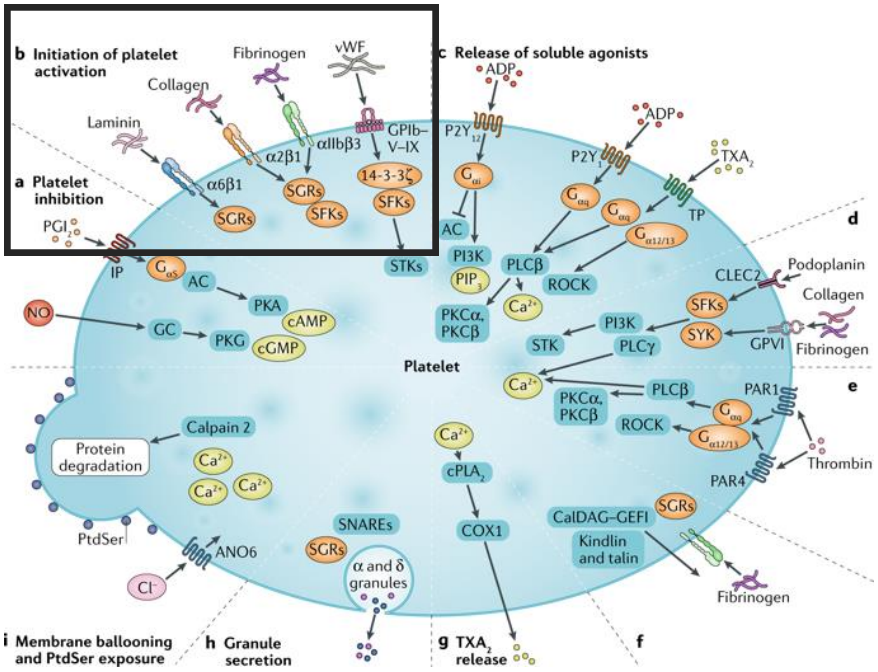

Figure 2.1 Schematic diagram of platelet structure including major signalling events and responses during platelet activation. Adapted from[37].

The disk shape platelet is supported by a cytoskeleton of microtubules, with receptors present on their surface, specifically glycoproteins Ib (GPIb) and IIb-IIIa (GPIIb-IIIa), highlighted in Figure 2.1. These receptors are responsible for mediating the contact reactions of platelet adhesion and aggregation[5]. Adhesion can be considered as the interactions that occur between the platelet organism and the contacting surface, whereas aggregation is the interactions that take place between platelets. The presence of a phospholipid membrane accelerates coagulation reactions and forms a spongy, open surface giving rise to an increased surface area for interaction with plasma factors.

The central focus of the work presented in this thesis is the study of platelet activity with the aim of attaining knowledge required to develop a physiologically relevant platelet function test to facilitate the assessment of platelet behaviour under

dynamic arterial shear flow conditions. As previously reported by Fuchs *et al.* vWF is required under arterial shear to enable platelet adhesion[38]. vWF is a blood-borne protein, further discussed in Section 2.4.

2.3 Platelets and Haemostasis

The term haemostasis relates to a set of interdependent reactions between a surface, normally that of a damaged blood vessel lumen, platelets and coagulation proteins[39]. Under normal haemostasis conditions, the site of injury is recognised by specific circulating proteins that adhere and uncoil leading to platelets becoming activated and recruited to the area of damage, which results in the formation of a thrombus. The mechanism by which these events occurs is complex and is said to be dependent on the rheological properties of the surrounding dynamic environment[40]. The response of these blood factors is diverse and dependent on the location within the vascular network in which the adverse event has occurred. Regardless of the mechanism by which haemostasis is initiated, platelets remain the main component for the formation of a blood clot that arrests bleeding[4].

The blood proteins that carry out the function of flagging vessel wall injury or insult are well defined[41] and exclude those proteins who carry out messenger activities such as hormones and cytokines. Table 2.1 shows the different categories of blood proteins and their respective function.

Table 2.1 Table detailing the major protein constituents within blood and their respective functions.

Blood Protein	**Function**
Albumins	Main constituent of blood proteins, accounting for over 50%. Produced in the liver and responsible for maintaining blood volume and pressure.
Globulin	Account for approximately 20% of plasma proteins and are responsible for enzymatic function and defence.
Fibrinogen	Important clotting factor responsible for ~4% of plasma proteins, which helps to stabilise platelet aggregates.
Clotting Factors	Responsible for haemostasis, examples of which are – fibronectin, Factor VIII and vWF, with vWF being most important in terms of platelet activation.
Regulatory Proteins	Regulation of gene expression.

Blood is a non-Newtonian fluid, i.e. it comprises particles circulating in a liquid medium and circulates around the body in a pulsatile flow environment controlled by the systolic and diastolic phases of the heart and the resulting blood pressure in the vessels. Depending on the blood flow shear rate within the body, the protein responsible for initial platelet recruitment may change; at shear rates below 500 s^{-1} fibrinogen arbitrates platelet activation whereas at shear rates above this, vWF is responsible[15]. Both coagulation proteins and platelets circulate freely in the body and are inactivated until such times as the vessel wall is damaged and sub-endothelial collagen is exposed. At the site of injury, the recognition and repair process begins with the interaction of GPIb receptors and collagen, causing vWF to adhere[42]. GPIb is the main surface receptor on platelets for vWF[43] and therefore without the presence of vWF, platelet adhesion and aggregation would not occur. The forces to which cells within the blood vessels are subject to include wall shear stress and circumferential

strain, with the former being dominant[5]. Therefore, for the purposes of this work, only the shear stress component will be considered. Platelet interactions with vWF are shear stress-dependant, and are thereby influenced by flow conditions within the blood[44–46]. Following adhesion, a series of reactions takes place, as follows:

a) Release of adenosine diphosphate (ADP)
b) Formation of small amounts of thrombin
c) Activation of the biochemical processes leading to thromboxane A_2 – a lipid produced by platelets.

These reactions act to recruit platelets to the site of injury and promote the formation of a platelet aggregate, leading to thrombus formation. As indicated previously, fibrinogen is the most important blood protein in terms of supporting platelet aggregation. Aggregation involves the bridging of platelets, via this fibrinogen protein, and is dependent on the presence of calcium ions (Ca^{2+})[5]. Thrombin mentioned, then binds directly to surface receptors on the phospholipid membrane of the platelets and so plays an essential role in platelet aggregation as it allows for Factor VIII to be released from vWF. For the purpose of this work, only the initial platelet adhesion and aggregation, mediated by vWF will be assessed.

2.4 von Willebrand Factor (vWF)

vWF is a large glycoprotein which is key to the correct functioning of platelet adhesion and initiation of later aggregation mechanisms. It can be distributed in the sub-endothelial ECM or within the blood serum, where it is able to circulate freely. Storage in the Weibel–Palade bodies (WPB) in the endothelium allows for release of vWF into the blood stream when injury to a vessel has occurred[47]. In addition, vWF is produced and released by megakaryocytes when platelets have been activated following vascular damage[48]. For the purposes of the work undertaken herein, only vWF

circulating in whole blood will be considered in the context of its ability to bind to a polymer surface and consequently interact with platelets.

Figure 2.2 represents the main steps of the vWF activation and its interaction with platelets on a damaged vessel lumen during the coagulation process, forming a thrombus[42].

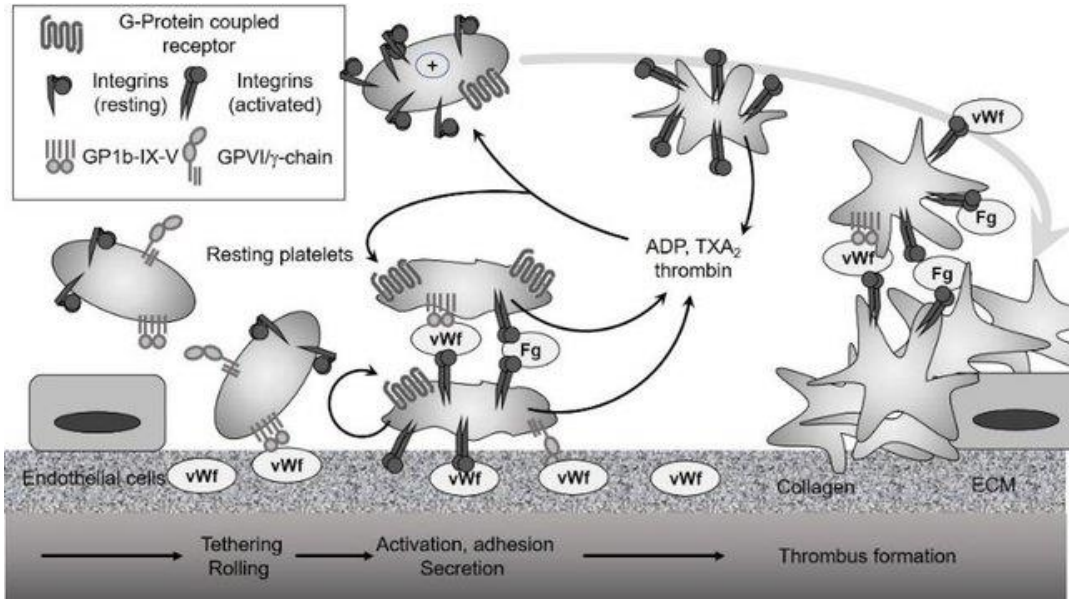

Figure 2.2 Schematic representation of vWF activation leading to platelet adhesion and aggregation to form a thrombus[49].

As with any protein, the structure of vWF is pertinent to its function. As shown in Figure 2.3 the basic vWF multimer, as recently updated by Zhou *et al*, consists of 2050 amino acids made up of various domains[50].

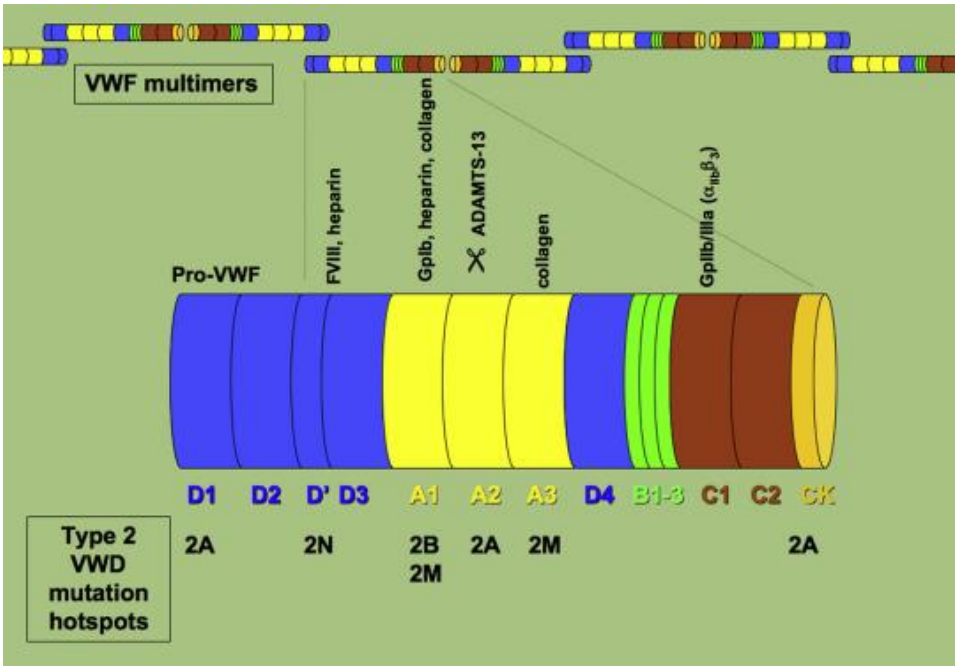

Figure 2.3 Schematic block representation of the basic structure of vWF, identifying specific binding domains and sites. Adapted from[7].

As such, vWF comprises 5 D-domains, 3 A-domains, 6 C-domains and 3 B-domains – more specifically the structure can be represented by the formula D1-D2-D'-D3-A1-A2-A3-D4-B1-B2-B3-C1-C2-CK. The monomers concerned are linked head-to-head and tail-to-tail to form ultra-long concatemers. Table 2.2 below describes the relevant roles of each of the domains.

Table 2.2 Key functions of specific domains within the vWF structure.

Domain name	Function
D1-D3	Responsible for disulphide linkage in formation in WPB and exhibit a binding site for factor VIII
A1	Binds to the GpIbα receptor
A2	Cleavage site for ADAMTS13 (must be uncoiled)
A3	Binds to collagen which becomes exposed when the vessel wall undergoes damage
C1-C6	Allows for length and flexibility especially within neutral pH environments.

The normal circulation of vWF in blood throughout the body occurs as a coiled structure due to the disulphide linkages caused by the D-domains, meaning that the A1 domain is not exposed therefore not allowing for any unnecessary platelet interaction with platelets via the GpIbα receptor[51,52].

As indicated previously, vWF has two roles in initiating and maintaining haemostasis: (1) it is responsible for the interaction with sites of injury[53] and (2) it is a carrier protein for Factor VIII. Under appropriate shear conditions of the type normally associated with arterial blood flow, vWF multimers that are located along a damaged sub-endothelial wall form transient tethers with the Gp-Ib-XI-V platelet receptor allowing of the initial contact and 'rolling' of platelets along the vessel wall. Shear stress (τ) is the frictional force that results from a fluid acting on an area parallel to its direction of flow. The shear rate (ϒ) can therefore be described as the change in velocity that occurs when one layer of fluid passes over another layer. These two parameters can be linked using equation (2.1):

$$\tau = \Upsilon x \mu \qquad (2.1)$$

where μ represents the dynamic velocity.

The capture of platelets from flowing blood under the correct arterial shear conditions is highly specific to the function of vWF[54]. At lower shear rates, platelets do not interact with vWF due to the disulphide bridges blocking the A1 domain. Aponte-Santamaria *et al.* have shown how the A2 domain can bind to the A1 domain so that the β3 strand is shielded, which is essential for GpIb binding to occur[55]. When the forces required to separate these two domains are met, their cleavage site becomes exposed, such that the A1 GpIbα receptor is revealed. Hence, these shear forces unravel the normally coiled vWF making available the relevant receptors for interaction with platelets. Yago *et al.* have suggested that platelet GpIb receptors and the vWF can form bonds up to a certain shear stress limit, after which the bonding will deteriorate, however there are no values specified for this value in the study[56]. Hence, the process can be seen as only resulting within a relatively narrow window of shear stress. For the purpose of this work, an arterial shear rate of 1500 s^{-1} will be considered as the conditions needed to represent the vWF-platelet interactions of whole blood capable of promoting thrombolytic response on the PS/PMMA polymer demixed surfaces of interest.

2.5 Relationship between Bleeding Disorders and vWF

Franchini *et al.* have suggested there is a strong association between blood group and the risk of bleeding. Individuals with A, B and AB blood groups have been shown to have an increase in incidences of thrombotic disease compared with those with blood group O[57]. It is also well known that the ABO blood groups are related to plasma vWF levels[53]. Sarode *et al.*[58] suggest that AB structures act on vWF to modulate platelet aggregation, and that these structures are related to increased levels and activity of vWF. On the other hand, those with blood group O have been shown to have the lowest levels of vWF and so their risk of bleeding was heightened[53,59]. Other bleeding

disorders result from various conditions such as: abnormal levels of platelets; reduced amounts of blood clotting proteins; or abnormal blood vessels[60]. Von Willebrand Disease (vWD) is a condition whereby blood lacks fully-functioning vWF[61]. Uncontrollable bleeding can therefore result from the associated impaired vWF-platelet interactions or due to a reduction in Factor VIII – a common comorbidity with vWD[62]. It is estimated that around 1% of the UK population have reduced levels of von Willebrand Factor, meaning that their blood cannot clot properly and that they may be prone to uncontrolled bleeding[63]. The Scientific and Standardisation Subcommittee (SSC), of the International Society on Thrombosis and Haemostasis (ISTH) have defined three classifications of vWD, as follows;

i. Type 1: partial quantitative deficiency of vWF
ii. Type 2: qualitative deficiencies, further divided into 4 subtypes;
    a. 2A
    b. 2B
    c. 2M
    d. 2N

    The subtype of Type 2 is dependent on the variant present.
iii. Type 3: patients represent a complete deficiency in vWF.

Type 1 vWD is the most common form, accounting for 40-70% of cases[7], while Type 3 is the rarest form, affecting 1 in 500,000 individuals[64].

The diagnosis of vWD by type, is critical to correctly diagnosing, monitoring and controlling abnormal bleeding. In this respect, the SSC-ISTH have determined the following criteria that need to be present in order to allow for the standardisation of a vWD diagnosis[6]:

i. Personal history of abnormal bleeding

ii. Family history of abnormal bleeding

iii. Reduced vWF levels

The problem with these criteria is that they are rarely present together and therefore the chance of misdiagnosis is high. Diagnosis of Type 1 is usually based on the presence of reduced quantity of integral plasma vWF. This diagnosis can be difficult in mildly affected individual's due to the natural fluctuation of vWF in circumstances of stress or inflammation[65]. The qualitative variants with type 2 individuals is based upon the specific defect in vWF present whether it is collagen-binding defects, lack of high molecular multimer vWF or faults in platelet receptor binding[66].

Currently, there is no single laboratory test available to screen for VWD and the associated bleeding risk. A diagnosis is made using several specific laboratory tests, making the process time consuming and labour-intensive. Figure 2.4 shows a typical flowchart process for diagnosis of vWD and other related bleeding disorders.

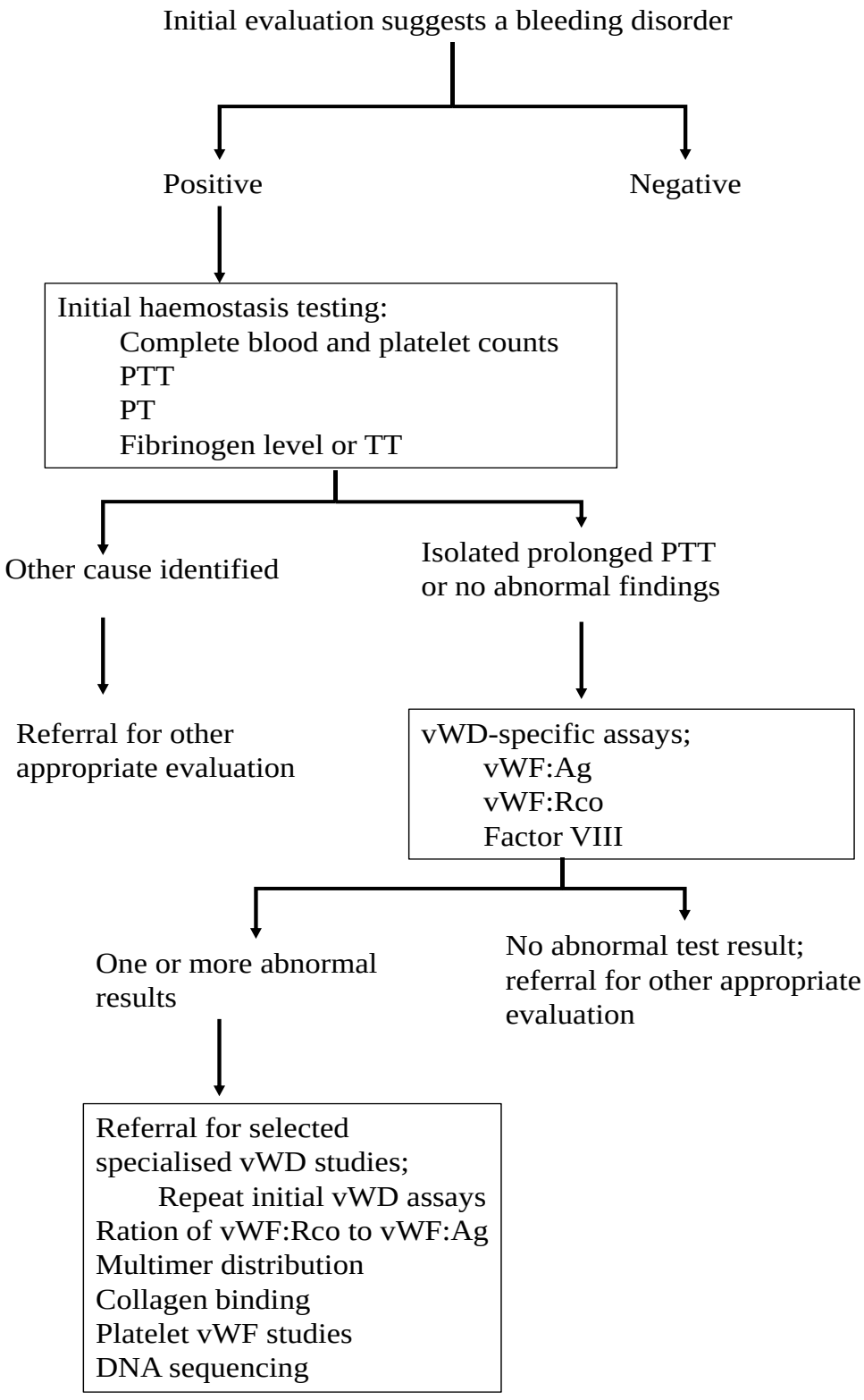

Figure 2.4 Current approach for the diagnosis of vWD Adapted from National Heart, Lung, and Blood Institute [67] .

2.6 Screening Tests for vWD Identification

There are number of ways to investigate vWF and platelet function *in vitro*, each of which has different advantages and limitations. The earliest platelet function test is the 'bleeding time' test developed in the 1900s[68]. The principal of operation of this procedure, is to determine the length of time taken for the onset of bleeding from a deliberate *in vivo* wound to stop. Although this is physiologically relevant, it is nonspecific and there can be significant errors introduced by measurements made by different individuals.

Platelet aggregometry was developed in 1962 by Born[69] and O'Brien[70] and is the basis of the current PFT gold standard. In its first iteration, the platelet-platelet interaction in whole blood is assessed using electrical impedance whereby two electrodes are placed in the sample volume and the direct impedance measured[71]. The addition of a suitable stimulatory reagent causes the platelets to be activated such that they aggregate to the electrodes. The impedance that is measured between the electrodes will then increase and can be plotted as a curve that relates to the rate of aggregation. The disadvantages of this method include poor reproducibility, expense and the fact that it is time-consuming[71,72].

A further development of a whole blood assay which monitors platelet aggregometry is the Rapid Platelet Function Assay, more recently known as VerifyNow (Accumetrics, San Diego, California). Here, fluorinated PS beads are combined with adenosine diphosphate (ADP) and reacted with whole blood to activate the platelets. Results are recorded by way of a change in optical signal intensity, representative of platelet aggregation[73,74].

The vWF: Ristocetin cofactor (Rco) assay is commonly used to measure vWF ability to bind to the GPIbα platelet receptor[66]. From this, the rate of Ristocetin-induced aggregation is related to functional activity of plasma vWF. Although this assay is widely used, it is limited by its high levels of variation[75]. Another commonly used screening tool is the vWF:Antigen (vWF:Ag). Various methods exist for this test including enzyme-linked immunoassay (ELISA) - where absorbance is measured and correlates to the concentration of vWF and Latex immunoassays (LIA) which utilise a change in optical density, due to agglutination, to determine vWF concentration[76]. vWF:Ag is highly reproducible; however, this approach only detects the presence of vWF, not its functioning[66].

More recently, developments in microfluidic platforms have been applied to the field of haemostasis based on research findings from flow assays[13,77,78]. Advances in this technology is now driving the development of many miniaturised analytical devices and requires less sample and reagent volumes, shorter analysis time while producing increasingly accurate results[79,80]. Hence, this approach offers a means to assess platelet function in systems which can mimic both the physiological and pathophysiological surroundings closer to those normally encountered *in vivo*[81,82]. In particular, flow assays lend themselves as a test for vWD due to the ability to create assemblies that can deliver the shear forces necessary to activate vWF uncoiling and associated platelet interaction, in a way that is difficult to incorporate within conventional assays[56,83]. The ISTH have issued guidelines for the creation of a suitable dynamic platelet flow assay[84]:

- Multiple shear rates
- Use of untreated whole blood
- Real-time monitoring of platelet activity

- Single-pass, small-capacity flow device
- Controlled collagen coating

The use of flow chambers for PFT measurement is not new and was introduced in the 19th century, when Bizzozero *et al.* developed the first apparatus of its type, where a microscopic slide was used to observe coagulation and thrombus formation[85]. This work was then further developed by Baumgartner *et al.*, who developed a device to investigate the interaction of blood with an exposed rabbit artery wall[86]. Subsequently, systems comprising the natural materials commonly found in the ECM such as collagen, fibrinogen and vWF have used in devices to study the flowing blood, with collagen being the most common substrate[87]. This technology has evolved more recently with the open flow chambers replaced by parallel plate systems to provide a more controlled volume, close to the measurement surface which can be more easily incorporated into an optical microscopy assembly with real time video capture[88–90].

Sakariassen *et al.* have reported a system devised to study the interaction of platelets with cultured endothelial cells. A coverslip coated with the cells was incorporated between two plates and blood was perfused over the surface at a flow rate of between 300 and 1100 s^{-1}. In this study, platelets did not adhere to cells at a flow of 765 s^{-1} but when these cells were removed, and blood perfused again platelet adherence was observed. Removal of the endothelial cells was reported to increase platelet adherence due to a preference for certain, fibrillar structures of the extracellular matrix[88]. In a related study, when blood was passed through a suitable parallel-plate chamber under shear rates ranging between 100 – 2600 s^{-1}, thrombus formation occurred of which resembled the in vivo process[91]. A key consideration of these flow-based methods is the use of whole blood at arterial shear rates. Platelet adhesion to collagen, has also been measured to indicate aggregation or thrombus[9].

Although it is a useful substrate material, there are many different types of collagen and this can mean that the test varies from device to device therefore making comparison across different devices difficult. In this regard, quality control is also difficult due to collagen having a non-uniform porosity which affects its mechanical properties[92,93]. Also, given that collagen requires dissolution in an acidic solvent to create a coating any residue may influence its properties[17].

The first commercial system to investigate the properties of whole blood was the PFA-100 (*Siemens Healthineers, USA*)[94] which measures the time taken for a clot to occlude blood flow through a nitrocellulose membrane, coated with collagen or ADP[73,95]. This test utilises blood mixed with citrate which is agitated at high shear rates. Application of this technology is aimed toward screening for bleeding disorders and monitoring antiplatelet therapies[81,96]. Compared with the previous devices, this is fast, simple and takes physiological shear rate into consideration. However, the main limitation with this technology is the fact that the time taken to occlude is not actually indicative of any individual bleeding disorder[78].

The next step in the evolution of flow-based assays for vWF/platelet testing involved the use of soft lithography, whereby topography was introduced to a surface to better control the spatial presentation of proteins[97]. Nalayanda *et al.*[98] have investigated cell rolling assays under haemodynamic conditions over a patterned surface. This system can assess both the receptor-ligand binding properties, along with making an accurate measurement of platelet adhesion onto a protein media. This platform again uses whole blood and as it flows over the surface, the platelets adhere where the specific binding protein is deposited.

Kent *et al.*[99] reported the development of a novel microfluidic device that is able to analyse the cell-surface interactions under relevant shear stress conditions. To date, these conditions have only been studied using basic microfluidic platforms[100–102]. The two fundamental considerations behind employing such a device to assess these interactions are as follows:

1. A reliable fabrication method to produce the appropriate test environment with a high degree of repeatability.
2. Understanding the structure and function of the active surfaces used to assess platelet function[103].

The parallel-plate flow chamber utilised here is capable of creating the conditions needed to study platelet behaviour under physiologically relevant arterial wall shear stress conditions[99]. This is due to the low aspect ratio of the channel, resulting in an almost constant wall shear force. The general set up consists of an inverted microscope, light source and video camera, aligned with the flow chamber which comprises a top plate with an inlet and outlet for the flow whole blood, which is connected to a syringe pump controlling the flow rate. The base plate of the device is then the test sensor surface on which the activity of contacting platelets is measured. The results from studies carried out by Kent *et al.* using this device suggest that it has the capacity to screen large sample populations at a relatively small cost, making it an important option for a point-of-care (POC) device that is suitable for clinical applications. This forms the basis of the dynamic platelet function assay (DPFA) system that is central to the research presented in this thesis.

2.7 The Dynamic Platelet Function Assay

As indicated earlier, the main limitation of current generation of platelet function assays is that they examine an endpoint in a static blood sample where platelet activity

is measured via stimulated aggregation. As such, these methods can miss vital platelet mechanisms such as 'rolling' of platelets along the surface, transient tethering and release and final adhesion. The dynamic platelet function assay (DPFA) developed by researchers at the Royal College of Surgeons (RSCI), Dublin is an example of such a parallel-plate flow chamber set up whereby the contacting diagnostic sensor surface is coated with immobilised human endogenous vWF protein[10–12]. This device couples the microfluidic flow chamber developed by Kent *et al.* with an inverted fluorescence microscopy and high-resolution video camera for real time visual analysis of fluorescently dyed platelets in regard to their adhesion and aggregation on a bottom plate test substrate. Lincoln *et al.*[12] have also proposed the use of this type of parallel-plate flow chamber for study of platelets in a controlled shear stress environment. In general, it consists of a top and bottom plate fabricated from poly (methyl methacrylate) (PMMA), with the top plate having the inlet and outlet connections for blood flow. In this case, the sensor substrate is a glass coverslip which can be coated with materials that meet many of the main requirements of a platelet function assay as indicated by the ISTH guidelines[13].

In the case of the RSCI-DPFA device, the sensor is a glass plate onto which endogenous vWF has been immobilised through an established incubation protocol. Platelets perfusing across this surface in whole blood via the inlet/outlet ports at arterial shear rates (1500 s^{-1}) recognise the presence of vWF and adhere to it if they are fully functional leading to aggregation and thrombus formation. The images recorded for platelets interacting with the surface are analysed using appropriate processing software[15,104]. Although not yet applied clinically, the outcomes from a range of studies carried out with this device suggest that it is indeed capable of discriminating between platelets with specific inherent activity.

Cowman *et al.* employed the DPFA system to investigate platelet function in very low birth weight pre-term neonates. Conclusions from this study detailed that platelet function significantly altered, leading to higher incidences of bleeding, when compared to full term neonates[11]. More studies from Cowman *et al.* look at dynamic platelet function in respect to aging, which reports the increase in platelet adherence on vWF with increasing age, more profoundly in females[104].

Allied to the physical properties of the DPFA system has been the development of an algorithm to facilitate a detailed analysis of the platelet kinetic behaviour over time[10,11,105,106] Motional parameters of platelets are measured to indicate behaviours such as speed and distance travelled. Application of this *in-silico* methodology further enhances the clinical relevance of the assay, building upon the visual interpretation of any microfluidic assay images[59,107]. Initial development of this algorithm was led by Ralph *et al.*[105] whereby six dynamic platelet parameters were identified, namely; Ntracks, % translocation, mean translocating velocity, fraction of static platelets, % unstable platelets and % surface coverage. Dunne *et al.* studied the influence of ABO blood group on vWF performance. Conclusions suggest that the platelets on Type O individuals have a greater number of translocating platelets (18.4 ± 3.5%) which is indicative of reduced engagement of the GPIIb/IIIa receptor, responsible for forming stable bonds[59]. Within this study four key parameters were measured – Ntracks, number of stably adhered platelets, mean translocating velocity and surface area covered by platelets on final frame, alongside five verified parameters; number of translocating platelets, mean translocation distance, % platelets in motion, % surface coverage and finally, adhesion rate. Verified parameters are said to have some important biological implications, but mainly correlate with the key factors [15]. Whilst this is a huge advancement in terms of understanding platelet function over time, a

significant limitation is the fact that it uses endogenous vWF, immobilised on the surface meaning that patient specific testing is not an option. Hence, if this issue can be resolved by the use of autologous vWF on the sensor surface while still being able to apply the kinetic analysis algorithm it would assist in enhancing the clinical diagnostic value of the technique overall.

As discussed earlier, the development of a patient specific substrate that is capable of entrapping autologous vWF from flowing blood at arterial shear rates ($1500s^{-1}$) and testing the function of platelets from the same sample is the core aim of the work undertaken here. Previous work by Bishop[14] and Ward *et al.*[108] has proposed that a surface created by spin coating a PS/PMMA polymer demixed solution onto a glass slide has the correct chemistry and topography to entrap autologous vWF from flowing blood in a way that allows for platelet function to be tested thereon. The application of polymer demixed surfaces in this regard is based on previous published results by Minelli *et al.*[109]. As indicated earlier, the work in this thesis seeks to create a clearly defined topography which can facilitate autologous protein/platelet interactions.

2.8 Polymer Demixed Nanotopographies for Platelet Assay Testing

Spin coating (also known as spin casting) of solutions of PS and PMMA in a suitable solvent has been shown to create thin film surfaces with sub-micron to nanoscale topographical features of the type known to provide for platelet interaction thereon. This coating technique, which was first used to apply coatings of paint using equipment designed by Emslie in 1958[110], is easy to use and inexpensive and have proved to be highly effective for depositing polymer films on a range of substrates[111–113]. In the case of polymer demixed solutions the substrate is accelerated rapidly at the desired rotational speed (RPM)[111]. The centrifugal force acting on the substrate

causes the liquid placed on it to flow radially across the surface, with excess being ejected off the edges. A polymer film is formed as the liquid layer thins and the solvent evaporates, with a thin film coating formed when all the solvent has been removed.

The creation of thin films via spin coating from polymer demixed solutions has been studied extensively during the last tens of years, and the process is now reasonably well understood[114]. The technique has been used to form surfaces to investigate the effect of surface topography on a range of biological systems including proteins and cells[115–117]. Due to the immiscibility of the polymers in the blend, the solution typically demixes during spinning[118] and produces a surface with unique forms of nanotopography due to the partially soluble particles of one component being distributed throughout the fully soluble phase of the other. Tanaka *et al.*[119] have researched the morphology of an immiscible polymer blend of PS and PMMA in w/w ratios of 30/70 and 50/50 in varying amounts of toluene solvent, dependant on thickness of film intended. Atomic Force Microscopy (AFM) was utilised to examine the microstructure where 100 nm films were reported to show a "*sea-island-like*" structure for 50PS/50PMMA blends whereas at the 30/70 ratio showed a more continuous phase-separate topography, with islands reaching up to 120 nm in height. Spin coating from a toluene solution is a common means for producing a '*thin, uniform polymer film*'[111].

Previous to 1997, the blending of PS and PMMA was studied in terms of their bulk demixing characteristics[120] and associated biochemical phase behaviour[119]. Walheim *et al.*[118] then investigated the phase morphology of thin films using this demixed polymer combination. They explored three fundamentals; the dependence of topography on the solvent used, effect of the substrate onto which the solution was spin cast, and lastly the evolution of these features towards equilibrium. Solvents that

they used included toluene, tetrahydrofuran (THF) and methyl ethyl ketone (MEK). From this study, it was found that if the solvent used is more suitable to dissolving the polymer component with the lower surface tension, then the surface features present will be sharp and well defined. However, if the solution is matched with the higher surface tension component the resultant features will be more rounded. These conclusions were made based on a 50/50 weight by volume mixture use as a 3% solution in the solvent.

In the case of this thesis, the PS/PMMA blend, both polymers are immiscible and phase separation takes place causing a relatively disordered topography. Generally, the solubility of the polymer increases when its solubility parameter is closer to that of the solvent. The Hildebrand solubility parameters of chloroform (9.3), PS (9.1) and PMMA (9.5) would mean that PS should be detected when spin coating with chloroform. However, this is reliant on the system reaching thermodynamic equilibrium[121] and the method used to detect surface chemistry[122].

Ton-That *et al.*[123] investigated the influence of the solution concentration and composition of the PS/PMMA mixture on the resulting morphology and thereby the overall structure of the coating. This mixture, like that to be used in this study, employed chloroform as the solvent. In each case, the surface was enriched with PMMA due to its high solubility in chloroform.

D'Sa *et al.* conducted a study with a range of PS/PMMA blends, 75/25, 50/50 and 25/75 in a 1% w/w chloroform solvent. Characterisation of these thin films showed a PMMA surface chemistry in all polymer blends. When PMMA is in excess, surface topography is reported to consist of a nanoisland topography with peaks showing an average peak height of 27.7 nm, with surface roughness values of R_a = 7.5 ± 0.8 nm and R_q = 9.3 ± 1.1 nm[115].

More recently, Fleming *et al.* reported how binary polymer blends can take the form of a nanotopography comprising islands, pits and ribbons, depending on the polymer concentration[124]. They have stated that islands with heights of 7 ± 2 nm are fabricated when a blend of 1% w/v 25% PS/75% PMMA, the solvent being chloroform, is spin coated onto glass slides. However, when PS concentration is increased to 50%, a morphology consisting of nanopits is observed, with depths of 8 ± 5 nm.

Minelli *et al.* employed the polymer demixing of PS and PMMA as a method for creating a substrate demonstrating features ranging from 40 – 400 nm[109]. The substrate was then treated with cyclohexane to remove the PS phase. These surfaces were exposed to whole blood and showed a higher density of platelets adhered to the larger surface features present. These authors found that platelet adhesion and further aggregation increased with structural features of ~400 nm. Although it was proposed that these surface features might also display a higher degree of vWF adsorption and that both size and shape of the surface features attained from spin coating from PS/PMMA polymer demixed solutions may have a major role in the way in which a protein interacts, this proposition was not pursued further.

Shenkman *et al.*[125] constructed a study to investigate the adhesion of platelets to a PS surface with ECM coated plates acting as a control. The most important finding from this work is that platelet adhesion to PS requires the presence of both fibrinogen and vWF, while in ECM fibrinogen is not required: and platelet adhesion to PS requires GPIIb and GPIIIb-IIa surface receptors, however in the ECM the surface receptor GPIIIb-IIa is not needed.

Most recently, Bishop *et al.* carried out studies using the RCSI-DPFA assembly to fabricate a synthetic surface to entrap vWF from whole blood under arterial shear[14].

Polymer demixed spin coated thin films were investigated with PS/PMMA blends of 25/75 and 50/50 w/w in 1% chloroform. Results show a positive response for platelet adhesion and inhibition studies revealed that this adhesion was indeed a result from vWF entrapment. However, the main limitation that remained was the lack of reproducibility of the surface to produce a repeatable platelet response. Attempts were made to overcome this by hot embossing PMMA with surface features similar to the spin coated nanotopography. However, no further results were published in regard to biological response.

It is clear from this review of the published literature that challenges still remain in regard to producing a reproducible coating topography by spin coating from a PS/PMMA demixed solution of the type required to entrap vWF and measure subsequent platelet activity thereon. The composition of this form of prothrombotic surface needs to have specific nanoscale topographical features. As indicated above, the work of Minelli *et al.* forms the basis of how whole blood interacts with a PS/PMMA polymer demixed surface with nano-features present. Polymer demixed blends of PS and PMMA at varying concentrations have been investigated and shown to provide features varying from 40-400nm[109]. Results attained suggest that feature size affects the capture of vWF and therefore increase platelet thrombus formation. Bishop *et al.*[14] carried out research on related polymer demixed PS/PMMA thin films and examined their behaviour in the RCSI-DPFA. Although the thin films produced entrapped vWF from flowing whole blood under arterial shear and interacted with platelets from the same solution, the process lacked the required reproducibility due to substrate variability. In particular, the topography produced was a combination of micron, sub-micron and nanoscale features.

Results presented within this thesis focus on the further refinement of surfaces created by spin coating of an already established polymer demixed solution (25PS75PMMA in chloroform)[14] to provide a more defined range of nanoscale features that provide for more reproducible vWF/platelet interactions. This has been achieved by both altering the polymer blend via the introduction of PS microspheres and by changing the spin coating ambient conditions. These new polymer demixed thin films are used as a substrate within the RCSI-DPFA parallel platelet flow chamber to yield an improved form of physiologically relevant autologous vWF platelet function assay with a sub-endothelial type topography[126]. The improvements sought here are considered in the context of attaining a clinical assay for the detection of vWD and its characterisation by type.

3. Materials and Methods

3.1 Polymer Demixed Spin Coating Solution Preparation

Polystyrene (PS), Molecular Weight = 290,000 Daltons and Poly (methyl methacrylate) (PMMA), Molecular Weight = 350,000 Daltons were purchased from Sigma Aldrich, UK and thoroughly mixed in a 25/75 weight to weight ratio (25% PS + 75% PMMA) after which a 3% weight to volume (3g per 100ml) solution was created in chloroform (Sigma Aldrich, UK) and placed on gently rotating mixing plate for 24 hours, to produce the stock 25PS75PMMA demixed spin coating blend. The chloroform used was amylene stabilised, with a density of 1.48 g/mol at room temperature. The core polymer demixed blend used here (25PS75PMMA in chloroform) was chosen based on a previous study[14] and acted as a baseline for further refinement of the resulting spin coated surface features.

The stock 25PS75PMMA solution was augmented with the addition of 50 μm PS microspheres (Thermo Scientific, UK) which were provided in aqueous media in 25 ml vials with 3,000 PS particles per 1 ml. 5 ml aliquots (15,000 microspheres) of the aqueous media were placed in a rigorously clean glass petri dish and baked in an oven at 60ºC overnight to remove the water. The dried particles were re-suspended in chloroform and used almost immediately. Ratios of 1:2, 1:4 and 1:8 were used to combine the PS beads in chloroform with the stock 25PS75PMMA blend to produce the spin coating solutions shown in Table 3.1. As before, each blend was placed on the rotating mixing plate for 24 hours before use in spin coating. It is important to note, that the assumption here was that all the microspheres were successfully introduced into the augmented 25PS75PMMA solutions.

Table 3.1 Augmentation of stock 25PS75PMMA blend by incorporation of 50 µm microspheres by way of 1:2, 1:4 and 1:8 ratios and the resulting number of microspheres per ml.

Ratio	**1:2**	**1:4**	**1:8**
Microspheres in aqueous solution (ml)	5	5	5
Amount of stock solution (ml)	10	20	40
Number of microspheres/ml	1500	750	375

3.2 Substrate preparation

Glass microscope slides (24x50 mm) (Paul Marienfeld GmbH & Co. KG, Germany) were used as the substrate onto which the polymer demixed solutions were spin coated to produce a coating. To ensure that they were free of any contamination, a washing protocol was carried out. A set of 10 slides were placed in a clean beaker containing 99% isopropanol (IPA) (Sigma Aldrich, UK) with care taken to ensure that they were kept apart. The beaker was placed in an ultrasonic bath (Ultrawave Ltd., UK) for 30 minutes. When finished, the slides were removed from the IPA solution, placed on a clean glass plate and left in a fume cupboard to air dry for two hours.

3.3 Fabrication of spin coated PS/PMMA thin films

Demixed polymer films were produced by dispensing the various PS/PMMA solutions onto the static glass slide until the surface was saturated (to the extent of the surface tension breaking) within the spin coating apparatus. Polymer controls of 3% w/v 100% PS and 100% PMMA in chloroform were spin coated and used as a baseline to identify the physical characteristics of each polymer. Solvent cast 100% PMMA thin films were also produced at room temperature, to demonstrate the influence of spin coating forces on thin film formation.

Two types of spin coater were used within this work; a G3P-8 (Speciality Coatings, Indianapolis) which employs a positive pressure nitrogen purge to ensure thin film uniformity whilst spinning and a VTC-100 compact spin coater (MTI Corporation, Richmond) which operates in air at atmospheric, i.e. without a purge.

The spin programme for the G3P-8 begins at 0 RPM and increases up to a maximum of 6000 RPM over a period of three minutes. The thin film coatings created within this system in a positive pressure nitrogen purge environment are referred to hereafter as positive pressure substrates.

The same spin coating programme could not be fully replicated for the VTC-100 instrument due to its built-in operational parameters Hence, in this case, the maximum parameters were used for time and speed – time 1 (T1): 2 minutes , speed 1 (S1): 2000 RPM, T2: 2 minutes, S2: 2000 RPM.

3.4 Substrate Nomenclature

Spin coated substrates are named throughout this thesis in accordance with the constituent formulation and any aspects of the process by which they were fabricated. The sample name and details of each spin coated substrate is shown in

Table 3.2. Samples were spin coated in a positive pressure (purged) nitrogen environment unless appended with the term “air”.

Table 3.2 Substrate nomenclature for spin coated thin films, with details of relevant constituents involved.

Sample Name	Specification
100PMMA	3% 100:0 PMMA:PS (Control sample)
100PMMA_sc	3% 100:0 PMMA:PS solvent cast (Control sample)
100PS	3% 0:100 PMMA:PS (Control sample)
25PS75PMMA	3% 25:75 PS:PMMA
25PS75PMMA_375	3% 25:75 PS:PMMA, +375 microspheres/ml
25PS75PMMA_750	3% 25:75 PS:PMMA, +750 microspheres/ml
25PS75PMMA_1500	3% 25:75 PS:PMMA, +1500 microspheres/ml
25PS75PMMA_air	3% 25:75 PS:PMMA, spun in ambient air pressure
25PS75PMMA_750_air	3% 25:75 PS:PMMA, +750 microspheres/ml, spun in ambient air pressure

3.5 Hot Embossing-Fabrication of Nanoscale Features on PMMA

Hot embossing was used to create the isolated nanotopography deemed to be effective for the entrapment of von Willebrand Factor (vWF) and the interaction of platelets from the same blood sample. PMMA sheets (Goodfellow, UK) with a thickness of 1mm, were cut into discs with a diameter of 90 mm and cleaned with 99.9% IPA before being dried with a lint free cloth. Hot embossing was completed using an EVG-520HE Hot Embosser (EVG Group, UK) under a contact from the University of Southampton Nanofabrication Centre using a stamp designed to a previous specification[14]. This stamp template has features which are the inverse of the topography required and once pressed into the thermoplastic polymer substrate surface at an elevated temperature, creates the actual features required in a highly organised manner.

The original (previously employed[14]) master stamp template was created using the services of a specialist supplier (NIL Technology, Denmark). This device comprised a fused silica disc of 90 mm diameter and 1 mm thickness onto which two channels of 35 mm in length and 5 mm width were created, shown in Figure 3.1. Each channel consists of an array of etched of pits created by semiconductor photolithographic processing techniques which have a 500 nm base diameter, a 100 nm apex diameter and are 50 nm in depth, meaning that embossing of this onto a surface should yield peaks of these dimensions. Each channel is shown within a marked area representing the dimensions (25 x 50 mm) of the bottom plate of a DPFA sensor substrate. Whereas both channels have features with the same dimensions, the interspacing between them differs; the first channel has a 1:2 ratio of feature to spacing, giving a 1000 nm interspacing between individual features while the second channel has a 1:1 ratio, thereby yielding 500 nm interspacing. The stamp is completed by application of a fluorinated silane-based anti-stick layer (ASL) on the surface to enhance its release from the PMMA surface post-embossing. Although successful in creating the required nanotopography, the native fused silicon master stamp template was fragile and broke after two embossing cycles. Hence, it was not possible to determine the effects of vWF-platelet activity on the embossed features in the respective flow channels.

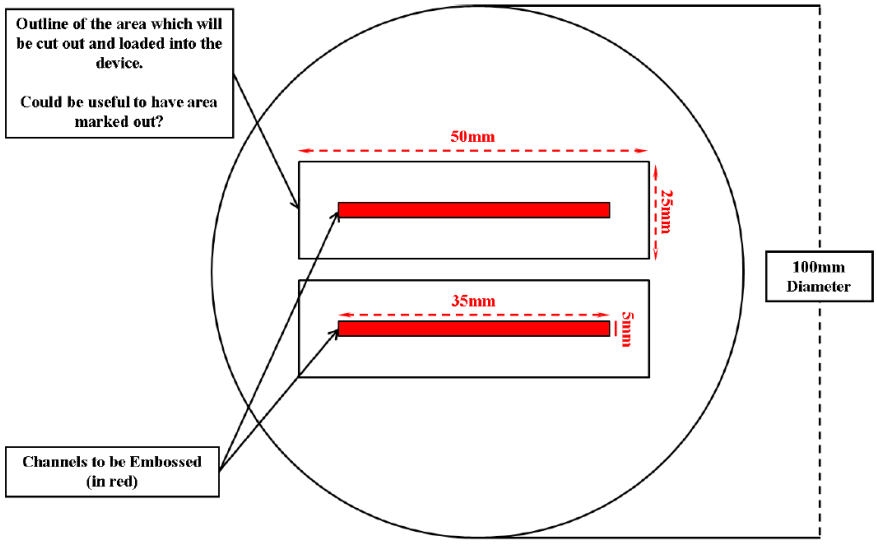

Figure 3.1 Schematic drawing of the hot embossing master stamp template highlighting the two (5 x 35 mm) channels within a marked area representing the dimensions (25 x 50 mm) of the bottom plate of a DPFA sensor substrate[14].

For the purposes of the studies carried out here, a second version of the stamp was created using the same design (Figure 3.1) but augmented during fabrication with a nickel layer, the purpose of which is to better dissipate the stresses encountered during the embossing process. This new stamp is otherwise the same in all other aspects regarding its form and function. In order to create the required nanoscale features with this upgraded stamp template, PMMA discs were cleaned with IPA (>99.5%) and allowed to dry vertically in air in a laminar fume hood. Just prior to embossing, a stream of dry nitrogen was used to remove any debris from both the stamp and PMMA surfaces.

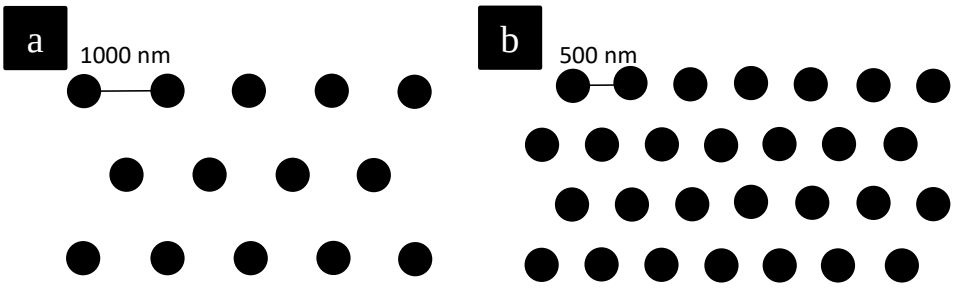

Figure 3.2 Sketch of hot embossing master stamp template showing (a) channel with 1000 nm feature inter spacing and (b) channel with 500 nm channel interspacing.

Embossing was then carried out using an EVG-520HE Hot Embosser (EVG Group, UK). The nickel coated master stamp was placed on top a blank silicon wafer of the same dimension and placed on the bottom of the system heating chuck. A PMMA disc was then aligned with the upper surface of the master stamp a backed by a second blank silicon wafer. The top of the heating chuck was now put in place and the assembly placed into the processing chamber of the instrument and heated above the glass transition temperature for PMMA (105˚C), to 135˚C. Once this temperature was achieved, the chamber was evacuated to a pressure of < 0.1 mbar and a force of 8.5 kN applied for 5 minutes. At the end of this time period, the temperature was reduced to < 100 ˚C commensurate with the glass transition temperature of the PMMA whilst maintaining the same applied loading force for an additional 5 minutes. The loading force was then removed and the PMMA allowed to cool to room temperature after which the chamber was vented, and sample removed. The process was then repeated to attain the number of embossed substrates required for subsequent studies, with the stamp and blank silicon wafers cleaned with IPA and dried in flowing nitrogen between each run.

Substrates were then cut to size using a CO_2 laser, for use within the DPFA assembly (25 x 50 mm). The VLS2.30 CO2 laser system (Universal Laser Systems Inc, Arizona, USA) operated with 10.6 μm laser wavelength, and 25W power. The cuts outs were made in the PMMA using vector mode at 100% power, and 25% speed.

3.6 Substrate Nomenclature

Details for substrate names used for the PMMA embossed substrates referred to throughout the body of the thesis are provided in Table 3.3.

Table 3.3 Substrate nomenclature and associated specification for PMMA embossed samples, with details of their specified interspacing.

Sample Name	**Specification**
Channel a	50 nm height and 500 nm base width 1000 nm interspacing
Channel b	50 nm height and 500 nm base width 500 nm interspacing

3.7 Characterisation of Substrate Surfaces

Physical and chemical characterisation of substrate surfaces produced by spin coating of PS/PMMA polymer demixed solutions in chloroform onto glass slides has been carried out for samples created in positive pressure (purge) of nitrogen and in air under normal ambient conditions. Likewise, the embossed structures created on PMMA have also been examined in respect of confirming the actual feature size and spacings produced. The methods used and their utility in the provision of the information sought, are outlined below.

3.7.1. Optical analysis

Optical microscopy was employed to examine the final distribution of PS particles within the amorphous PMMA component of the spin coated PS/PMMA demixed surfaces (see

Table 3.2). Images were obtained using a Nikon TS Eclipse 100 phase-contrast microscope (Nikon, UK), equipped with a x20 objective and Nikon CoolPix5400 camera fitted with a MXA5400 microscope adapter. Data was collected in phase-contrast mode which works by converting phase shifts of the light energy to brightness changes in the image. For the purposes of these studies, phase-contrast microscopy was found to be superior to the standard bright field technique, as it has the ability to better identify fine details which are usually invisible in normal optical views of highly transparent materials. The coating formed on each slide was imaged in three areas across the sample surface:– centre, off centre and the edge, as shown in Figure 3.3. Post-acquisition, images were modified to include a scale bar using ImageJ software (NIH, Bethesda, USA).

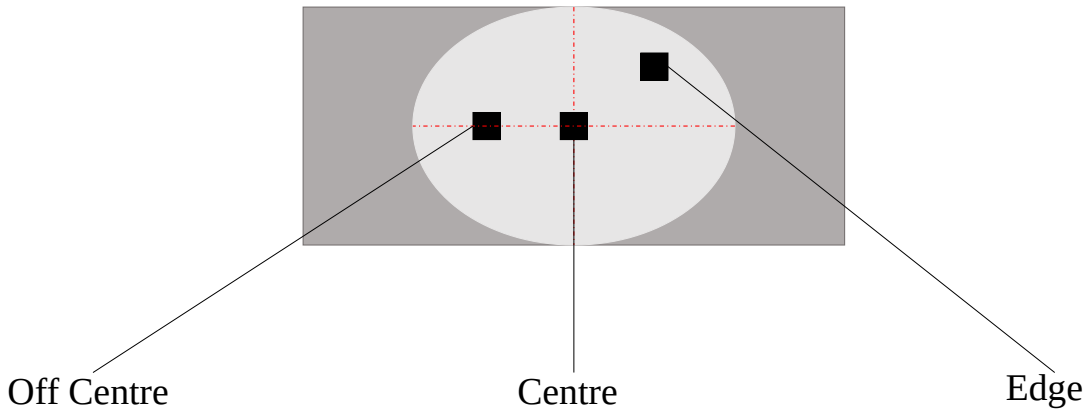

Figure 3.3 Diagram showing the three distinct areas (centre, off-centre and edge) on spin coated PS/PMMA samples imaged by optical microscopy in phase contrast mode.

3.7.2. Atomic Force Microscopy (AFM)

AFM was used to measure and spatial map the surface topography of the PS/PMMA spin coated samples at the sub-micron to nanometre scale. The technique was also used to identify and confirm the dimensions of features created by hot embossing PMMA with the nickel augmented stamp (including feature spacing). All

measurements were performed using a Veeco Digital Instrumentation Dimension 3100 AFM (Bruker Axs, UK) system operating in tapping mode whereby the silicon tip oscillates at a frequency at or close to the resonant frequency of the cantilever. In this work, a scan rate of 0.96 Hz was employed to create scanning areas ranging from 10 – 40 μm^2. Deflection of the tip is caused by van der Waals forces and electrostatic attractions/repulsions between atoms on the surface and the tip. These deflections are measured in terms of the change in amplitude and are then translated into topographical information via a pseudo-colour plot of the xyz co-ordinates. Image analysis was carried out using NanoScope Analysis software (v1.5, Bruker Axs, UK). Data was processed by initially using first order flattening to account for sample tilt and/or piezoelectric non-linearity, before a 3D construction of the scanned area is made. Surface roughness was subsequently recorded as both R_a (arithmetic mean roughness) and R_q (root mean square roughness) values. Only height descriptors were measured for each substrate to identify changes in feature size. Line profiles of the peak-to-peak height and peak-to-peak amplitude were obtained from the image data sets at a fixed position perpendicular to the xy scan direction. These data outputs were used to assess the number of features present and their regularity across this area of the surface. In all cases, a minimum of three spin coated sensor substrates (n=3) were used in each experiment, with triplicate measurements then made on each of these individual samples.

3.7.3. X-ray Photoelectron Spectroscopy (XPS)

XPS is a highly sensitive surface analysis technique used to acquire chemical information about the uppermost region of a material or coating. The XPS depth of analysis is determined by the mean free path of photoelectrons that are produced by incident X-rays, in that only those close to the surface are detected, namely in the

uppermost 5 to 10nm. By measuring the kinetic energy (KE) of the detected photoelectrons their original binding energy (BE) can be determined using equation 3.2.

$$BE = hv - KE - \varphi \qquad (3.2)$$

where BE = binding energy

hv = incident x-ray energy (Plank's constant × x-ray frequency)

KE = kinetic energy

φ = work function of the spectrometer (constant)

The equation above is incorporated within the Vision processing software (v2.10 Kratos, UK) integrated within the spectrometer so that values are shown as BE. As the BE values are unique to specific elements, their presence can be used to identify the composition of a materials surface or a coating with high surface depth specificity. Moreover, the BE position (after correction for any surface charging effects) can provide additional information regarding the chemical state of the elements concerned. This is particularly useful for polymeric materials as the carbon 1s (C1s) electrons are sensitive to the attendant bonding conditions that are present.

The polymer demixed thin film coatings created by spin coating PS/PMMA solutions in chloroform onto glass slides were subject to XPS analysis to gain information on the resultant surface chemical composition. A Kratos Ultra Delay Line Detector system (Kratos Analytical, UK) was used throughout with samples introduced into the analysis chamber operating at a pressure of 1 × 10-9 mbar via fast access load-lock and transfer chambers, allowing for sample degassing and removal of water vapour. Spectra were recorded using an aluminium X-ray source (Kα X-rays

at an incident energy of 1486.6 eV) operating at a pass energy of 160 eV, with a spot size of 600 µm to acquire initial wide energy survey scans (WESS) of BE versus photoelectron counts per second. Based on the polymeric nature of the coating of interest, high resolution spectra for the carbon (C 1s) and oxygen (O 1s) regions were collected at a reduced pass energy of 20 eV. Due to the insulating nature of PS/PMMA materials, in situ charge neutralization was applied via a low energy electron gun operating with a filament current of 1.95 A and a charge balance of 3.3 V, working in tandem with a magnetic immersion lens. In all cases, a minimum of three spin coated sensor substrates (n=3) were used in each experiment, with triplicate measurements then made on each of these individual samples.

All spectral data were processing using CasaXPS software (v2.3.19, CasaXPS, UK). As a first step, a post-acquisition correction for any residual charging effects was made by calibrating the C-C aliphatic peak in the C 1s region to 285.0 eV. Quantitative values for the relative percentage atomic concentration (% atomic concentration) were derived from the spectra using the area under each spectral envelope as a function of the tabulated values of Scofield X-ray cross-section values ratioed to the intensity F1s peak set to unity. Peak fitting was used to deconvolute the high-resolution spectra thereby yielding information on specific bonding environments present. In all cases, peaks were fitted using the Scienta ESCA 300 database[127] and the beta-shifted carbon component was identified within the aliphatic carbon peak. Constraints were applied at values ± 0.3 eV from these published reference values.

3.7.4. Contact angle

Water contact angle uses the balance between cohesive forces occurring between liquid molecules, and the adhesive forces between the liquid molecules and a contacting material to give a measure of wettability which can be used to characterise

the degree of hydrophobicity/hydrophilicity of a surface. The basic equation for the relationship between contact angle and surface energy is provided in equation 3.1;

$$\gamma\_sv = \gamma\_sl + \gamma\_lv \cdot cos\theta \quad (3.1)$$

Where γ_sv= surface energy

γ_sl=solid-liquid interface

γ_lv=liquid-vapour interface energy

θ=contact angle

In this work, a Cam 200 Optical Contact Angle Metre (KSV Instruments, Finland) was used to measure the water contact angle for the various substrates of interest. Samples were placed on the instrument stage and a 5 µl drop of water dispensed onto the surface. The contact angle was measured from static video image with both the left and right edges of the droplet-surface interface measured and reported as an average value. The depth analysed varies from 3-20 angstroms (Å) and spatial resolution is approximately 1 mm. A minimum of 3 measurements per sample, across 3 samples were completed for each sample set.

3.8 Biological Assessment of Substrates – Dynamic Platelet Function Assay (DPFA)

Haematological assessment of each substrate fabricated within this research was measured using the Dynamic Platelet Function Assay (DPFA) system developed by the Royal College of Surgeons in Ireland (RCSI), Dublin, Ireland [15,99,104]. This RCSI-DPFA system comprises a parallel flow chamber architecture for platelet function testing and the schematic for which is shown in Figure 3.4. The parallel plate flow chamber comprises a top plate with a pre-cut flow channel and input/output ports

which is placed on top of the various glass slide substrates spin coated with a PS/PMMA layer or the embossed PMMA samples. A self-adhesive gasket is used to seal the two parts of the assembly together and thereby create the discrete flow path within the flow chamber.

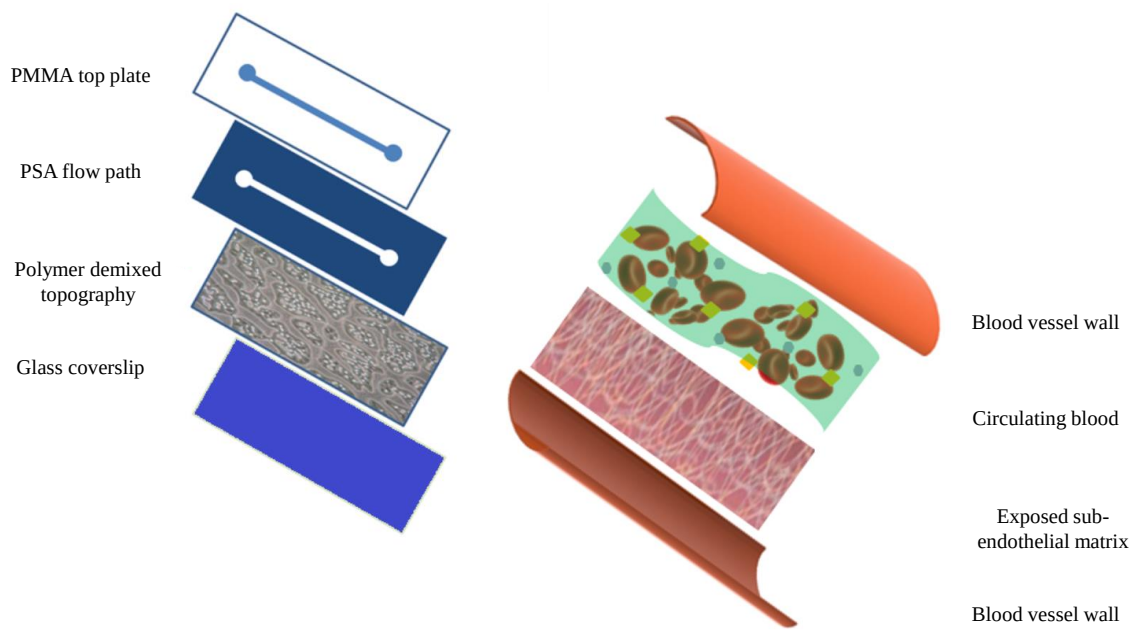

Figure 3.4 Schematic breakdown of the synthetic substrate incorporated with the DPFA top plate, representing the simplified in vivo environment.

3.8.1. Blood collection

Blood donors within this research were healthy volunteers who had not taken any medication that is known to affect platelet function, and all gave informed consent for their participation. Blood collection was carried out under clinical conditions at Beaumont Hospital, Dublin, Ireland. Blood was taken through a 19-gauge Sarstedt Safety Needle into an S-Monovette 9NC collection tube (Sarstedt, Wexford, Ireland) containing the anticoagulant solution trisodium citrate dihydrate (final concentration of 0.32%, 1:9 ratio of citrate to blood). Donor age and gender were recorded. Platelet indices were measured at the time of donation using a Sysmex KX21N (Sysmex, Kobe, Japan) blood analysis apparatus. A complete blood count (CBC) was collected

which details % amount blood cells (leukocytes, erythrocytes, platelets) and platelet indices. Of these values, the platelet count (PLT), mean platelet volume (MPV), haematocrit (HCT) and platelet-large cell ratio (P-LCR) were monitored. These four platelet indices were considered due to their link to platelet activation[128]. All donors had a platelet count within the accepted normal range of 150 – 450 x10^3/µl [3].

3.8.2. Dynamic Platelet Flow Assay (DPFA) Measurements

The assembled flow chambers were mounted on a Zeiss Axiovert-200 epifluorescence inverted microscope (Zeiss, Ireland). The fresh blood samples from volunteer donors were placed in a Eppendorf tube and 1µM 3-3'-dihexyloxacarbocyanine iodide (DIOC6), a lipophilic dye that emits light at 488nm, added to stain the platelets.

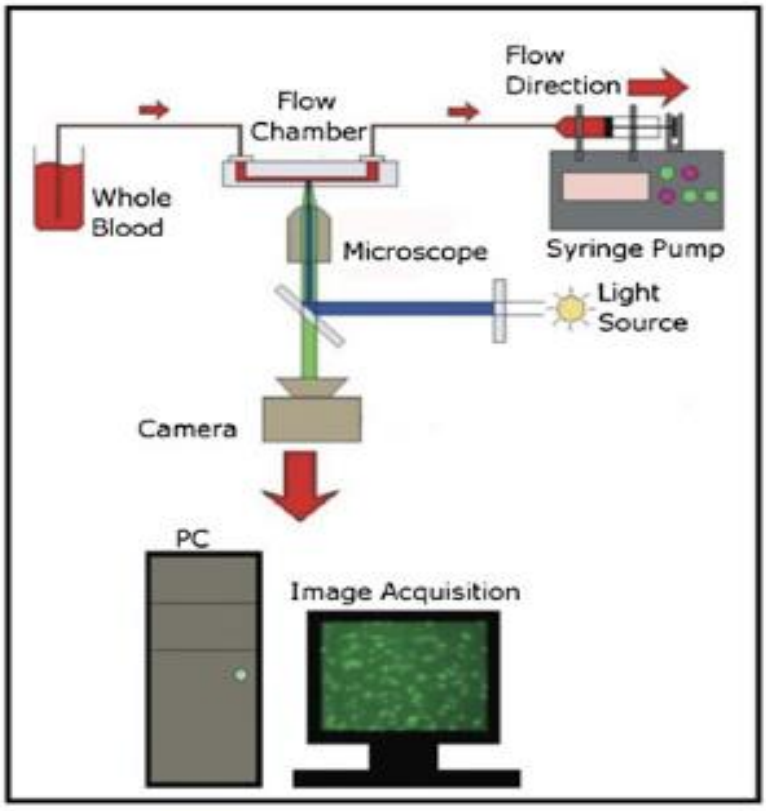

Figure 3.5 Schematic representation of the Royal College of Surgeons, (Dublin Ireland) Dynamic Platelet Function Assay (RCSI-DPFA) test apparatus[104].

Figure 3.5 shows the assembled DPFA process where a NEMESYS syringe pump was then used to perfuse the "stained" whole blood across the parallel flow path at flow rate (Q) of 75 μl/min corresponding to an arterial shear rate (γ) of 1500 s^{-1} equivalent to that experienced on the inner lumen of small arteriole vessels. Fluorescent images of the flow path were obtained using a vacuum-cooled (-80 ˚C) digital iXON EM+ CCD camera (Andor Technology, UK) in video capture mode connected to a MetaMorph (Molecular Devices Ltd., UK) and illuminated with an Osram 103-W light source equipped with a fluorescein iosthiocyanate (FITC) filter set (Chroma Technology Corp, Vermont, USA) providing excitation and emission at 490 nm and 528 nm, respectively.

At the outset of the blood perfusion process, the video stream is monitored in real time and when the first platelet sticks to the surface, a recording of 1000 images at 19 frames per second (fps) is attained with a x20 objective lens (field of view 502 x 501 pixels). This is immediately followed by capture of 1 frame every 2 seconds over a 4-minute period (120 frames), designated as the time lapse sequence. This protocol was kept consistent with previous work completed using the DPFA assembly[14,15]. In all cases, a quantitative assessment of the platelet interaction with the surface was undertaken, based on measurement taken from the final frame (i.e. 120/120) of this latter image acquisition sequence.

3.8.3. Calculation of the platelet surface coverage

At the end of the analysis sequence, images were imported into the ImageJ software package (NIH, Bethesda, USA) where they were adjusted in terms of brightness and contrast to provide for clear differentiation between the adhered platelets and the background surface features. These data files were then imported into the "Volocity" image processing software package (Perkin-Elmer, UK) and the platelet interaction

surface coverage calculated using the ‘find objects by % intensity’ tool. This analysis was carried out with acceptance limits set to values of 45 (lower limit) and 100 (upper limit). Figure 3.6 shows the outcomes achieved by processing (a) the raw (.tiff file) image to attain (b) adjustment of brightness/contrast in ImageJ and (c) subsequent representation of fluorescent pixel counts in the Volocity®.

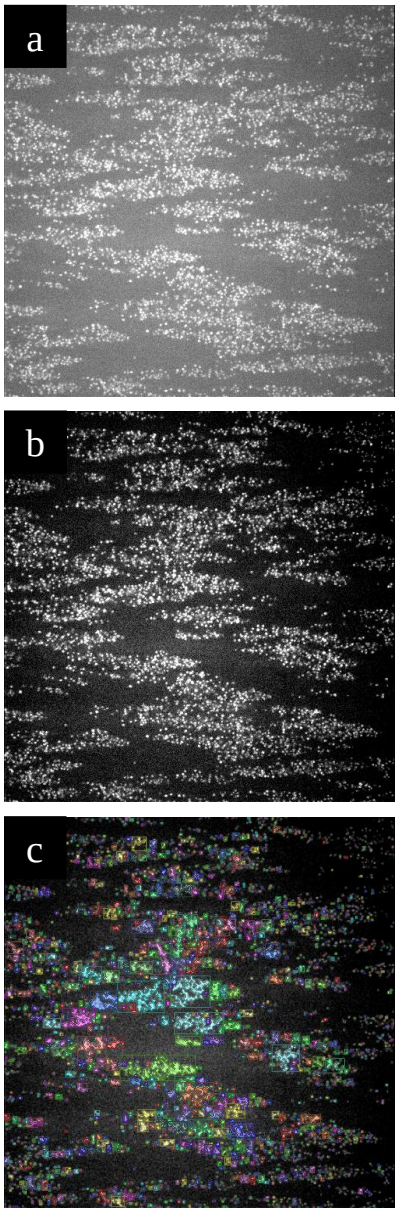

Figure 3.6 Image analysis processing steps from (a) raw .tiff frame through (b) ImageJ brightness/contrast adjustment and (c) fluorescent pixel counts using Volocity®.

Areas of interaction were measured in respect to the pixels associated with the adhered platelets and % surface coverage calculated by dividing these values by the total number of pixels present.

3.8.4. Analysis of dynamic platelet tracking parameters

Image stacks were analysed using an algorithm routine devised to interpret information relating to the dynamic kinetics platelets on the immobilised vWF substrate sensor surface[15,59,104]. In this regard, platelet adhesion and aggregation involves a series of reversible and irreversible actions which can be described by a set of four equations, the origins and development of which are described by Ralph *et al.* [105]. For ease of understanding, these equations have been included;

$$\frac{d\mathrm{Ntrack}}{dt} = K_{on}N_0 \tag{3.3}$$

$$\frac{dN_{platelet}}{dt} = K_{on}N_0 - K_{off}N_{platelet1} - K_{on2}N_{platelet1} \tag{3.4}$$

$$\frac{dN_{platelet2}}{dt} = K_{on2}N_{platelet} \tag{3.5}$$

$$\frac{dN_{platelet}}{dt} = \frac{dN_{platelet1}}{dt} + \frac{dN_{platelet2}}{dt} \tag{3.6}$$

where K_{off} = detachment rate

K_{on2} = stable adhesion

K_{on1} = transient adhesion

$N_{platelet}$ = number of platelets within field of view

$N_{platelet1}$ = number of platelets transiently adhered

$N_{platelet2}$ = number of platelets stably adhered

N_{tracks} = total number of platelets that appear within the whole image stack

N_0 = Platelet Count (PLT) × volume

Based on these equations, a range of kinetic parameters associated with platelet-surface interactions have been investigated for the spin coated PS/PMMA samples created herein. The reporting and interpretation of this data are then based on the biological relevance of each of the parameters described in Table 3.4.

Table 3.4 Description of parameters measured within the algorithm used to quantify dynamic platelet kinetics on spin coated PS/PMMA surfaces.

Parameter	**Description**
Ntracks	Total number of valid platelets recorded, with the exclusion of very short or very small platelets which are deemed to be potential noise. Reduction in the number of Ntracks indicates a poor level of VWF entrapment and therefore low levels of platelet interaction.
Fraction stably adhered platelets	The number of platelets that are stably adhered to the surface presented as a fraction of Ntracks. This is defined as those that move < 1.5 times their own radius over the 1000-frame analysis. Biologically, this refers to the number of platelets that initially interact with autologous VWF and remain 'stably-adhered' to the surface.
Mean Translocating Distance (μm)	Mean distance travelled by translocating platelets: a decrease in this value may indicate increased signalling within the platelet which leads to faster activation of GP IIb/IIIa, reducing the distance a platelet travels before stably adhering to the surface.
Mean Translocating Velocity (μm/s)	The mean velocity is an indication of how fast platelets are translocating. A reduction in platelet translocation speed may signify, in biological terms, increased signalling within the platelet causing faster activation of GP IIb/IIIa, which causes adhesion.
Fraction Sticking	Denotes the number of platelets which adhere and remain on the surface, regardless of whether they translocate or not.

Using the algorithm in its original form showed slight discrepancies in the adhesion rate which, when considered, was assumed to be due to the difference in image capture rate (30fps for endogenous samples) so an adjustment was made to account for capture at 19fps. Some variation was observed in the number of platelets on the surface at the beginning of real-time monitoring and so the equations needed to be amended to correctly include the time zero effect which changes the boundary condition ($N_{platelets}$ = Ntracks at t=0 of observation). The parameters were augmented to include a parameter called 'Fraction Sticking' derived from the binding rate analysis as: "k_on,2 / (k_on,2 + k_off)". It denotes those platelets that adhere and remain on the surface,

irrespective whether they translocate or not. Throughout this body of work, this modified platelet algorithm will be referred to as the ‘autologous platelet algorithm’.

3.9 Statistics

All experiments were conducted with a minimum of three replicates so that statistical comparisons could be made. Where appropriate, statistical analysis was performed using Prism software (v8.0.2, GraphPad Software Inc., USA). T-tests were used where there were only two sample sets, with p value < 0.05 to determine statistical difference. The results are presented as mean ± standard deviation, unless otherwise stated.

4. Surface Properties to Induce a Direct Thrombogenic Response within a Dynamic Platelet Function Assay

4.1 Introduction

Rapid and accurate platelet function testing (PFT) is essential for the diagnosis of bleeding disorders such as von Willebrand disease (vWD). Moreover, the need for a dynamic assay that is capable of analysing platelet behaviour over appropriate time periods under physiologically relevant conditions has been well recognised[12,13]. As described previously in this thesis, current platelet function assays are limited by way of their static form of operation, i.e. they do not take account of vital physiological conditions such as the effects of the shear rate that is present in pulsatile flowing blood[72,129,130]. Recent advances in the area of PFT have involved the use of a bespoke parallel platelet flow chamber that is capable of passing small volumes of blood over an assay sensor surface under physiologically relevant levels of wall shear force[131,132]. These flow chambers employ a substrate which is functionalised with a chemical or a protein capable of interacting with platelets in order to create a standardised approach to a clinical diagnosis. A significant advancement in this area has been the development of an assay that uses a sensor substrate that has been coated with immobilised von Willebrand Factor (vWF)[12,104]. While this form of dynamic platelet function assay (DPFA) is a significant advancement on the current approach to PFT, it is clear that it could be further improved by the inclusion of a sensor surface that is capable of entrapping vWF directly from the whole blood that flows over it, such that subsequent platelet interaction occurs in the same sample, thereby yielding a patient-specific DPFA device[99].

Previously published studies have shown that platelets can interact directly (adhere transiently, roll, stick, etc.) with polymer systems that have certain forms of surface nanotopography[14,109,133]. However, one of the critical limitations of this form of surface processing is a lack of reproducibility in the resulting surface features. In this chapter, a means to enhance the regularity of the surface topography that is created by spin coating a polystyrene (PS)/poly (methacrylate) (PMMA) demixed solution onto glass substrates has been explored. In particular, the polymer demixed thin film deposition process has been augmented by the introduction of specific numbers of 50μm diameter PS microspheres to create a more regular and reproducible distribution of the surface topographical features. 50 μm microspheres were selected as they were outside the range of average particle size distribution for the PS (Mw=290,000) used in the core demixed blend (25PS75PMMA in chloroform). Addition of this size of microspheres was chosen so that they would be large enough to disrupt the original PS distribution during spin coating without causing a drastic change in resulting features i.e. the desire is for the formation of nanopits as opposed to nanoisland features. The ability of these PS/PMMA + 50 μm PS spin coated surfaces, to facilitate platelet interactions from whole blood that is passed over them at arterial shear rates, has been investigated with the aim of creating a form of a more reproducible patient-specific DPFA assay.

In all cases, the distribution of PS in PMMA that results from spin coating solutions has been examined by optical microscopy (OM); the resulting topographical features characterised by atomic force microscopy (AFM) and the associated surface chemistry confirmed by x-ray photoelectron spectroscopy (XPS). Collaboration with Royal College of Surgeons, Dublin has facilitated the use of a well characterised DPFA system (that normally operates with immobilised vWF assay substrates) to

study the nature and scale of platelet interactions on the novel PS/PMMA substrates with and without 50 μm diameter PS microspheres in blood that is flowing at arterial shear rate (1500 s^{-1}).

4.2 Properties of 25PS75PMMA Polymer Demixed Surfaces

Based on a consideration of the findings from prior work[14], thin film spin coated surfaces created from a 25% PS/75% PMMA solution in chloroform (25PS75PMMA) were deemed to be the starting point for refinement of the DPFA substrate. Specifically, the topographical features created from this specific polymer demixed system has been proven to be capable of entrapping autologous vWF so to provide the conditions for platelet binding thereon[14,15]. In order to fully understand the chemical and topographical properties of the 25PS75PMMA surface, elemental composition analysis, physical characterisation and haematology testing were carried out. In this way, the resulting data will act as a baseline for subsequent refinements of the system within the context of the DPFA requirements.

Optical micrographs for three distinct areas (edge, centre and off-centre) across the spin coated 25PS75PMMA substrate surface are shown in Figure 4.1 and indicate that the PS is distributed within PMMA in two distinct patterns: (i) honeycomb-like structures located primarily at the centre of the spin coated layer and (ii) striations which are seen to radiate outwards from the centre of the slide. This patterning can be explained by the use of a spin coating fabrication technique, in that the radial striations result from the centrifugal force pulling the casting solution outwards upon rotation. Since this force is at its lowest at the centre of the glass slide, a more disorganised structure occurs where the solution is not under centrifugal force to the same extent.

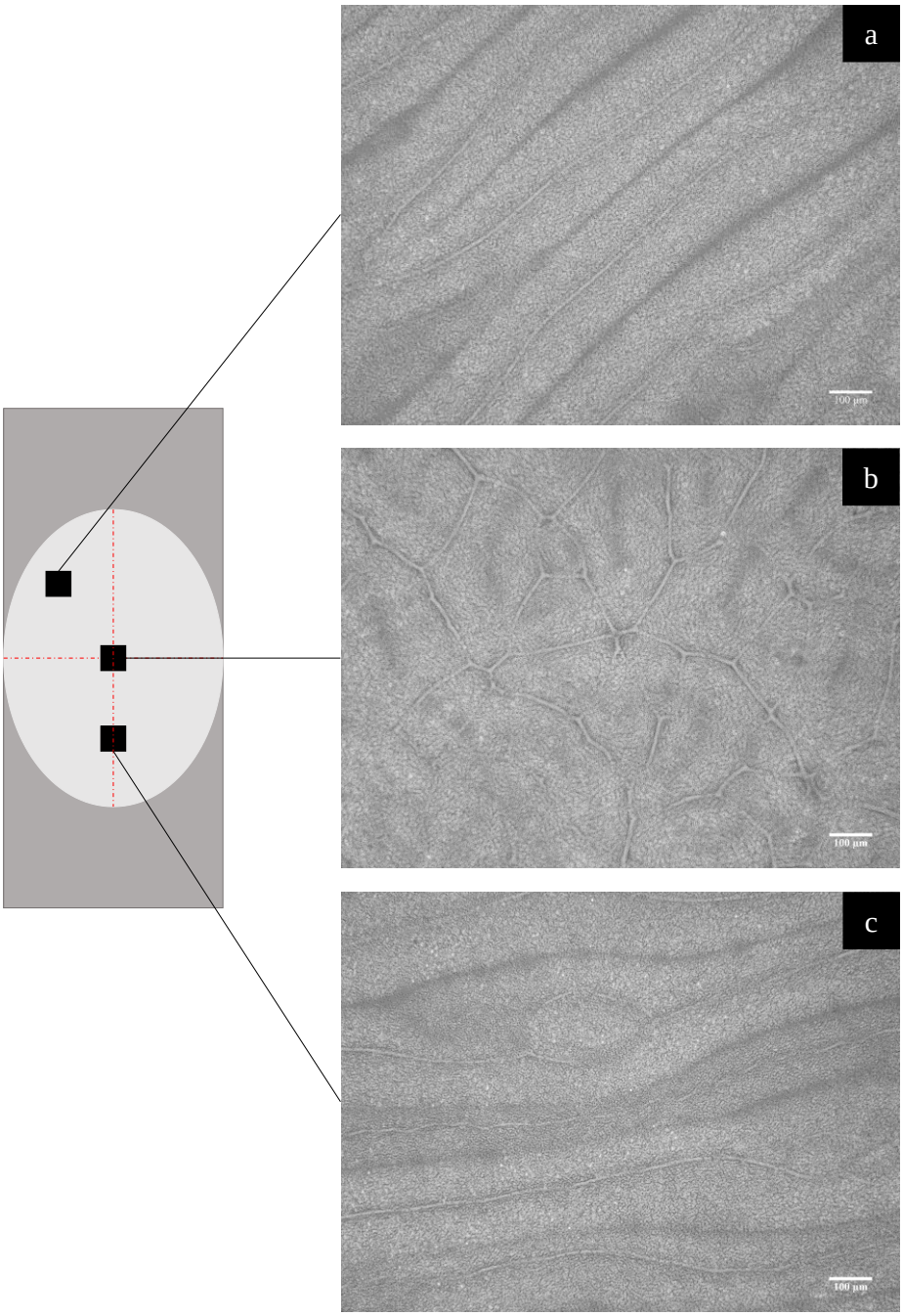

Figure 4.1 Optical micrographs of (a) edge, (b) centre and (c) off centre areas for a spin coated 25PS75PMMA substrate. Scale bar 100 µm.

By way of a comparison, the 25PS75PMMA solution was dispensed onto a glass slide using a standard solvent cast protocol and left to dry in air, to investigate what happens

in the absence of centrifugal force. Optical micrographs for these surfaces are shown in Figure 4.2.

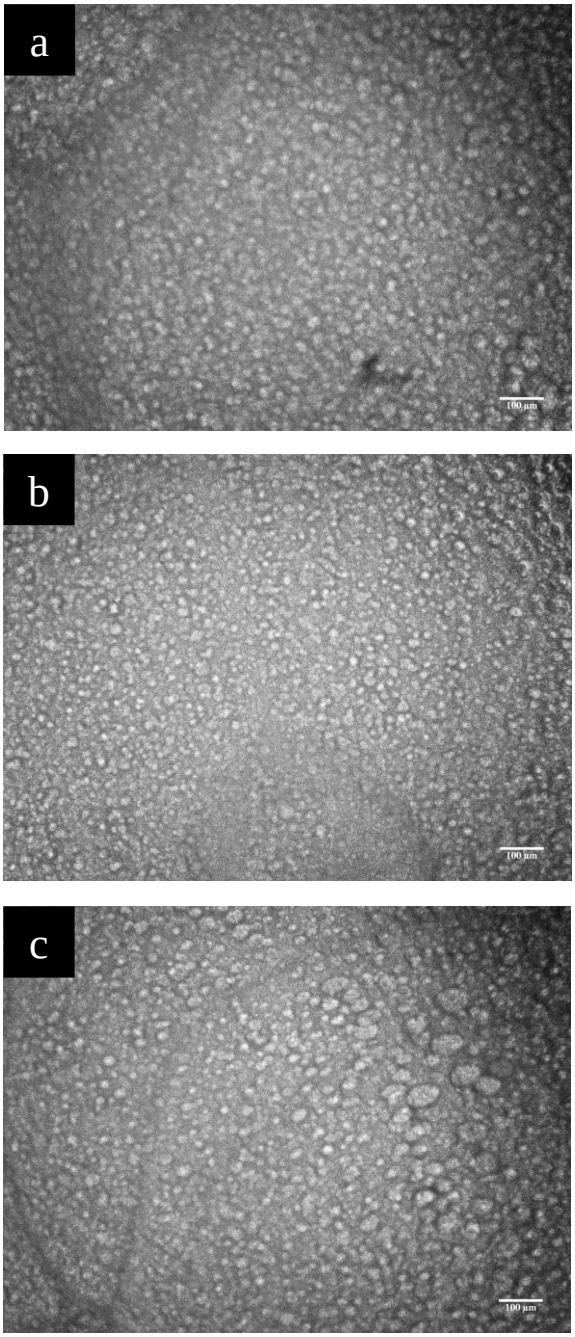

Figure 4.2 Optical micrographs for (a) edge, (b) centre and (c) off centre locations of an air-dried 25PS75PMMA substrate. Scale bar 100 µm.

In this case, the two distinct patterns seen previously for the spin coated samples are absent; with the PS distributed as particles throughout the PMMA component thereby confirming that the striations and honeycomb structures seen in Figure 4.1 are indeed a result of the centrifugal forces which occur when the substrate is spun.

Figure 4.3 (a)-(c) shows 10 µm x 10 µm 3D pseudo-colour AFM images for the areas examined by optical microscopy (i.e. edge, centre and off-centre) recorded in tapping mode, alongside line profiles for the 25PS75PMMA sample generated across the x-y midpoint of each of the 10 µm x 10 µm AFM images. In general, the 25PS75PMMA substrate presents a topography which represents a combination of poorly defined micron size features, overlaid with somewhat rounded nanoscale structures.

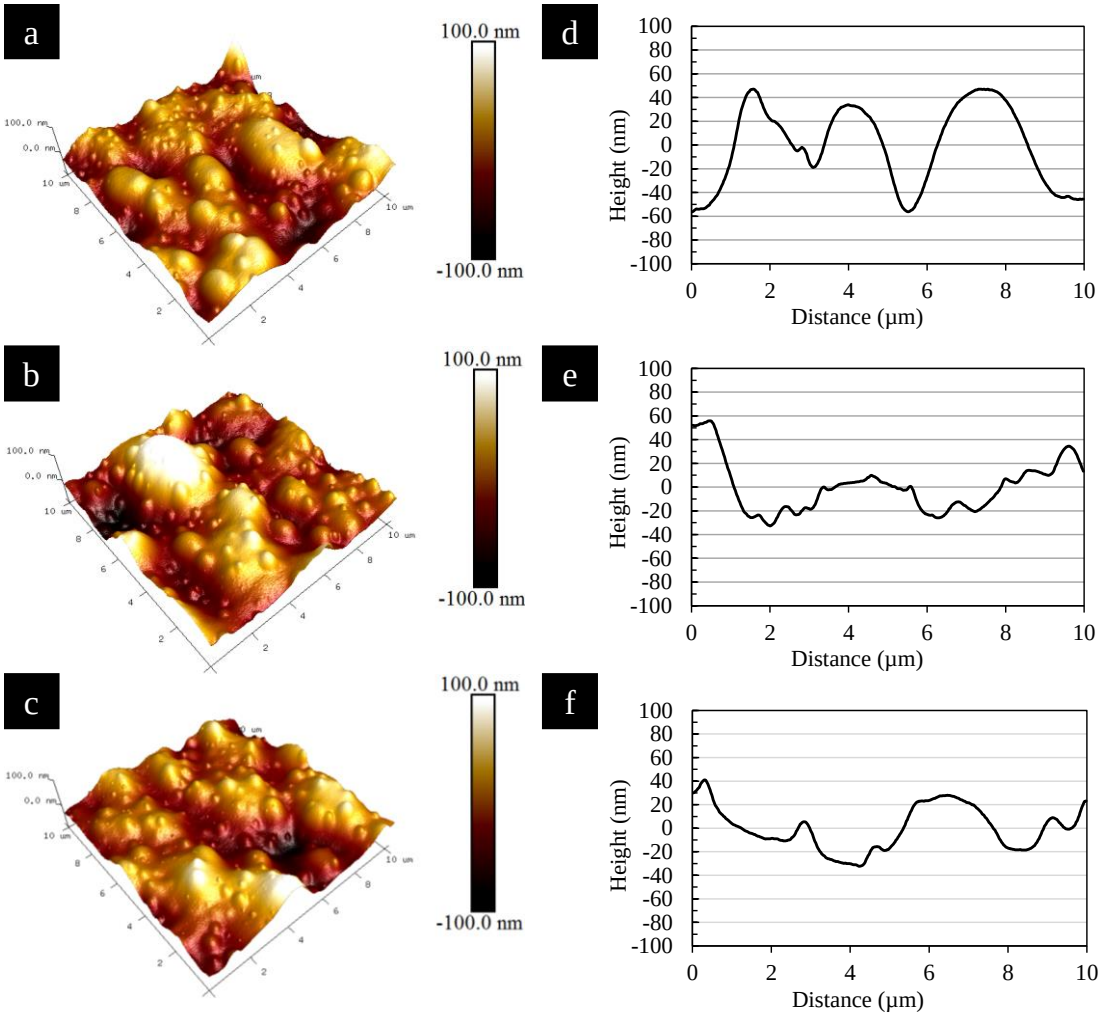

Figure 4.3 10 µm x 10 µm 3D pseudo-colour AFM images of (a) edge, (b) centre and (c) off centre areas of a spin coated 25PS75PMMA substrate (colour scale ± 100 nm) with corresponding line profiles of the (d) edge, (e) centre and (f) off centre generated from x-y midpoint.

Figure 4.3 indicates that the topography of this 25PS75PMMA polymer demixed surface is a combination of micron scale features with FWHM in the range ~ 2 to 4 µm and nanoscale features with FWHM in the range ~ 100 nm to 1 µm. The feature heights are in the range -70 nm to +50 nm. The corresponding surface roughness values, R_a and R_q, are 12.93 ± 4.06 nm and 15.85 ± 4.72 nm, respectively.

Polymer controls were introduced as a baseline for comparison. Three different surfaces were used – solvent cast PMMA, 100% spin coated PMMA and 100% spin coated PS. Figure 4.4 provides 3D pseudo-colour AFM images from 10 µm x 10 µm areas of 100% PMMA and 100% PS spin coated films on glass substrates, respectively. AFM analysis was not possible on solvent cast PMMA substrates due to their high magnitude of roughness. Surface calculated roughness parameters for spinc coated PMMA are R_a = 0.32 ± 0.01 nm, R_q = 0.53 ± 0.02 nm and for PS are R_a = 0.96 ± 0.01 nm, R_q = 1.33 ± 0.04 nm which indicate that each polymer results in a generally smooth spin coated layer surface.

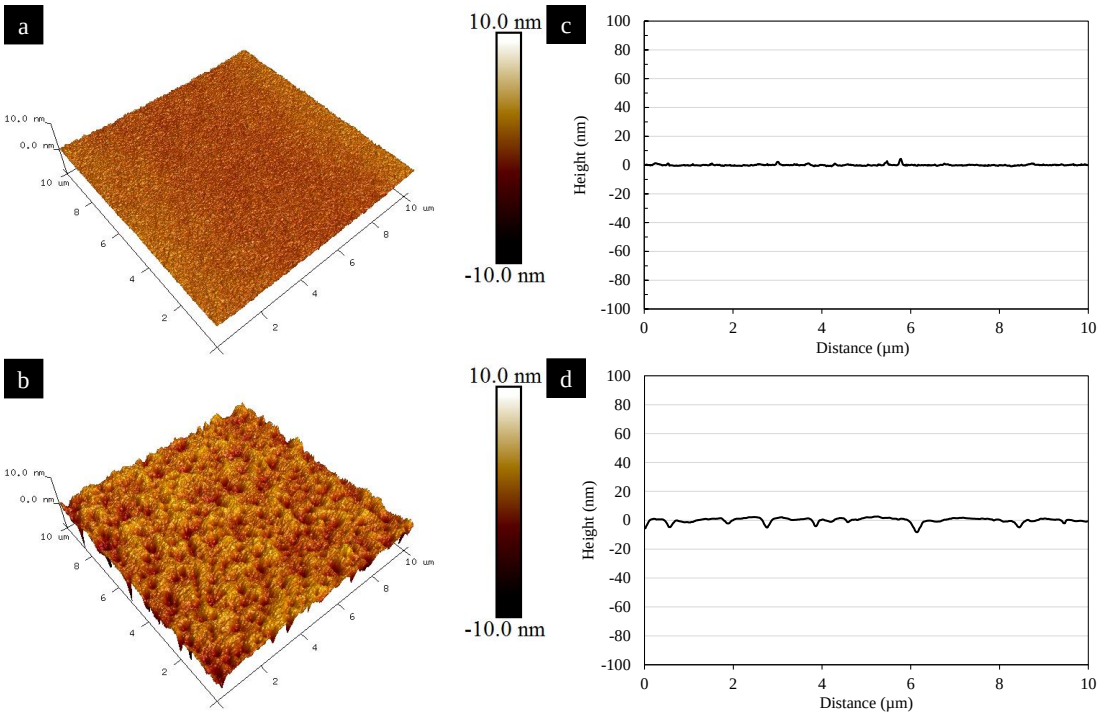

Figure 4.4 10 µm x 10 µm 3D AFM images of surfaces created by spin coating solutions of 100% (a) PMMA and (b) PS in chloroform with corresponding line profiles of the (d) PMMA and (e) PS generated from x-y midpoint.

Interestingly, the PS surface exhibits nanoscale pitting whereas PMMA surfaces show nano-protrusions. This explains the topography that is observed for the 25PS75PMMA system under the centrifugal force conditions experienced during spin coating. Surface chemistry analysis of the spin coated 25PS75PMMA sample was carried out to determine the chemical composition of the surface region. Figure 4.5 shows (a) a typical wide-energy survey scan (WESS) and associated high-resolution spectra for (b) the carbon (C 1s) and (c) the oxygen (O 1s) regions.

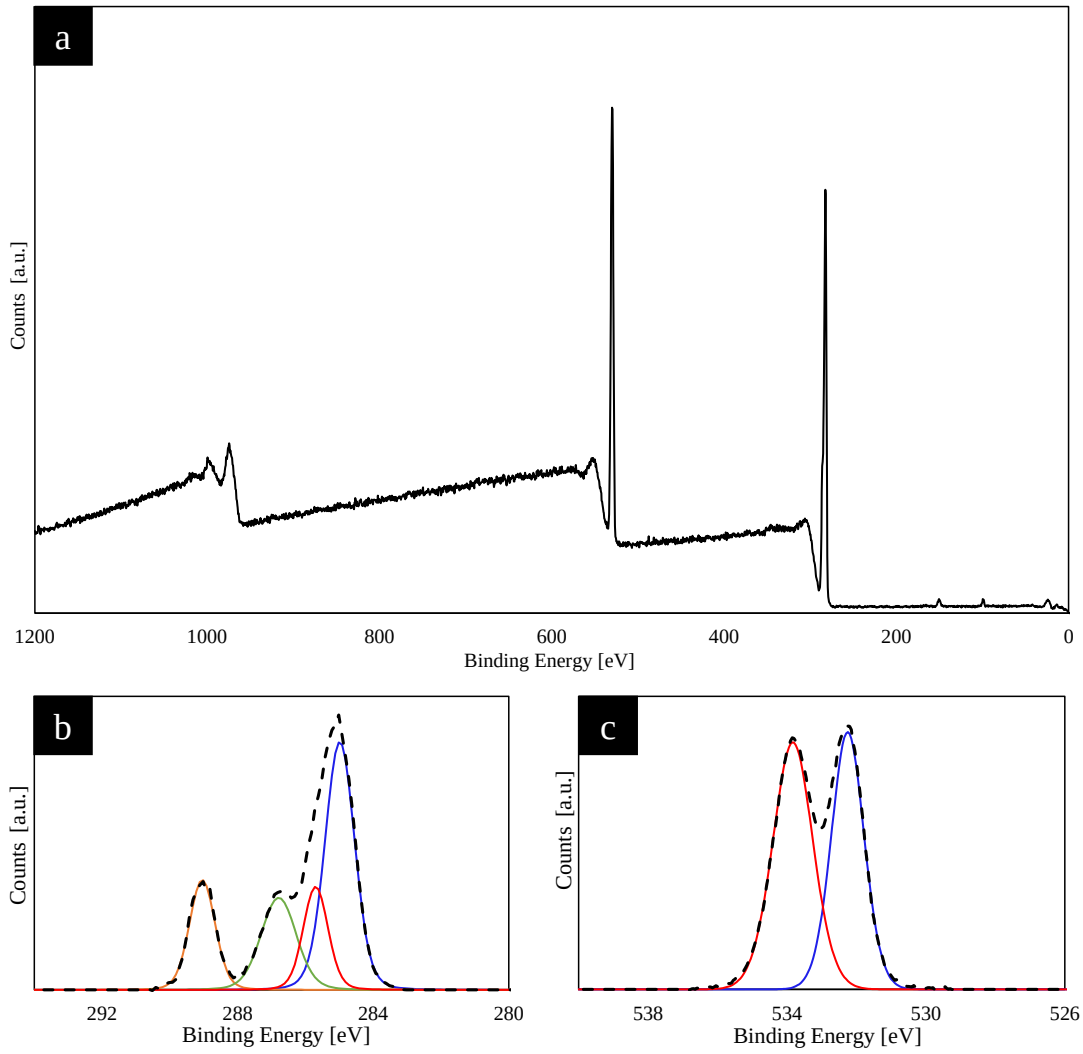

Figure 4.5 XPS spectra for spin coated 25PS75PMMA surfaces on glass substrates: (a) WESS, (b) C 1s and (c) O 1s spectra.

Charge correction was applied via calibration of the C-C aliphatic peak to 285.0 eV. Overall, four peaks were identified within the C 1s region at 285.0, 285.7, 286.8 and 289.0 eV; relating to C-H hydrocarbon, C-C-O beta-shifted carbon, C-O methoxy group carbon and O-C=O carbonyl bonding, respectively. Analysis of the O 1s component indicated a doublet consisting of two peaks at 529.1 and 530.7 eV, corresponding to C=O carbonyl and O-C methoxy group.

The corresponding quantitative data for this substrate is displayed in Table 4.1 along with those of obtained for the polymer control samples, for comparison. The data are reported as the average (n=3) % atomic concentration for both C 1s and O 1s contributions ± standard deviations.

Table 4.1 XPS derived % atomic concentration values of both C 1s and O 1s contributions for polymer demixed 25PS75PMMA sample with data for pristine PMMA and PS.

Sample Type	Sample	% C 1s	% O 1s	% C 1s	% O 1s
Solvent Cast PMMA	1	75.96	24.04	75.98 ± 1.04	24.02 ± 1.04
	2	77.02	22.98		
	3	74.95	25.05		
100% PMMA	1	80.53	19.47	80.23 ± 0.37	19.77 ± 0.37
	2	80.35	19.65		
	3	79.82	20.18		
25PS/75PMMA	1	76.56	23.44	78.41 ± 1.60	21.59 ± 1.60
	2	79.23	20.77		
	3	79.43	20.57		
Solvent Cast 25PS75PMMA	1	76.47	23.53	76.47 ± 0.24	23.53 ± 0.24
	2	76.71	23.29		
	3	76.24	23.76		
100% PS	1	100			
	2	100			
	3	100			

Hence, these spectral data indicate that the surface chemistry is definitively only that of PMMA.

4.3 Biological Assessment of 25PS75PMMA Polymer Demixed Surfaces

DPFA measurements were carried out on the spin coated 25PS75PMMA samples as per the set up shown in Figure 3.5 Samples were mounted in the flow chamber assembly and flushed with phosphate buffered saline (PBS) *in situ*. Whole blood from a healthy donor (designated as Healthy Donor 1) that had been labelled with the

lipophilic dye 3,3′-dihexyloxacarbocyanine iodide (DIOC6), was perfused across the flow channel surface at an equivalent arterial shear rate of 1500 s^{-1} for a total of 240 seconds. A profile of the blood from Healthy Donor 1 is provided in Table 4.2 including platelet count and the factors that influence same. Platelet interactions with the spin coated 25PS75PMMA surface were recorded by fluorescent microscopy using a CCD camera at a rate of 1000 frames at 19 frames per second, followed by 120 frames taken as 1 frame every 2 seconds over a 4-minute period, designated as the time lapse sequence. The final frame (120/120) of the time lapse was then used to calculate the % platelet surface coverage on the substrate.

Table 4.2 Blood profile for a healthy donor consisting of platelet count and additional platelet indices used for 25PS75PMMA DPFA measurements.

Name	Donor1_220617	**Haematocrit (HCT)**	44.2%
Age	24	**Platelets (PLT)**	$217_{x10}{}^{3}/\mu L$
Blood Type	O	**Mean Platelet Volume (MPV)**	10.3fL
Gender	Female	**P-LCR**	25.8%

Figure 4.6 shows a typical final frame from the 120/120 frame of the time-lapse fluorescent microscopy image set with adhered platelets seen as bright spots and clusters against the dark background.

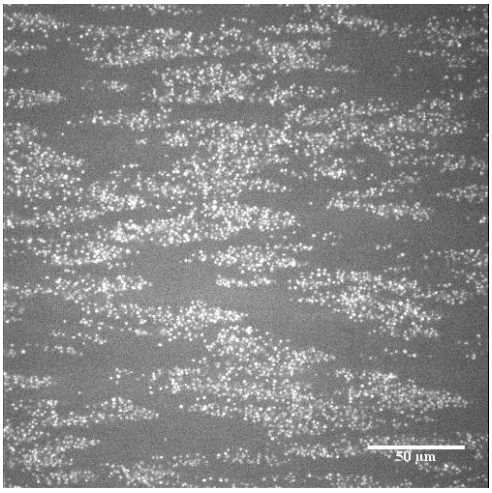

Figure 4.6 Final frame (120/120) from the time lapse sequence for a spin coated 25PS75PMMA substrate showing positive fluorescent platelet adhesion. Scale bar 50 µm.

To further investigate the scale of platelet interaction with this surface, quantitative image analysis was carried out to obtain a value for total percentage surface coverage. A surface coverage of 14.5% was calculated for the spin coated 25PS75PMMA substrate (Figure 4.6). However, one single test is not robust enough to determine feasibility.

In order to investigate the reproducibility of the platelet function measurements on the spin coated 25PS75PMMA substrate, a second set of experiments were performed at n = 5 using the same donor blood (Health Donor 1 – Table 4.2). Figure 4.7 (a) – (e) shows the final frame images (120/120) from the time lapse sequence for each of the five replicate surfaces.

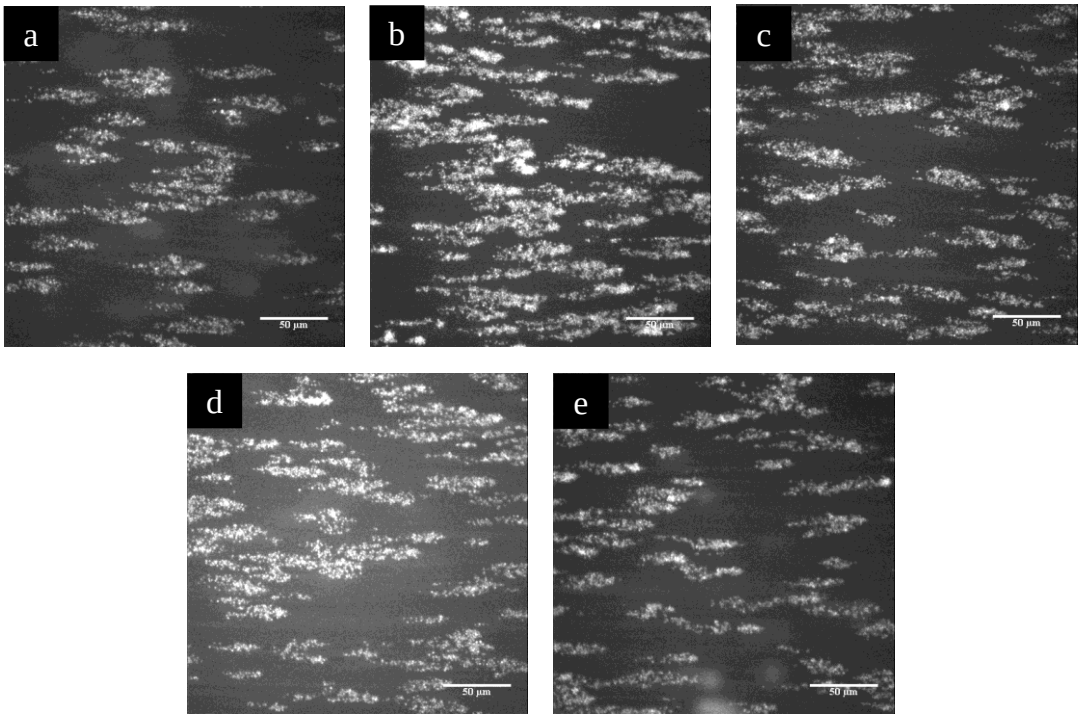

Figure 4.7 Fluorescence micrographs of whole blood DIOC6 labelled platelets in frame 120/120 for each 5 replicates (a) to (e) of the spin coated 25PS75PMMA surface. Scale bar 50 µm.

The calculated surface coverage for the five individual substrates are provided in

Table 4.3 with the average value determined to be 13.9 ± 6.6%.

Table 4.3 Average % surface coverage (n = 5) and standard deviation values for 25PS75PMMA spin coated surface.

Solution	Sample	% Coverage	Average	Standard Deviation
25PS75PMMA	1	7.94	13.89	6.60
	2	24.64		
	3	14.85		
	4	12.70		
	5	9.30		

Consideration of the high standard deviation value that is associated with the measurements within this sample set reflects the spread of values of the calculated percentage coverage. In order to better understand the platelet activity over time rather than solely at the 120/120 time point, the platelet interactions within frames at intervals across the time lapse sequence were selected and analysed. Figure 4.8 shows the still frames at 0, 60, 120, 180 and 240 seconds. The presence of adhered platelets in image (a) is noted and is deemed to be due to the recording of 1000 frames initially to allow for the threshold accumulation of vWF to facilitate platelet adhesion.

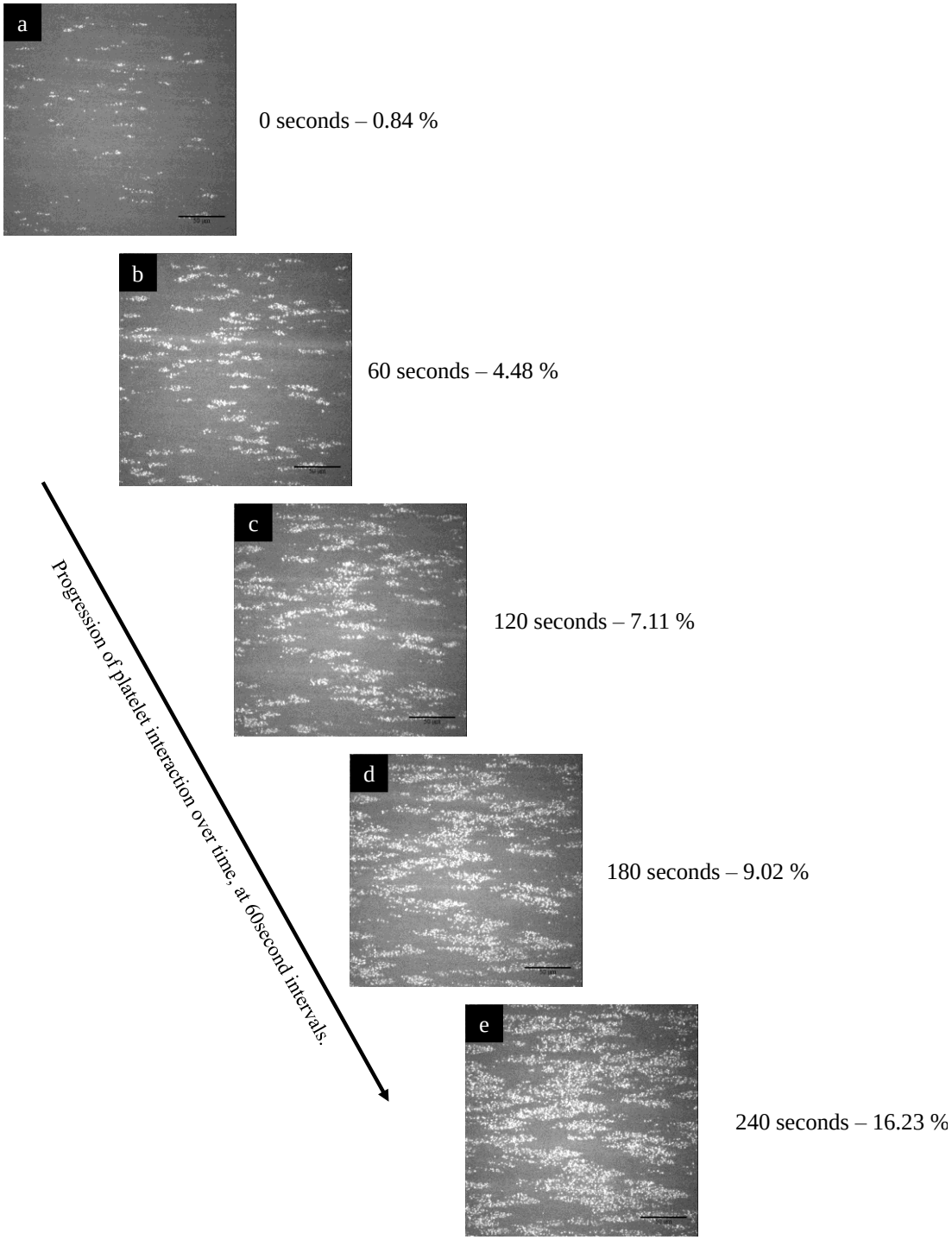

Figure 4.8 Images of platelet interaction with the spin coated 25PS75PMMA surface across at (a) 0, (b) 60, (c) 120, (d) 180 and (e) 240 seconds. Scale bar 50 µm.

Platelet growth can be seen across five timepoints within the time lapse series, to follow a linear formation where vWF strings have evidently adhered. Further

quantitative analysis of the percentage surface coverage for these static images are also recorded. Platelet interaction escalates by way of a 15.39% increase across the 4-minute period. Between frame (a) and (b) surface coverage grows by 3.64%, however from this point up until (d) 180 seconds, this rate of growth decreases before a last upsurge of an additional 7.21% of platelets covering the substrate. At this stage, platelets are now forming thrombi and both vWF and platelets are causing platelet activation.

4.4 Properties of Augmented Polymer Demixed Surfaces

Variance seen within the 25PS75PMMA study, would suggest that a more reproducible PS/PMMA demixed topography may produce a more consistent platelet interaction. To this end, uniform PS microspheres of diameter 50 µm, were introduced into the 25PS75PMMA spin coating solution in varying ratios as follows: 1:2 (1500 microspheres/ml), 1:4 (750 microspheres/ml) and 1:8 (375 microspheres/ml). The PS microspheres to base demixed PS/PMMA blend ratios selected for investigation were chosen as a starting point, to determine the number of microspheres required to have an effect on surface topography. This decision was incorporated with the anticipation of disrupting the fluid mechanics which were previously at play, in a bid to create a modified topography[134].

Optical micrographs for two distinct areas (edge and centre) on substrate surfaces created by spin coating from 25PS75PMMA solutions augmented with (a, b) 1500, (c, d) 750 and (e, f) 375 PS microspheres/ml are shown in Figure 4.9. Further analysis of the off-centre area was suspended due to the fact that blood does not come into contact with this area. These data indicate that the PS is still distributed within the PMMA in two distinct patterns: (i) honeycomb-like structures located primarily at the centre of

the spin coated layer and (ii) striations which are seen to radiate outwards from the centre of the slide. As was the case for the standard 25PS75PMMA spin coated surface (Figure 4.1), this patterning is a consequence of the centrifugal force pulling the casting solution outwards upon rotation, such that the centre of the sample has a more disorganised structure.

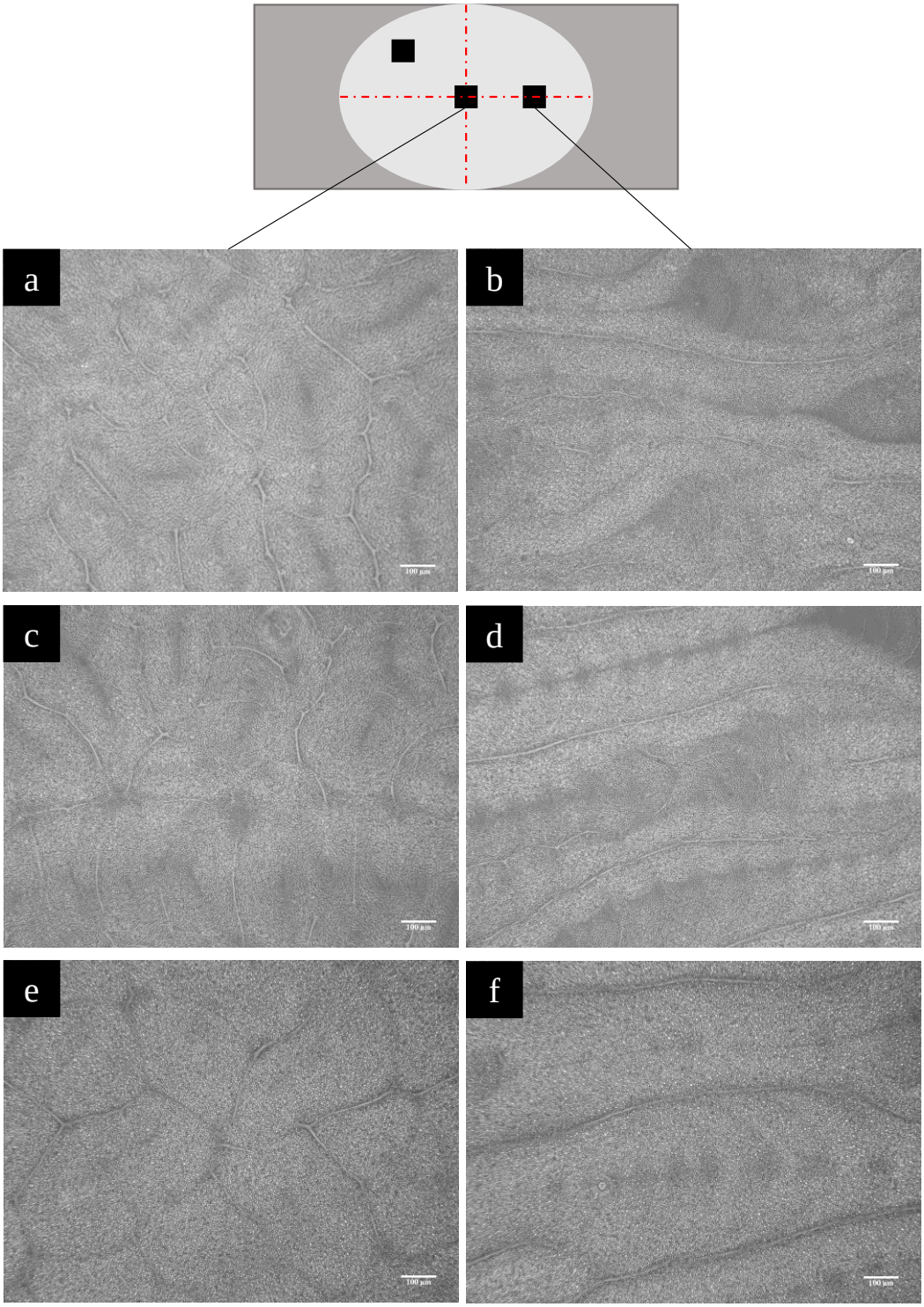

Figure 4.9 Optical micrographs for (a, b) 25PS75PMMA_1500, (c, d) 25PS75PMMA_75 and (e, f) 25PS75PMMA_375 thin films taken at the central area (a, c, e) and edge area (b, d, f) of the slide. Scale bar 100 µm.

AFM was employed to determine whether the introduction of the PS microspheres yielded any discernible differences in topography for the spin coated demixed polymer surfaces. Figure 4.10 shows 10 μm x 10 μm 3D pseudo-colour AFM images and line profiles, representative of the topography of spin coated films created from 25PS75PMMA solutions augmented with (a, d) 1500 (b, e) 750 and (c, f) 375 PS microspheres/ml. In general, the resulting microstructure is similar to that obtained for the 25PS75PMMA solution, comprising a combination of pits and islands across the surface with micron size features overlaid with nanoscale structures as per previous research findings[14,109,133].

However, increasing the number of 50 μm PS microspheres/ml in the spin coating solution results in a more regularly defined set of surface features. The associated line profiles indicate that addition of +375 microspheres/ml results in the same mixed micro/nano-scale topography as seen in the 25PS75PMMA base solution with microscale features of FWHM ~ 2-3 μm overlaid with nanoscale structures of FWHM ~ 100-500 nm (Figure 4.10 (f)). The corresponding data for spin coated surfaces created with +750 microspheres/ml (Figure 4.10 (e)) show slightly more refined features with peak heights ranging up to 30 nm-50 nm. The image and line profile data for the +1500 microspheres/ml spin coated surface show features that are significantly more regulated ranging in FWHM from ~ 100 nm up to 1 μm. Clearly, not only has the number of features present increased but they present a more ordered surface.

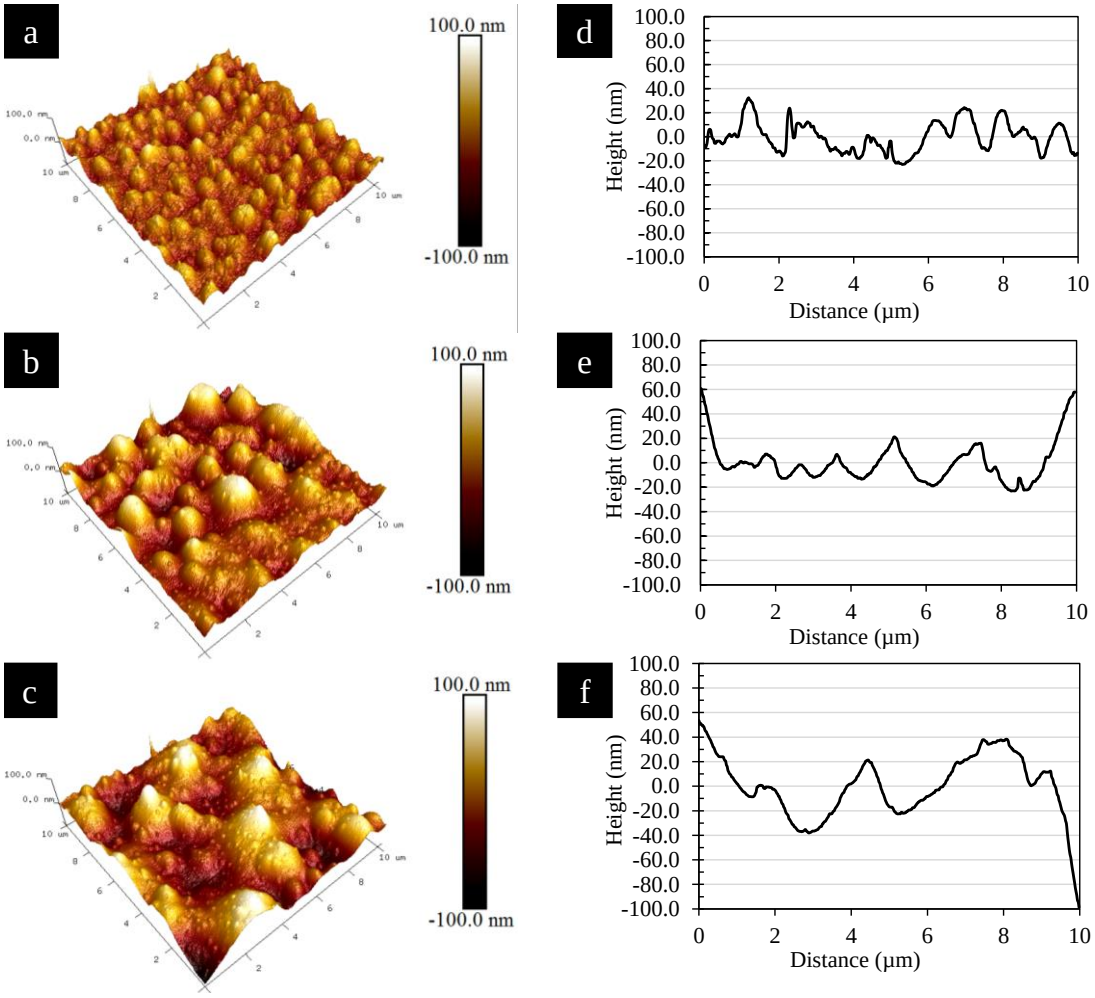

Figure 4.10 10 µm x 10 µm 3D pseudo-colour AFM images of spin coated thin films created by augmenting the 25PS75PMMA base solution with microspheres (colour scale ± 100 nm) at 1500 (a) 750 (b) and 375/ml (c) with corresponding line profiles generated from the x-y midpoint.

XPS was again used to determine the nature of the surface chemistry of the spin coated 25PS75PMMA thin films created from solutions with various amounts of 50 µm PS microspheres.

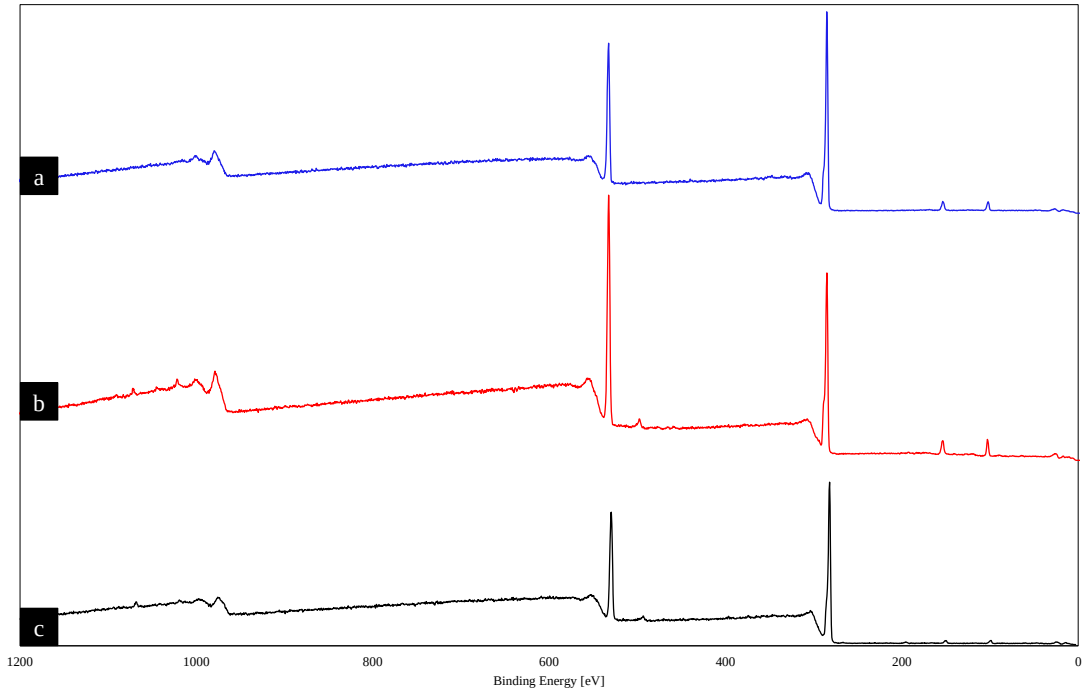

Figure 4.11 WESS for the augmented polymer blends corresponding to (a) 25PS75PMMA_1500, (b) 25PS75PMMA_750 and (c) 25PS75PMMA_375.

Figure 4.11 shows WESS data for each solution which are all very similar to that seen for the 25PS75PMMA thin film (Figure 4.5). The corresponding deconvoluted high-resolution spectra for the C 1s and O 1s regions are provided in Figure 4.12.

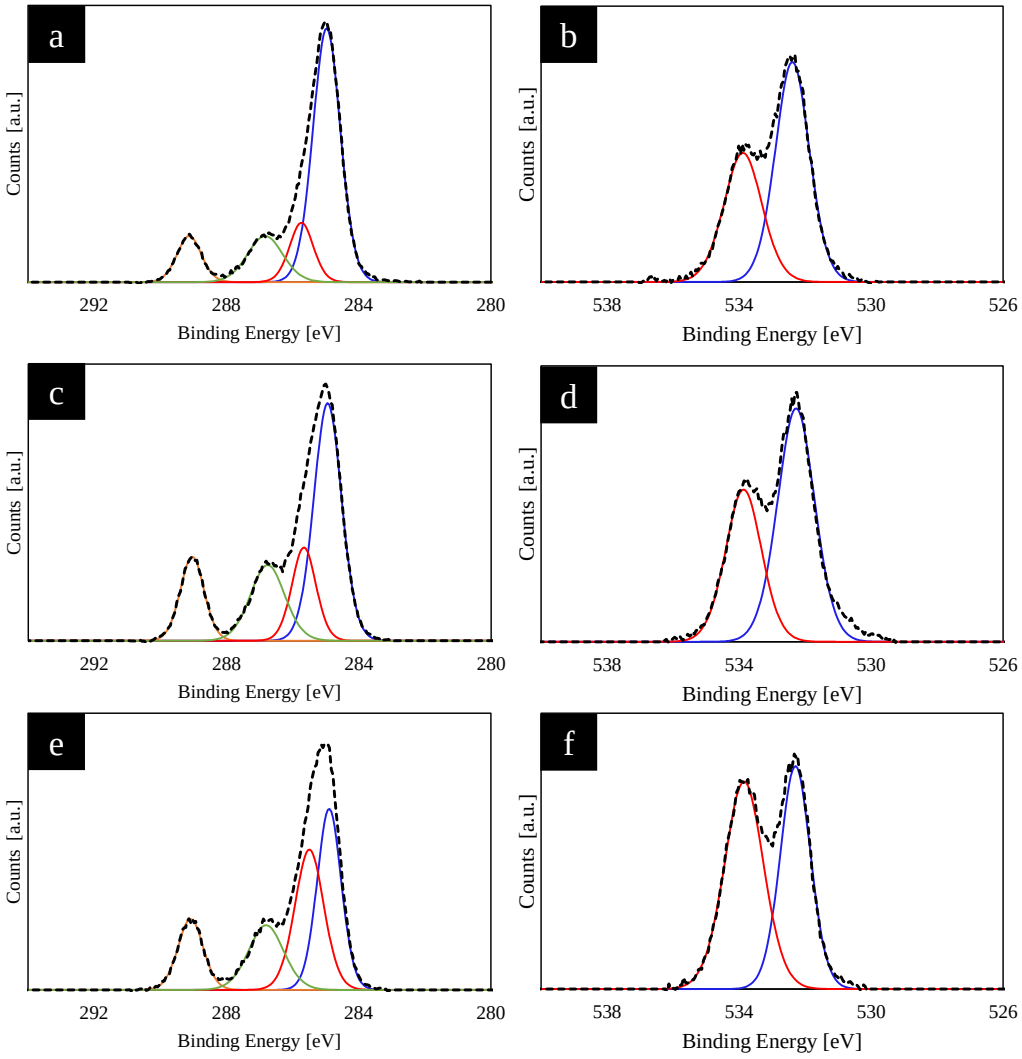

Figure 4.12 XPS high resolution spectra spin coated surfaces created from (a, b) 25PS75PMMA_1500, (c, d) 25PS75PMMA_750 and (e, f) 25PS75PMMA_375 solutions.

Charge correction was once again applied by way of the C-C aliphatic peak to 285.0 eV. As the number of microspheres/ml increase, so too does the intensity of the C-H aliphatic carbon peak at 285.0 eV, whilst the contribution from the O-C peak at 533.8 eV decreases. Quantitative analysis of atomic concentration (%) for O 1s and C 1s is recorded in Table 4.4. Broadly speaking, all augmented substrates contain the four carbon environments associated with PMMA alongside the O 1s doublet.

Table 4.4 XPS derived % atomic concentration values of both C 1s and O 1s contributions for augmented polymer demixed 25PS75PMMA blends.

Sample Type	Sample	% C 1s	% O 1s	% C 1s	% O 1s
25PS75PMMA_ 1500	1	80.28	19.72	80.13 ± 1.59	19.87 ± 1.59
	2	81.64	18.36		
	3	78.47	21.53		
25PS75PMMA_ 750	1	80.26	19.74	78.45 ± 2.96	21.55 ± 2.96
	2	80.06	19.94		
	3	75.04	24.96		
25PS75PMMA_ 375	1	78.52	21.48	77.28 ± 1.10	22.72 ± 1.10
	2	76.89	23.11		
	3	76.42	23.58		

As indicated previously, PMMA has an average % atomic concentration of 76% C 1s and 24% O 1s. Augmented substrates show a mean % atomic concentration for O 1s ranging from 19.9% up to 22.7%. When compared with the previous 25PS75PMMA surface and polymer controls, all substrates display a typical PMMA chemistry. Slight fluctuations within the sample may be indicative of surface contamination or a change in the orientation of the polymer chain[135].

4.5 Biological Assessment of Augmented Polymer Demixed Surfaces

Representative platelet interactions for each of the microsphere augmented substrates are shown in Figure 4.13, using blood from Healthy Donor 1 (Table 4.2). These samples were run individually as one-off analyses to assess the feasibility of the substrates for use in the DPFA.

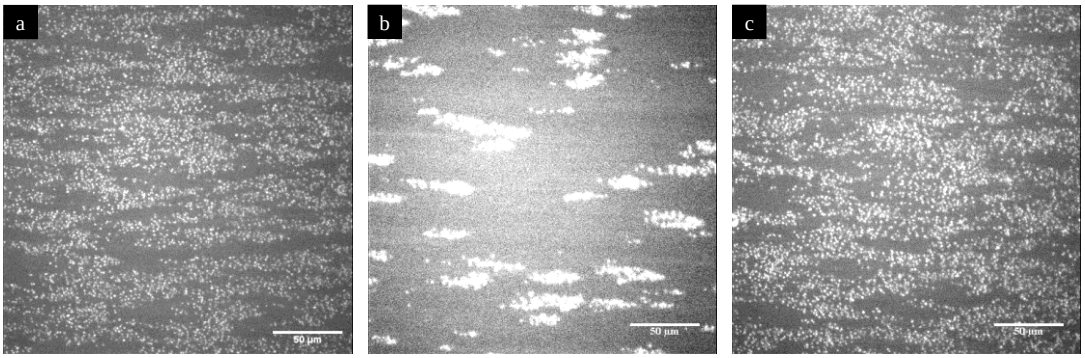

Figure 4.13 Time lapse frame 120/120 images for platelet interactions on (a) 25PS75PMMA_1500, (b) 25PS75PMMA_750 and (c) 25PS75PMMA_375 spin coated surfaces. Scale bar 50µm.

A visual inspection of these images suggests that platelet activity is more pronounced on the 25PS75PMMS_375 surface (Figure 4.13(c)). Final frame analysis confirmed that 25PS75PMMS_375 had the highest platelet coverage of 24.8%, followed by the 25PS75PMMA_750 with 6.8% with the 25PS75PMMA_1500 surface producing a surface coverage of 26.2%. As indicated earlier, AFM characterisation of the 375 microspheres/ml films showed them to have a very similar topography of the original 25PS75PMMA surfaces and as the key objective here is to develop a DPFA substrate which has a more pronounced nanotopography, it was decided not to pursue this surface in further blood studies.

As the 25PS75PMMA_750 and 25PS75PMMA_1500 surfaces showed differences in resulting topography, both were further investigated in respect to their reproducibility (n = 5) in platelet function measurements using Healthy Donor 1 blood (Table 4.2). Figure 4.14 (a-e) shows the 120/120 image frame in the time lapse sequence for each 25PS75PMMA_750 sample with the corresponding quantification data provided in Table 4.5.

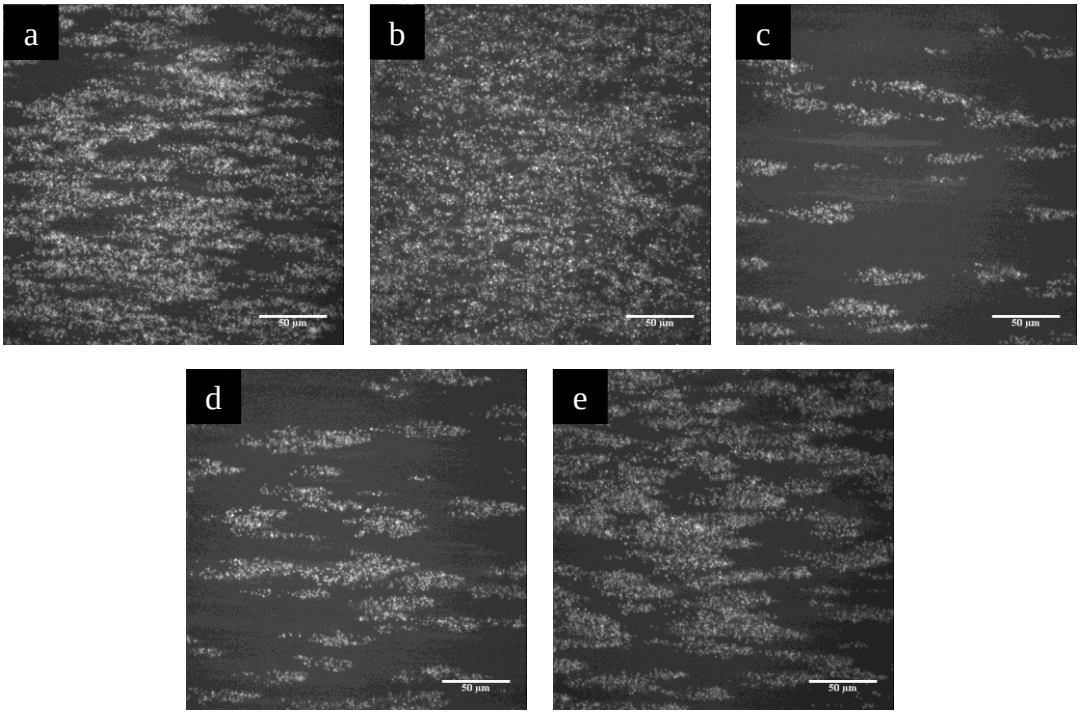

Figure 4.14 Fluorescence micrograph images at the 120/120 frame in the times lapse sequence of whole blood DIOC6 labelled platelets adhered to the 25PS75PMMA_750 spin coated surface of each of 5 replicates (a – e). Scale bar 50 µm.

Visual inspection indicates a high level of platelet adhesion on three out of five replicates (a, b and e) with (c) and (d) having a reduced level of interaction, as compared to the standard 25PS75PMMA thin film substrate. The average surface coverage value of 19.08% is the highest of any sample studied to date. However, the large value for the standard deviation (12.6) confirms the sample to sample variation.

The corresponding 120/120 image frames in the time lapse sequence for the 25PS75PMMA_1500 sample set (n = 5) are provided in Figure 4.15 (a)-(e), with the corresponding quantification data provided in Table 4.5.

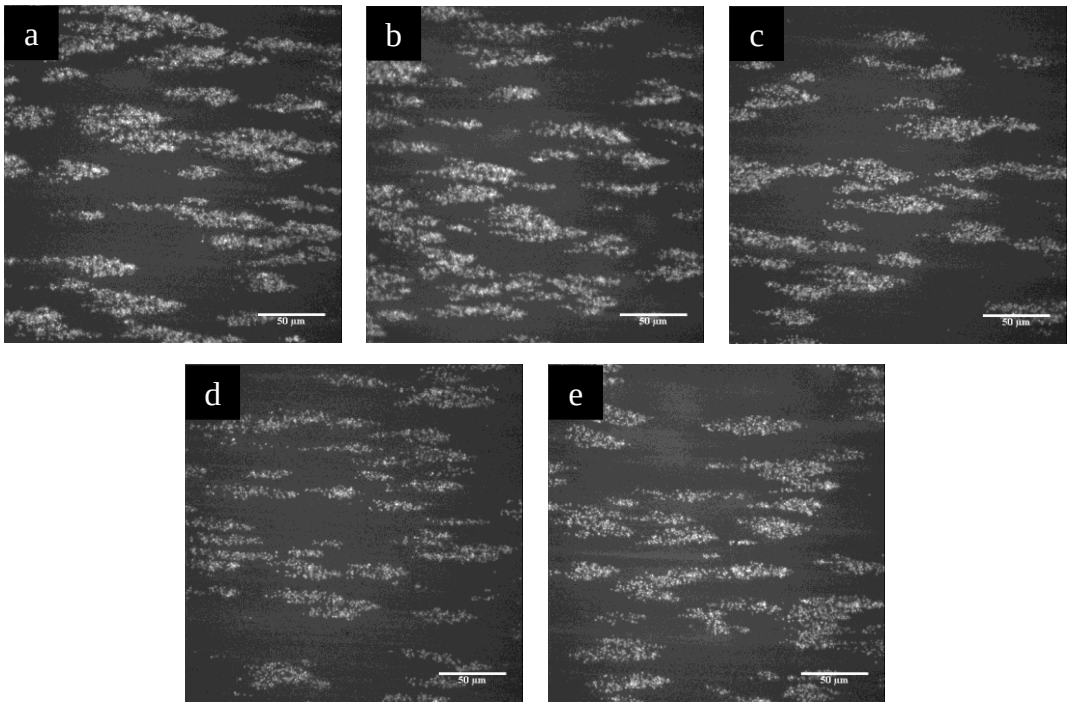

Figure 4.15 Fluorescence micrograph images at the 120/120 frame in the times lapse sequence of whole blood DIOC6 labelled platelets adhered to the 25PS75PMMA_1500 spin coated surface of each of 5 replicates (a – e). Scale bar 50 µm.

Platelet interaction in this substrate, can be said to follow similar trends as the base 25PS75PMMA substrate. Analysing the mean and standard deviation of the replicate studies, show the 25PS75PMMA_1500 substrates have a lower overall % of surface coverage alongside a significantly lower standard deviation. This would suggest that this surface may be more reproducible in terms of a diagnostic application.

Table 4.5 Quantitative image analysis data of average % surface coverage and standard deviation for spin coated surfaces created with 25PS75PMMA augmented with 750 and 1500 50 µm PS microspheres/ml.

Solution	Sample	% Coverage	Average	Standard Deviation
25PS75PMMA_750	1	32.50	19.08	12.59
	2	28.65		
	3	3.65		
	4	8.37		
	5	22.22		
25PS75PMMA_1500	1	16.76	10.88	4.11
	2	13.00		
	3	10.34		
	4	6.82		
	5	7.47		

However, the main goal here is to fabricate a surface with topography which is capable of eliciting a platelet response across the whole area, to yield as close to 100% surface coverage as possible. From this perspective, it was determined that the similarity between the 25PS75PMMA surface coverage of 13.89% and the 1500 microspheres/ml substrate coverage of 10.88% meant that moving forward focus was put on the base 25PS75PMMA substrate alongside the most different substrate, in this instance 25PS75PMMA_750.

In order to better understand the nature of the 25PS75PMMA_750 surface microstructure in more detail, five 40 µm x 40 µm areas across the 800 µm long flow channel of the DPFA device (left, mid-left, centre, mid-right and right areas) on each of the 5 replicate samples were examined by AFM to give a total of 20 areas analysed in all. Figure 4.16 shows representative 40 µm x 40 µm 3D AFM images samples of the left, mid-left, centre, mid-right and right areas of the distance.

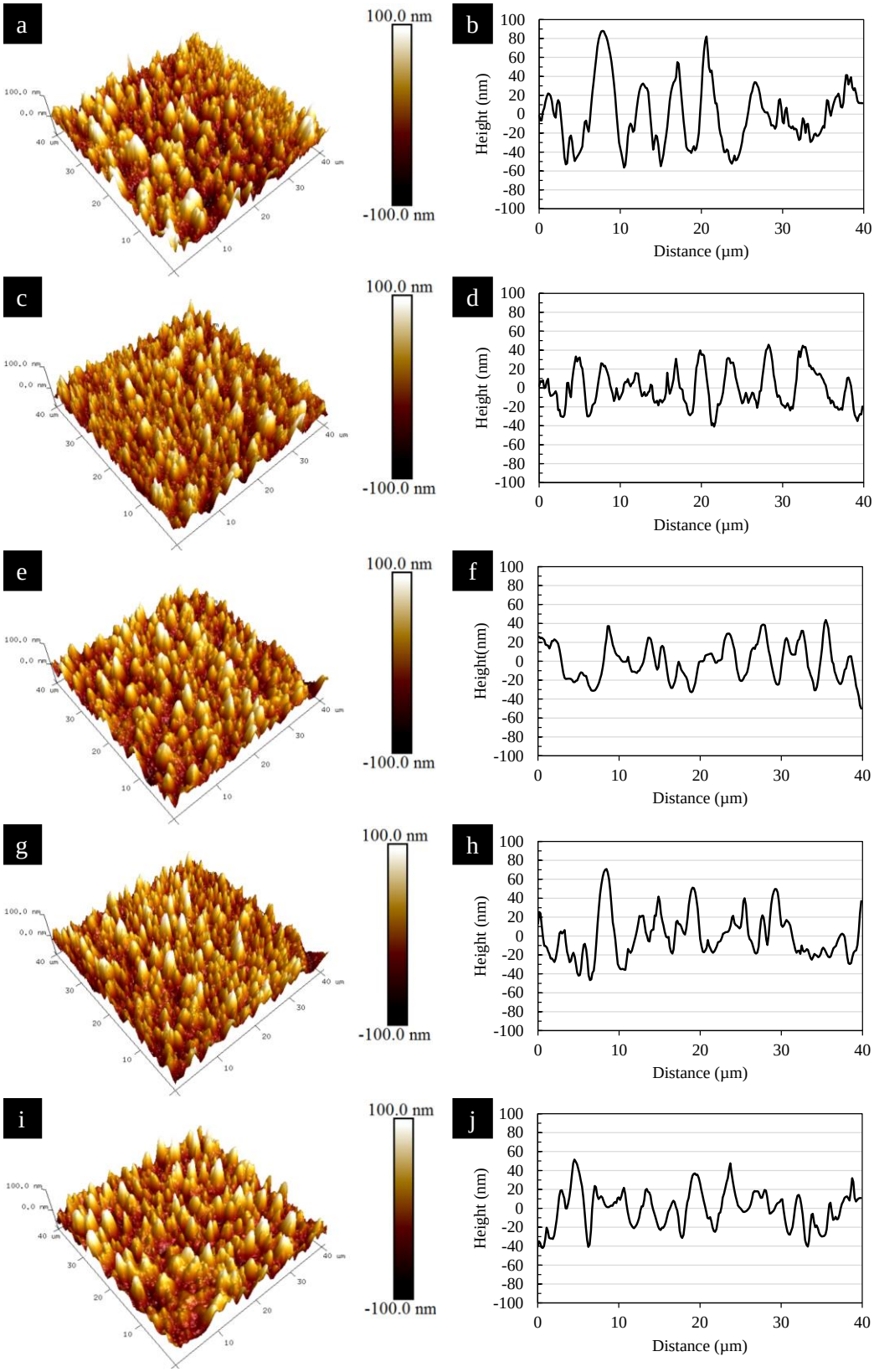

Figure 4.16 40 µm x 40 µm 3D AFM images of the nanotopography at the (a) left, (c) mid-left, (e) centre, (g) mid-right and (i) right sections of the channel (colour scale ± 100 nm) with corresponding line profiles generated from the x-y midpoint.

Surface roughness reported as R_a and R_q values, for the 25PS75PMMA_750 surface along with data for the standard 25PS75PMMA substrate and a 100% PMMA spin coated thin film are provided as averages in Table 4.6.

Table 4.6 AFM derived mean (n = 20) surface roughness (R_a) and root mean square roughness (R_q) values calculated from AFM data along the 800 µm channel study. Data for a spin coated 25PS75PMMA and 100% PMMA substrates included for comparison.

	100% PMMA		**25PS75PMMA**		**25PS75PMMA_750**	
	Ra (nm)	**Rq (nm)**	**Ra (nm)**	**Rq (nm)**	**Ra (nm)**	**Rq (nm)**
Average	14.12	21.58	26.06	32.82	19.46	24.45
Standard Deviation	5.19	6.24	2.69	3.36	1.89	2.22

The data for the 25PS75PMMA_750 surface returns an average $R_a = 19.46 \pm 1.89$ nm and $R_q = 24.45 \pm 2.22$ nm compared to values of $R_a = 26.06 \pm 2.69$ nm and $R_q = 32.82 \pm 3.36$ nm for 25PS75PMMA and $R_a = 14.12 \pm 5.19$ nm and $R_q = 21.58 \pm 6.24$ nm for the 100% PMMA spin coated sample. Surface roughness parameters show that there is a statistically significant difference ($p = 0.05$) between the AFM data obtained for each sample. These data indicate that the inclusion of the PS in PMMA has a moderate effect on the overall surface roughness but does influence the nature of the topography that results. Whereas, the spin coated 100% PMMA surface (Figure 4.4 (a)) has a very regular and relatively smooth microstructure, introduction of 25% PS creates the micron scale structure overlaid with nanosized features (Figure 4.3). Introduction of the PS microspheres maintains the general polymer demixed micro/nano-scale surface structure but with slightly more pronounced nanofeatures.

4.6 Dynamic Evaluation of Platelet Behaviour

To enhance the evaluation of platelet function on the PS/PMMA spin coated polymer demixed surfaces, their dynamic interactions were assessed using a bespoke autologous platelet algorithm, which has been modified slightly from that used within the DPFA system operating with an immobilised vWF substrate. This process is undertaken using an extended 1000-frame image stack that includes a capture period prior to the on-set of thrombus formation in the time lapse video capture. In this way, both initial and later stage vWF-platelet interactions were measured using Donor 1 blood. As a direct comparison, the Donor 1 blood was also tested on the immobilised standard DPFA assay substrate (Figure 4.17).

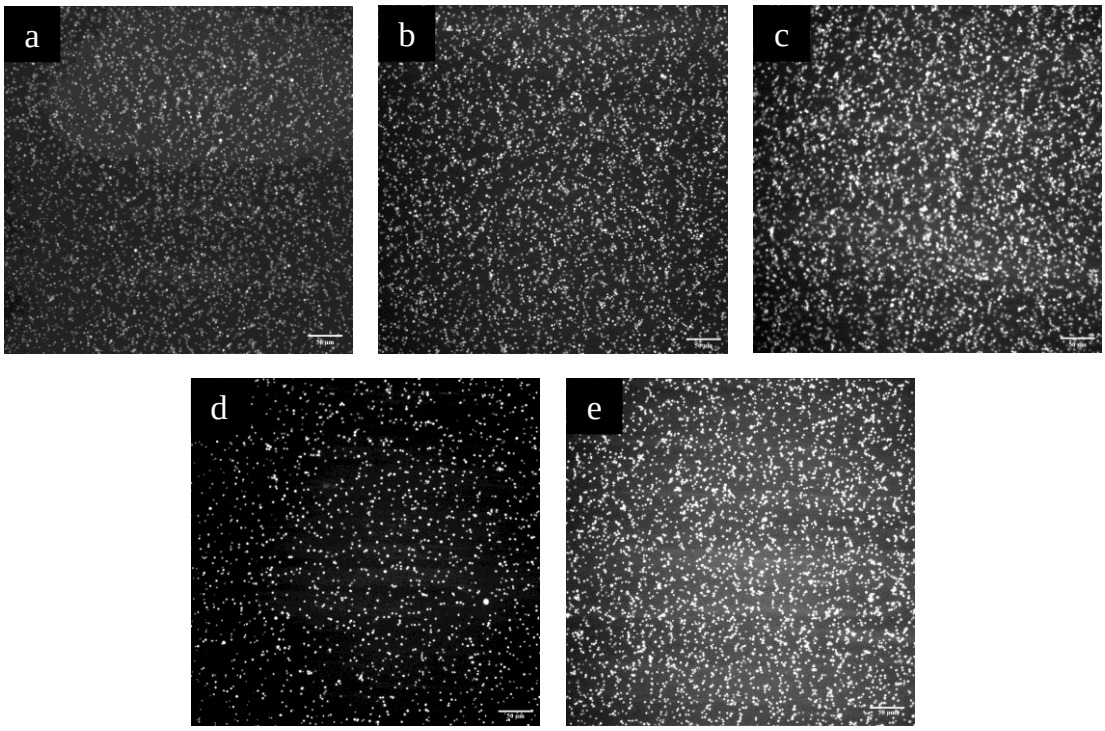

Figure 4.17 Fluorescence micrograph images at the 600/600 frame in the standard protocol sequence of whole blood DIOC6 labelled platelets adhered to the control, a vWF immobilised surface of each of 5 replicates (a – e). Scale bar 50 µm.

Several dynamic parameters were analysed by way of real-time tracking of individual platelets within the autologous algorithm, with the results shown in Table 4.7.

Table 4.7 Dynamic platelet parameter values and blood indices derived for the algorithm analysis for Donor 1 blood on each spin coated surface, with inclusion of the data from the standard immobilised vWF assay included for comparison (n = 5).

Dynamic Parameters	Immobilised vWF	25PS75PMMA	25PS75PMMA _750	25PS75PMMA _1500
Ntracks	4985 ± 1009	129 ± 49	527 ± 695	143 ± 70
Fraction of Stably Adhered	0.45 ± 0.02	0.76 ± 0.01	0.73 ± 0.05	0.74 ± 0.04
Mean Translocating Distance (μm)	4.64 ± 0.29	2.26 ± 0.29	2.50 ± 0.63	2.97 ± 0.68
Mean Translocating Velocity (μm/s)	2.41 ± 0.35	1.23 ± 0.81	1.69 ± 0.76	1.63 ± 0.77
Adhesion Rate ($x10^3$ s^{-1})	19.12 ± 4.88	0.50 ± 0.21	2.52 ± 3.52	0.60 ± 0.30
Detachment Rate (s^{-1})	0.29 ± 0.12	1.06 ± 1.03	0.37 ± 0.47	0.78 ± 1.32
Fraction Sticking	0.46 ± 0.10	0.37 ± 0.12	0.35 ± 0.14	0.31 ± 0.10
Platelet Indices*				
Platelet Count ($x10^3$/μl)	217	217	217	217
Haematocrit (%)	44.2	44.2	44.2	44.2
vWF (IU/dL)	47.6	47.6	47.6	47.6

** No standard deviation values are reported for the platelet indices due to a single blood sample having been used for this analysis to eliminate a potential source error.*

The data for the main dynamic parameters is shown in Figure 4.18. In comparison with the standard DPFA substrate control, the number of platelets (Ntracks) and the platelet adhesion rate are substantially lower. The fraction of platelets sticking on the spin coated PS/PMMA polymer demixed substrates is similar to each other and also to the control. However, the fraction of stably adhered platelets is similar amongst spin coated substrates but differs significantly from the control. Overall, the platelets appear to travel more slowly and over shorter distances on the synthetic surfaces, as compared to their behaviour on the immobilised vWF substrate.

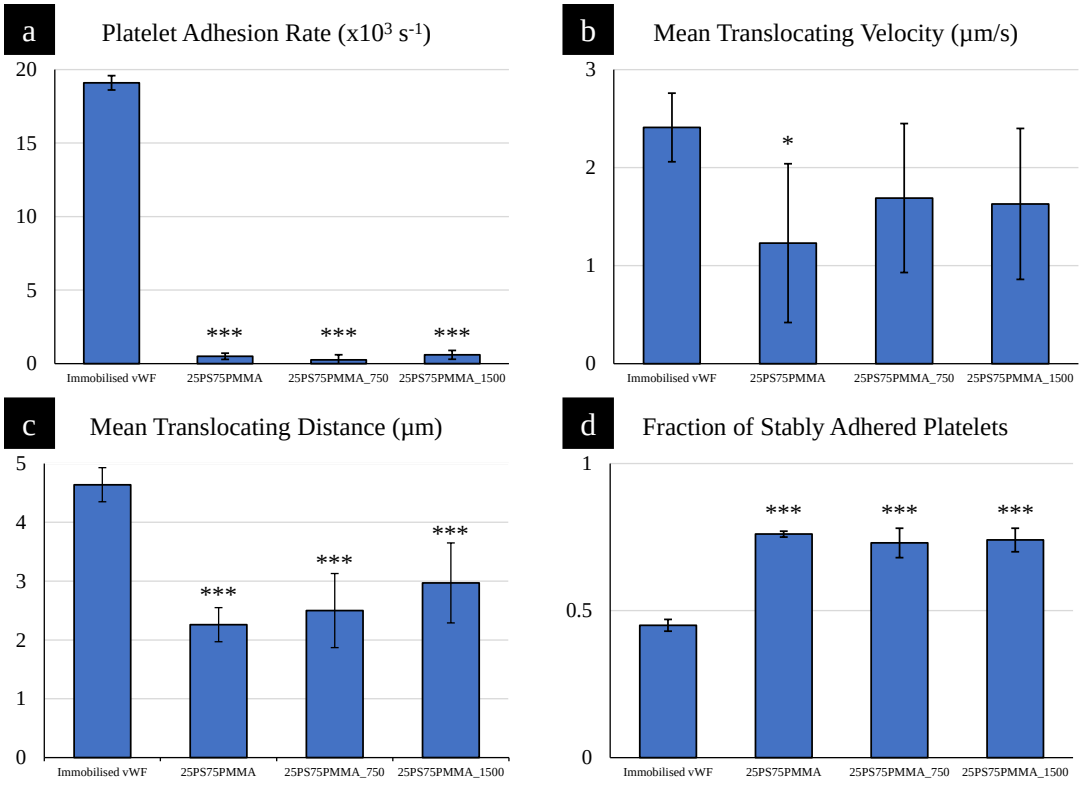

Figure 4.18 Graphical representation of four dynamic parameters, complete with statistical difference compared against the control using immobilised vWF (left). P value = 0.05.

4.7 Discussion

The goal of the work reported in this chapter was to identify the surface characteristics (both physical and chemical) of spin coated PS/PMMA polymer demixed surfaces that provide a means to direct their interaction with platelets in flowing blood at arterial shear (1500 s^{-1}) in the context of the requirements of the DPFA system. As indicated previously, the blood glycoprotein vWF is required to facilitate platelet adhesion and aggregation *in vivo*, i.e. as per the process that occurs in the event of damage to the endothelium. Hence, if a positive platelet response is observed from the PS/PMMA polymer demixed surfaces, then this is due to their capability to entrap vWF from flowing blood. Moreover, the environment in which this occurs also supports the subsequent uncoiling of the vWF which is essential to allow it to bind platelets. In this regard, the 3% 25PS75PMMA demixed system used as the starting point for this work has been shown to support platelet interactions by the direct vWF entrapment, uncoiling and binding[15]. Bishop *et al.* completed inhibition studies that involved use of the vWF-inhibiting 5D2 antibody and the platelet GP1b binding site inhibiting AK2 antibody which confirmed that no platelet activity occurred without the required binding conditions being met[14].

Optical analysis of thin film coatings fabricated from spin coating of the 25PS75PMMA polymer demixed blend solution in chloroform onto glass slides show two distinct patterns of the PS distributed in the PMMA: (i) honeycomb-like shapes in the centre of the slide and (ii) striations present radiating outwards. As long ago as 1900, Bernard Marangoni[136] observed hexagonal patterns on thin film layers and attributed the effects to buoyancy-driven convection associated with gradients in surface tension[137]. More recently, Mokarian-Tabari *et al.*[138] have investigated the morphology of thin films prepared using solutions of PS/PMMA blends and concluded

that high evaporation rates cause instabilities as the film forms, resulting in the formation of Marangoni type cells. In the context of spin coating, a surface tension gradient forms due to the differing rates of evaporation of the chloroform solvent between the air-liquid interface and the bulk of the solution. As the film thins under the centrifugal force associated with the spinning substrate, the instability increases causing wave-like changes in the film that result in sudden fragmentation of the insoluble component (PS) into numerous lateral areas[139] that are then isolated when the PMMA solidifies due to loss of solvent. Hence, the formation of an attendant surface microstructure is due to the resulting distribution of the PS in the PMMA.

The topographies that are created as a result of spin coating of polymer blends have been heavily researched for a range of biomedical applications[19,140,141], including the study of platelets thereon[29,142]. As indicated above, the specific topography of the spin coated 25PS75PMMA surface is deemed to be a consequence of centrifugal force in tandem with the demixing of the PS and PMMA in chloroform. AFM analysis of this surface reveals that it comprises micron-scale features overlaid with a nano-scale topography. The 25PS75PMMA features range from -50 nm and +70 nm in height and FWHM values anywhere between 100 nm to 4µm and these values are consistent with measurements reported in other studies[115]. D'Sa *et al.* reported average feature heights for a thin films spin coated from a 1% 25PS75PMMA solution as 27.7 ± 4.4 nm[115] with the difference in results reported here deemed to be due to the concentration of polymer solution employed. It is known that nature and scale of the topographical features created in this way can be linked to the PS weighting in the demixed formulation. Polymer controls of 3% 100% PS and 100% PMMA in chloroform were used to identify the single topographical traits of each polymer. 100% PS spin coated films yielded a pitted landscape with pits reaching a depth of -7.50 nm. In contrast,

100% PMMA thin films portrayed a surface with protrusions between 1-4.5 nm high with FWHM values of approximately 10 nm. From this, it can be understood why a 50PS50PMMA blend produces a mixed nano-island/pit topography[133], whereas if PMMA is over this 50% threshold, a landscape of primarily islands are created[14].

From XPS analysis of the surface chemistry, the spin coated 25PS75PMMA thin film was found to be solely that of PMMA within the uppermost 5-10 Å limit of the technique with no evidence of PS at the associated detection limits of (ca. 0.1% atomic concentration). The high-resolution spectra for O 1s and C 1s regions correspond directly to those determined by Beamson and Briggs[127] for thin film PMMA in respect to the occurrence of four distinct carbon and two oxygen environments. At a theoretical level, the published literature would suggest that the component with a lower surface energy should enrich the surface[143], which in this case it would mean that PS should be detected. However, the results obtained here can be explained by the thin film not reaching thermodynamic equilibrium[121] due to the nature of the spin coating process involved. In this case, the polymers in question have insufficient time to reach equilibrium such that the resulting chemistry is attributed to other factors, namely; substrate type[118], film thickness[144] and solvent volatility[145]. This also applies to the solvent cast 25PS75PMMA substrate, whereby the volatility of the chloroform results in a PMMA surface chemistry, due to equilibrium not being reached before evaporation. Further evidence for these effects are indicated by previous studies on physical and chemical characteristics of polymer demixed films[146] which illustrate the same resulting PMMA dominant surface chemistry as presented in this work. This PMMA enrichment of the uppermost surface can, in the main, be described by way of solvent effects[119]. PMMA has a significantly higher solubility in chloroform than PS and therefore under centrifugal force, the latter component is more

quickly diminished from the moving solution, forming a base layer which is subsequently coated with the still-fluid PMMA before total solvent evaporation leading to solidification. Tanaka *et al.*[144] have also observed this behaviour for PS/PVME blends. Ton-That *et al.* have explained how a PS/PMMA blend in chloroform segregates into a bilayer system consisting of two distinct PMMA and PS phases[146]. These distinct layers then undergo phase separation by the solvent gradient mechanism[147].

The regularity or otherwise of the PMMA dominant surface chemistry across the 25PS75PMMA thin film was analysed. A large zonal analysis of the 25PS75PMMA thin film system, comprising an 80-spot XPS study[14], reports an average % atomic concentration of 25.03 ± 0.6% for O 1s and 74.97 ± 0.6% for C 1s with no statistically significant change in values across the regions analysed.

As expected from previous studies, the 3% 25PS75PMMA spin coated surfaces exhibit a positive platelet response that is a consequence of topographical features and conditions being suitable for entrapment of vWF from whole blood that is flowing under arterial shear[108]. PMMA in its native form is deemed to be bioinert, however, when its surface is modified this material has been reported to support both cell[115,148,149] and platelet[14,15,108] response, as included in previous studies. The nature and magnitude of this response is influenced by the surface structures[150]. However, there is conflicting evidence regarding the optimum topography to improve platelet adhesion. Koh *et al.* explored the effect of topography on platelet adhesions and reported that the optimal range of pillars on a surface needed to be between 300 nm and 800 nm in height, 100 – 200 μm wide and with interspatial distances of <200 nm[142]. Alternative polymers like poly(lactic-co-glycolic acid) (PLGA) have also been shown to support platelet adhesion when both pristine and nanotextured surface are

used[151]. However, the data obtained from this previous study showed that irregularities occurred that were deemed to be due to the carboxylic acids groups within the graphite substrate that is formed as a result of the surface processing. Hence, it was not deemed to be appropriate for the work carried out here

Platelets can be seen to adhere in linear formations (Figure 4.8) suggesting that during the early stages of blood flow, vWF multimers adhere to spin coated 25PS75PMMA substrate. Platelet adhesion levels are seen to increase by 8.18% from frames (a) – (d) with a net increase in coverage and this is nearly doubled by an additional 7.21% surface coverage that occurs between the (d) 180 and (e) 240 second time points. The nature of the interaction of this time period suggests that a both platelet-platelet and platelet-surface interactions are involved, with the latter time points focusing on platelet-platelet interaction and thrombus growth[151]. The long, string-like nature of vWF means that it is highly responsive to shear forces. It is known that secreted uncoiled vWF chains are 100-1000 μm long when they initially bind to the surface of a damaged endothelium, surface *in vivo*. This would then suggest that the vWF that has attached to the 25PS75PMMA substrate polymer surface has quickly uncoiled in a way that exposes GP1b receptors to provide the correct orientation for platelets to subsequently adhere.

Although the 3% 25PS75PMMA spin coated surfaces are directing platelet adhesion, the nature of the variation introduced by the fabrication process indicates that they do not offer the reproducibility necessary to ensure clinical diagnostic accuracy as part of the DPFA. Specifically, although they entrap vWF leading to subsequent patient-specific platelet interactions, there is variation across the flow region that is greater than that seen for the current immobilised vWF substrates. This observation is consistent with that of Minelli *et al.* whose PS/PMMA spin coated

surfaces also adhered platelets after exposure to (static) whole blood. However, overall coverage was sporadic with most platelets found to be adhered to larger surface features[133].

In a bid to create a uniform and reproducible surface topography that can direct a more consistent platelet response, PS microspheres of 50 μm diameter were added to the 3% 25PSPMMA spin coating solution. It is proposed that introduction of these microspheres will disturb the centrifugal fluid mechanics during spin coating in a way that better regulates the micro/nano-scale topographical features produced. The principle of operation here is similar to that employed previously by Ton-That *et al.*[123,142]. Consideration has also been given to not introducing a third system to the blend and keep the percentage PS as close to the standard 25% as possible by adding small quantities in the range +375 to +1500 microspheres/ml of 25PS75PMMA spin coating solution.

Optical microscopy analysis of surfaces with +375 microspheres/ml showed no discernible change being seen at this scale and also had little or no effect on the surface topography beyond that of the standard 25PS75PMMA system as seen in the associated AFM data. Increasing this number to 750 microspheres/ml does have a positive effect on the surface features with both regularity and size being affected. The average surface features are in the height range 40-50 nm with FWHM of approximately 1 μm. Increasing the number of microspheres further to +1500 microspheres/ml, produces coatings with surface features which are more regularly distributed across the area analysed by AFM (10 μm x 10 μm). The average feature heights are now in the range 20 nm to 50 nm and FWHM is approximately 500 nm. As was the case for the standard 25PS75PMMA films, the surface chemistry is still deemed to be that of PMMA only, as determined by XPS analysis. However, the C 1s

regions do differ slightly in terms of the relative intensities of the four components which is suggestive of small differences in polymer orientation on the surface. Increase in the intensity of the carbon peak at 285.0 eV, coincides with a decrease in the oxygen peak at 533.8 eV. This may be attributed to an increase in the PS microspheres therefore increasing the C 1s contribution, or it may be a case of a change polymer chain orientation[152].

All the spin coated surfaces produced from 25PS75PMMA solutions augmented with 50 μm PS microspheres have been shown to be capable of vWF entrapment and to direct the uncoiling of same, to directly facilitate platelet adhesion. The surfaces created with 375 microspheres/ml shows similar surface coverage to that seen for samples created with standard cast solutions. However, in the case of the surfaces with the topography resulting from the presence of 750 microspheres/ml, the average surface coverage by platelets is greater than both the 25PS75PMMA and 25PS75PMMA_375 surfaces, with distribution more evenly occurring across the whole region imaged. Some sample to sample (n = 5) variation in platelet surface coverage was observed for this surface type. Additional checks indicated that the R_a and R_q values were very similar for all three areas measured in each of five samples. Notwithstanding the changes to the surface topography, the corresponding 25PS75PMMA_1500 samples show a platelet response that is again like the standard 25PS75PMMA surface. This suggests that not only is the topographical feature size important, but so also is the regularity of its distribution across the region of interest. Based on these findings, it is the 25PS75PMMA_750 surface features that are deemed to be an improvement on the provision of a polymer demixed surface that is capable of entrapping autologous vWF for use in the DPFA device, although it is recognised that its reproducibility still needs to be further improved.

Although the 25PS75PMMA_750 surface appears to provide superior amounts of platelet adhesion compared to 25PS75PMMA, this is only based on the field of view coverage at the 120/120 time point. Hence, it is not clear if this behaviour is comparable with that observed on the standard immobilised vWF substrate. In the case of the latter analysis, a computer algorithm has been developed to better analysis the dynamic behaviour of the platelets which is applied to real-time image stacks to analyse number of platelets, platelet velocity and even distance travelled[59]. This algorithm has been applied to each of the spin coated surfaces, alongside a set of control surfaces (immobilised assay) and statistical comparisons were made. A minor modification has been made to the original code to allow for more accurate calculation of platelet attachment and detachment rates (k_{on}, k_{off}) on the synthetic surface[107]. Based on interpretation of the 120/120 frame image it may be assumed that the standard, immobilised vWF assay is superior in terms of the field of view platelet coverage, thereby suggesting that this surface is better at capturing platelets. However, it is important to also consider the dynamic behaviour of platelets on the spin coated PS/PMMA polymer demixed surface in order to evaluate how the topography and surface chemistry can entrap vWF from flowing blood.

Statistical analysis of the dynamic parameter data from the various surfaces showed significantly lower adhesion rates for all spin coated surfaces when compared to the immobilised vWF substrate. In a previous study, type O blood donors (n = 33) were tested on the immobilised vWF surface and an average value of 273 ± 130 Ntracks was recorded[59]. However, the type O Donor 1 blood used here had a higher average Ntracks of 4985 ± 1009, a value which was on average ~18 times greater than that recorded for the synthetic surface. However, the actual values for the spin coated PS/PMMA demixed surfaces are closer to the published results. The main reason for

this difference may be attributed to the fact that the control surface has vWF in abundance, and in the correct conformation to adhere platelets instantaneously. By contrast, the spin coated surfaces require time for the vWF from the (Donor 1) flowing blood to accumulate on the surface and for it to subsequently uncoil before platelet adhesion can take place. Critically, Ntracks is a parameter which presumes that platelet interactions happen independently, and since it is evident from the fluorescent images that this is not the case for some of the spin coated surfaces, in that clumping due to platelet-platelet interactions is present, this may explain the large deviation of the 4985 ± 1009 value recorded for Donor 1 (Table 4.7) compared to the previously published blood group O results.

The velocity at which platelets travel across the 25PS75PMMA (1.23 ± 0.81 μm/s) is about 50% of that seen in the immobilised vWF assay data (2.41 ± 0.35 μm/s). Interestingly, this value does not change to any great extent for the PS microsphere augmented surface. The mean translocating distance travelled by platelets reduces from 4.64 ± 0.29 μm for the immobilised vWF control to 2.26 μm for 25PS75PMMA and 2.97 μm for 25PS75PMMA_1500. The relevant data from the published large cohort Type O donor study (n = 33) shows an average velocity of 4.60 ± 2.10 μm/s and a mean translocating distance of 5.77 ± 1.80 μm [59]. Donor 1 (type O) values on the immobilised vWF control also show values close to this range. Platelet translocating speed and distance on spin coated PS/PMMA surfaces appear to increase with introduction of PS microspheres, but there is no significant statistical difference between these substrates.

The control surface had significantly less (0.45 ± 0.02) fraction of stably adhered platelets, i.e. those that have travelled less than 3 μm, when compared to each of the spin coated PS/PMMA polymer demixed surfaces, range 0.73 – 0.76. This is

consistent with the behaviour observed for the translocating distance of platelets which was also reduced on the same surfaces.

There are no previous literature reports on these types of algorithm-derived dynamic platelet parameters in respect to polymer demixed thin films. Therefore, more studies are required to enable the validity of such datasets to be confirmed. However, it can be stated that as the vWF protein from flowing blood is indeed entrapped naturally by the PS/PMMA topography, in a manner that causes attachment mechanisms, that may not always be robust enough to withstand arterial shear thereby causing a higher detachment rate on the polymer demixed surfaces compared to those employing immobilised vWF.

In summary, the fabrication of spin coated polymer demixed thin films on glass slides that are capable of entrapping autologous vWF in a form that can induce subsequent platelet interactions within the same patient blood sample, has been completed. These substrates show promise for use within a dynamic assay system; however, reproducibility of this surface is a limiting factor in its clinical utility. In an aim to improve this, the inclusion of varying numbers of 50 μm PS microspheres in the 25PS75PMMA blend was explored and showed a means of regulating the topographical features without changing the attendant surface chemistry. In particular, the addition of +750 microspheres produces highly reproducible surface features (50 μm high; 1 μm FWHM) that entraps vWF in a manner that provides for an increased coverage across the field of view. However, there are still limitations to this surface and so within the next chapter we explore the manipulation of topography on a grander scale, looking at spin coating conditions to modify features and regularity of same, whilst continuing with blood studies to assess platelet adhesive properties to surfaces. The algorithm-based dynamic parameter assessment of platelet activity provides

additional insight into how the vWF-platelet interactions differ on the surfaces studied here.

5. Influence of an Ambient Atmospheric Pressure During Spin Coating on Polymer Demixed Surface Features

5.1 Introduction

The work presented in the previous chapter shows that the topography of PS/PMMA polymer demixed thin films can be modified by way of introducing uniform microspheres into the casting solution while maintaining the same (PMMA only) surface chemistry. This effect has been attributed to a change in fluid dynamics that occur within the solution and the centrifugal forces that act during its distribution across the substrate in advance of solvent evaporation and associated coating formation in the presence of a positive pressure of nitrogen gas. To further understand the role that the gaseous environment and pressure has on these attendant surface properties, spin coating of the PS/PMMA solutions has been carried out under an ambient (air) atmospheric pressure[153].

These spin coated thin films have been examined by optical microscopy (OM), atomic force microscopy (AFM) and x-ray photoelectron spectroscopy (XPS). Platelet interactions thereon have been investigated in the DPFA system using blood flow at arterial shear rate (1500 s^{-1}) from both a single donor and using different blood types to evaluate both inter- and intra-assay variation.

5.2 Properties of 25PS75PMMA_air Polymer Demixed Surfaces

Optical micrographs from the centre and edge of the 25PS/75PMMA polymer demixed thin films created by spin coating in air at atmospheric pressure (25PS75PMMA_air), are shown in Figure 5.1. As observed previously, there are striations and honeycomb patterns present that are indicative of the PS distribution within PMMA that result from the centrifugal forces experienced during the spin

coating process. However, whereas these images show feature that are similar to those observed for the nitrogen-spun systems (Figure 4.1), they are more well defined and evenly distributed here.

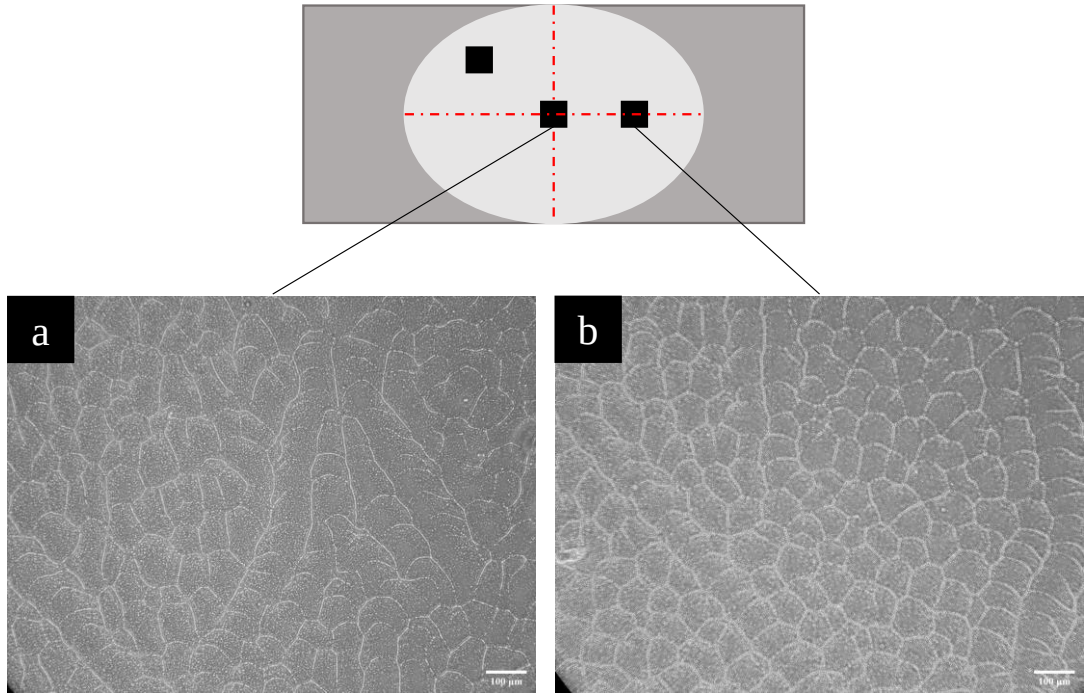

Figure 5.1 Optical micrographs of (a) centre and (b) edge areas for a spin coated 25PS75PMMA_air substrate. Scale bar 100 µm.

Notwithstanding the slight differences in PS distribution observed here, it is not possible to make a definitive statement regarding the role of air at atmospheric pressure versus nitrogen at a positive pressure. Figure 5.2 shows 40 µm x 40 µm 3D plots and corresponding line profiles for 25PS75PMMA_air substrates at three distinct areas across the slide surface.

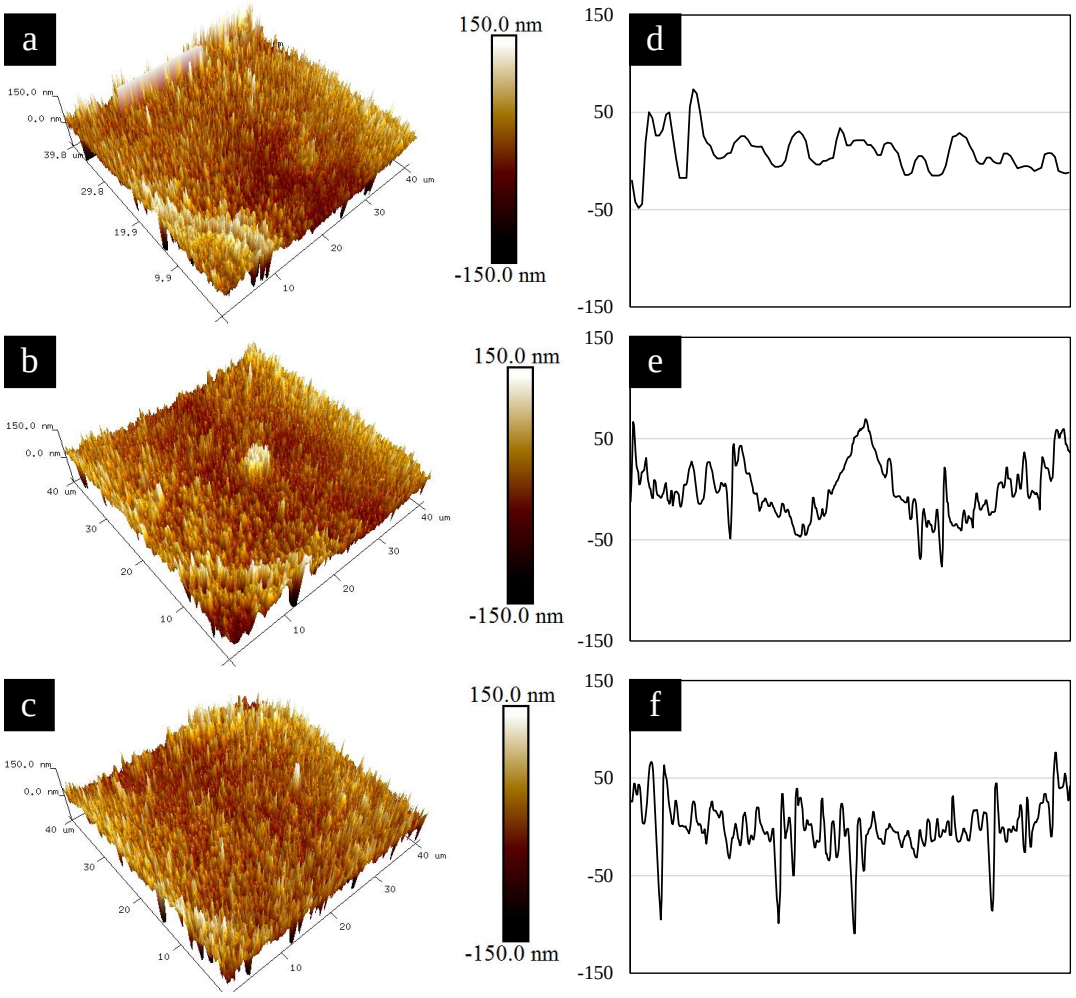

Figure 5.2 40 µm x 40 µm 3D pseudo-colour AFM images at (a) edge, (b) centre and (c) off centre areas of spin coated 25PS75PMMA_air thin film surface (colour scale ± 150 nm) with corresponding line profiles generated from the x-y midpoint.

The topography that results here is different to that seen for the samples produced in the presence of a positive pressure of nitrogen during spin coating (Figure 4.4). In this case, the features observed have full width half maximum (FWHM) values ranging from 500 nm to 1 µm and peak to valley heights ranging from -100 nm to +75 nm. It is important to realise that these areas are on a larger scale as opposed to the 10 µm x 10 µm areas. This change was implemented to enable a larger scale analysis of the surface, to gain a better insight into the random topography spin coating produces.

The corresponding AFM derived surface roughness indicate average R_a and R_q values of 22.30 ± 0.60 nm and 31.10 ± 2.50 nm, respectively.

Chemical analysis by XPS was employed to determine what, if any, effects spin coating at atmospheric pressure in air has on the resulting polymer surface chemistry. Figure 5.3 shows (a) WESS and associated high resolution peak fitted spectra for the (b) C 1s and (c) O 1s regions.

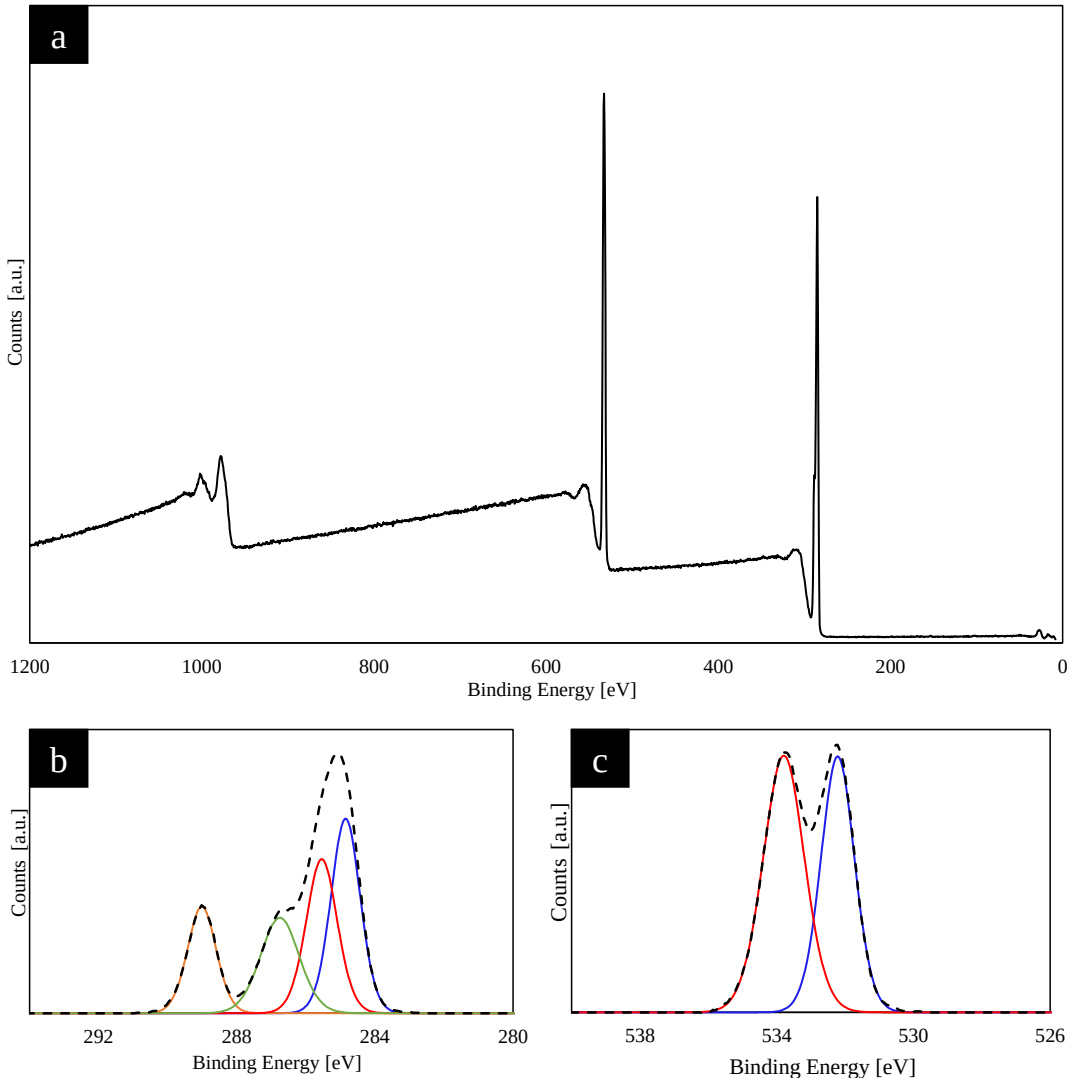

Figure 5.3 XPS spectra for spin coated 25PS75PMMA_air surfaces on glass substrates: (a) WESS (b) C 1s and (c) O 1s spectra.

As described earlier, the most intense aliphatic C-C peak attributed to adventitious carbon on the 25PS75PMMA_air sample was set to 285.0 eV as a means of additional charge correction. Thereafter, the four expected carbon environments associated with PMMA are seen to be present for this sample. Peaks are observed at 284.86, 285.55, 286.77 and 289.02 eV, relating to C-H hydrocarbon, C-C-O beta-shifted carbon, C-O methoxy group and O-C=O carbonyl bond, respectively. C-H and beta-shifted carbon peaks have been identified separately for completeness. Analysis of the O 1s region indicated a doublet consisting of two peaks at 532.23 and 533.80 eV, corresponding to O=C carbonyl and O-C methoxy group oxygen. Quantification of the % atomic concentration is shown in Table 5.1.

Table 5.1 XPS derived % atomic concentration data for peak fitted C 1s and O 1s contributions in 25PS75PMMA_air sample.

Spot	C-H (%)	C-C (%)	C-O (%)	C=O (%)	O=C (%)	O-C (%)	% C1s	% O1s
1	32.69	21.40	28.22	17.69	44.49	55.51	76.46	23.54
2	32.92	20.20	29.92	16.96	45.85	54.15	77.09	22.91
3	34.82	21.31	26.68	17.20	45.31	54.69	76.87	23.13
Average	33.48	20.97	28.27	17.28	45.22	54.78	76.81	23.19
Standard Deviation	1.17	0.67	1.62	0.37	0.68	0.68	0.32	0.32

5.3 Biological Assessment of 25PS75PMMA_air Surfaces

The 25PS75PMMA_air substrates were then subject to DPFA analysis using the same protocol as that applied in Chapter 4. Whole blood from the same donor (Healthy Donor 1) was used initially to enable a direct comparison with the data presented for the samples spin coated in the presence of a positive pressure of nitrogen. The profile

and platelet indices for this donor blood measured at the date DPFA analysis is shown in Table 5.2.

Table 5.2 Blood profile for a healthy donor consisting of platelet count and additional platelet indices used for 25PS75PMMA_air DPFA measurements.

Name	Donor1_181022	**Haematocrit (HCT)**	31.2%
Age	24	**Platelets (PLT)**	$224x10^3/\mu L$
Blood Type	O	**Mean Platelet Volume (MPV)**	10.8fL
Gender	Female	**Platelet-Large Cell Ratio (P-LCR)**	29.7%

Figure 5.4 shows the final frame fluorescence images (120/120) from the time lapse sequence for five replicates of the 25PS75PMMA_air surface.

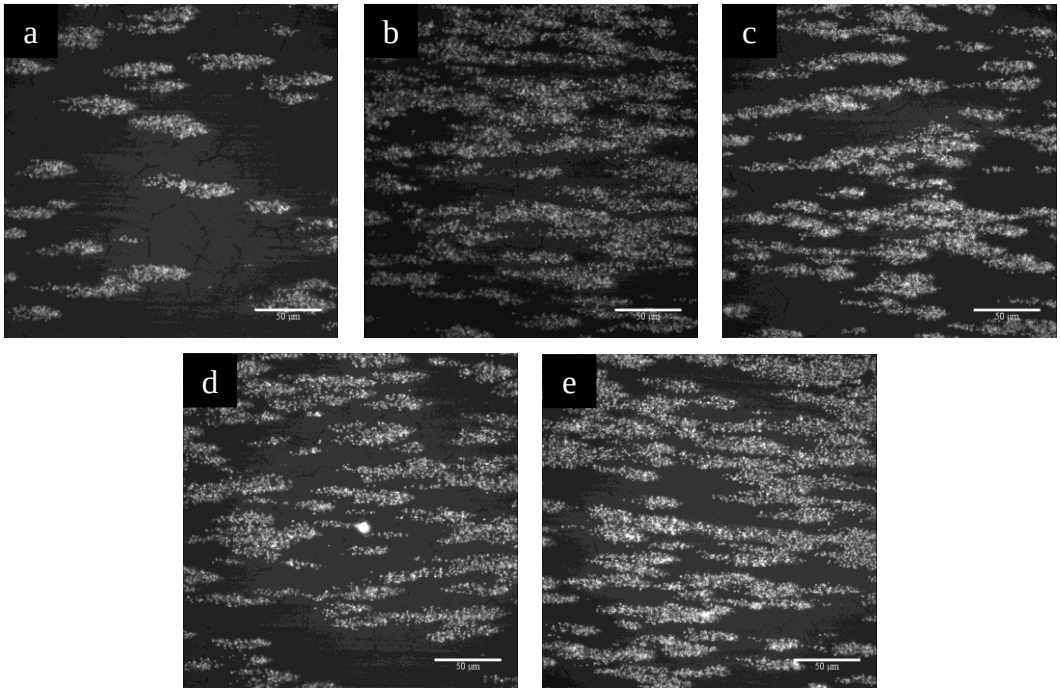

Figure 5.4 Fluorescence micrographs of whole blood DIOC6 labelled platelets in frame 120/120 for each of 5 replicates (a) to (e) of the spin coated 25PS75PMMA_air surface. Scale bar 50 µm.

Upon visual inspection, all five samples display significant amounts of platelet interaction with only replicate (Figure 5.4 a) showing a noticeably smaller amount of adherence at the 120/120 time point. The 'brighter' areas on the images indicate the formation of 3D thrombi building in the flow channel. The calculated percentage surface coverage values are provided in Table 5.3 and report an average coverage of 17.30 ± 6.80%.

Table 5.3 Average % surface coverage values (n=5) and standard deviation for 25PS75PMMA_air spin coated surface.

Sample	% Coverage	Average	Standard Deviation
1	8.0	17.30	6.80
2	14.1		
3	20.0		
4	18.0		
5	26.2		

The surface coverage here has increased by approximately +4% as compared to the value seen for 25PS75PMMA substrates spin coated in nitrogen (Table 4.3) while the standard deviation values calculated in both cases is very similar. Interestingly, it is quite clear that replicate (a) in Figure 5.4 makes a large contribution to the standard deviation value here. If only replicates (b) to (e) are used in this calculation, the average coverage increases to 19.60% and the standard deviation reduces to 5.00%.

In order to better understand platelet activity over time for this sample, images of replicate (c) (selected at random) at 60 second intervals between 0 and 240 seconds are shown Figure 5.5.

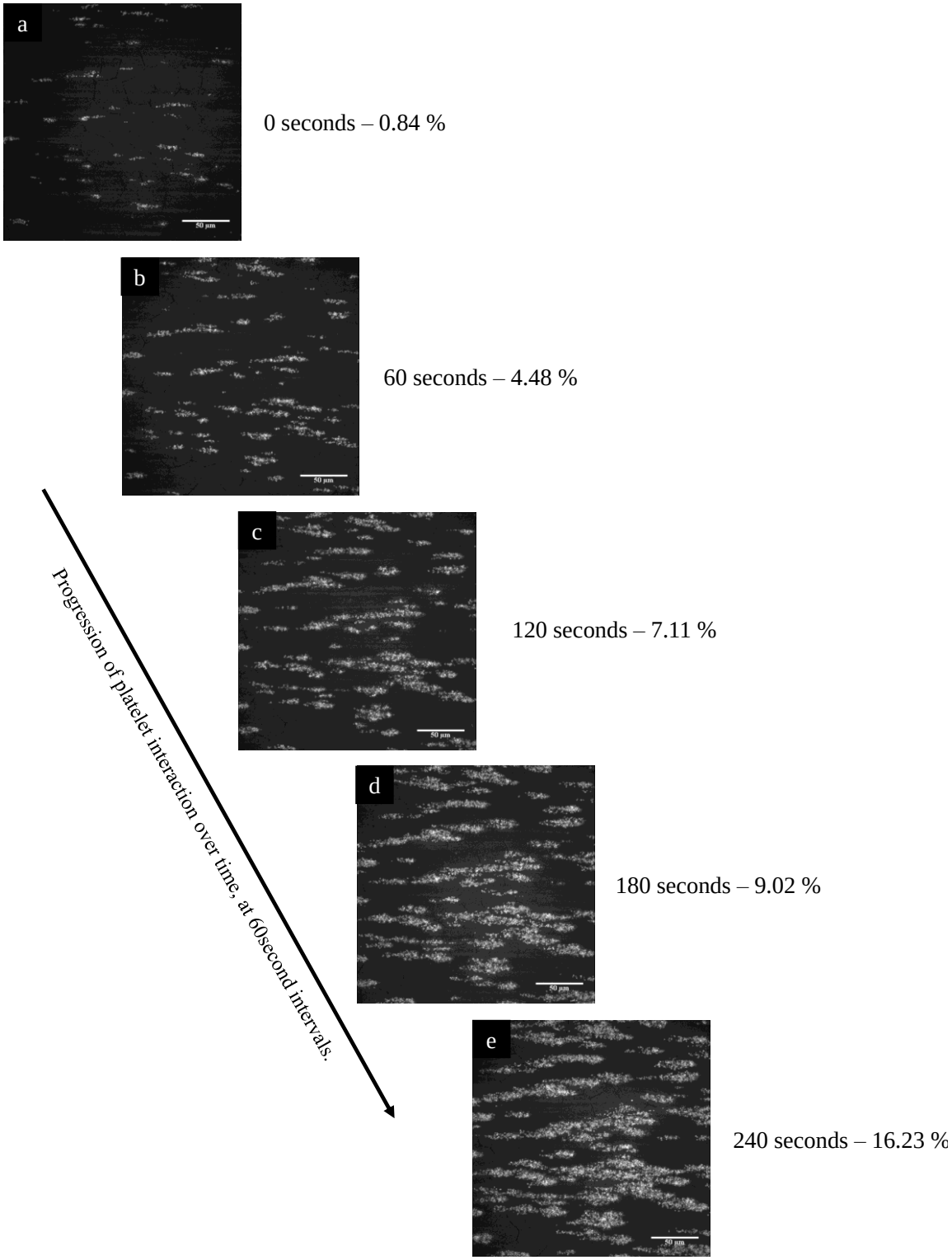

Figure 5.5 Fluorescence images of platelet interaction with the 25PS75PMMA_air surface at (a) 0, (b) 60, (c) 120, (d) 180 and (e) 240 seconds. Scale bar 50 µm.

The presence of platelets at time 0s (Figure 5.5 (a)) is due to the previous data collection period of 1000 frames at 19 fps, which leads to some initial adhesion. Platelet growth is observed in horizontal line formations once again, which supports the argument of von Willebrand Factor (vWF) uncoiling in a string conformation.

5.4 Properties of 25PS75PMMA_750_air Polymer Demixed Surfaces

Figure 5.6 shows representative optical micrographs for thin films surface created by spin coating a 25PS75PMMA solution in chloroform augmented with +750 50µm PS microspheres per ml, in air at atmospheric pressure (25PS75PMMA_750_air). No change is observed in these micrographs compared to those recorded for the 25PS75PMMA_air sample (Figure 5.1) with the PS distribution within the PMMA still resulting in striations and honeycomb-like assemblies. Again, these structures appear more ordered than those created by spin coating the same solution in nitrogen.

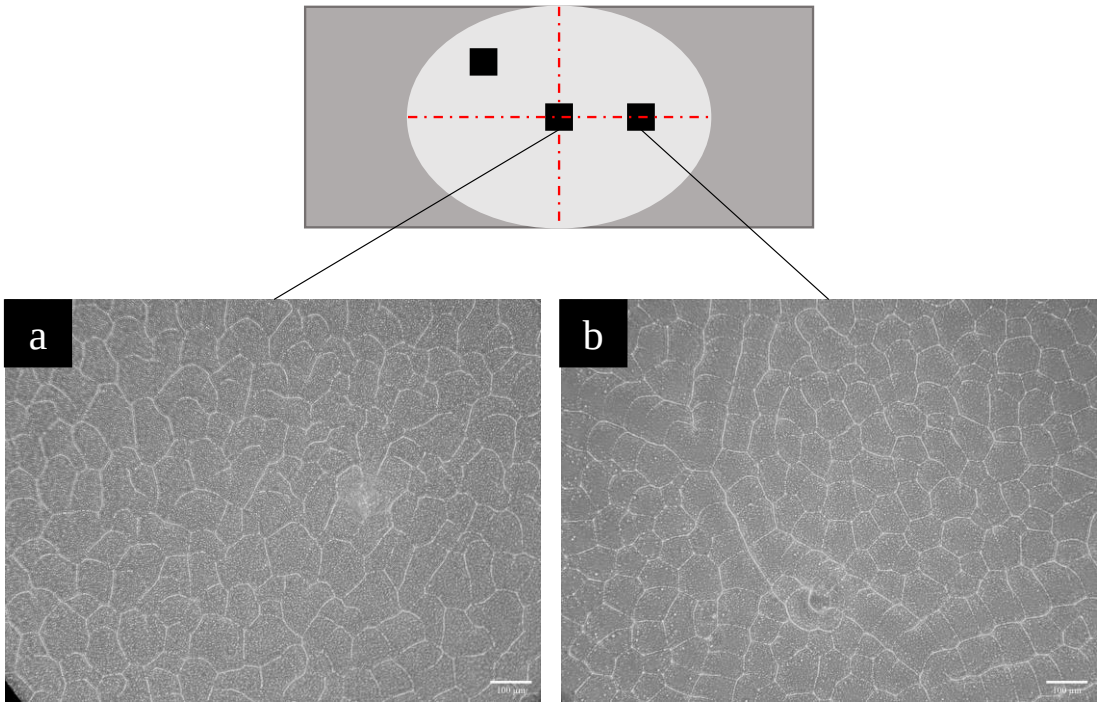

Figure 5.6 Optical micrographs of (a) centre and (b) edge areas for a spin coated 25PS75PMMA_750_air substrate. Scale bar 100 µm

The AFM pseudo-colour 3D plots and line profiles for the 25PS75PMMA_750_air sample are shown in Figure 5.7. As before, these are 40 µm x 40 µm scans to enable a more comprehensible picture of the topography within the channel to be presented.

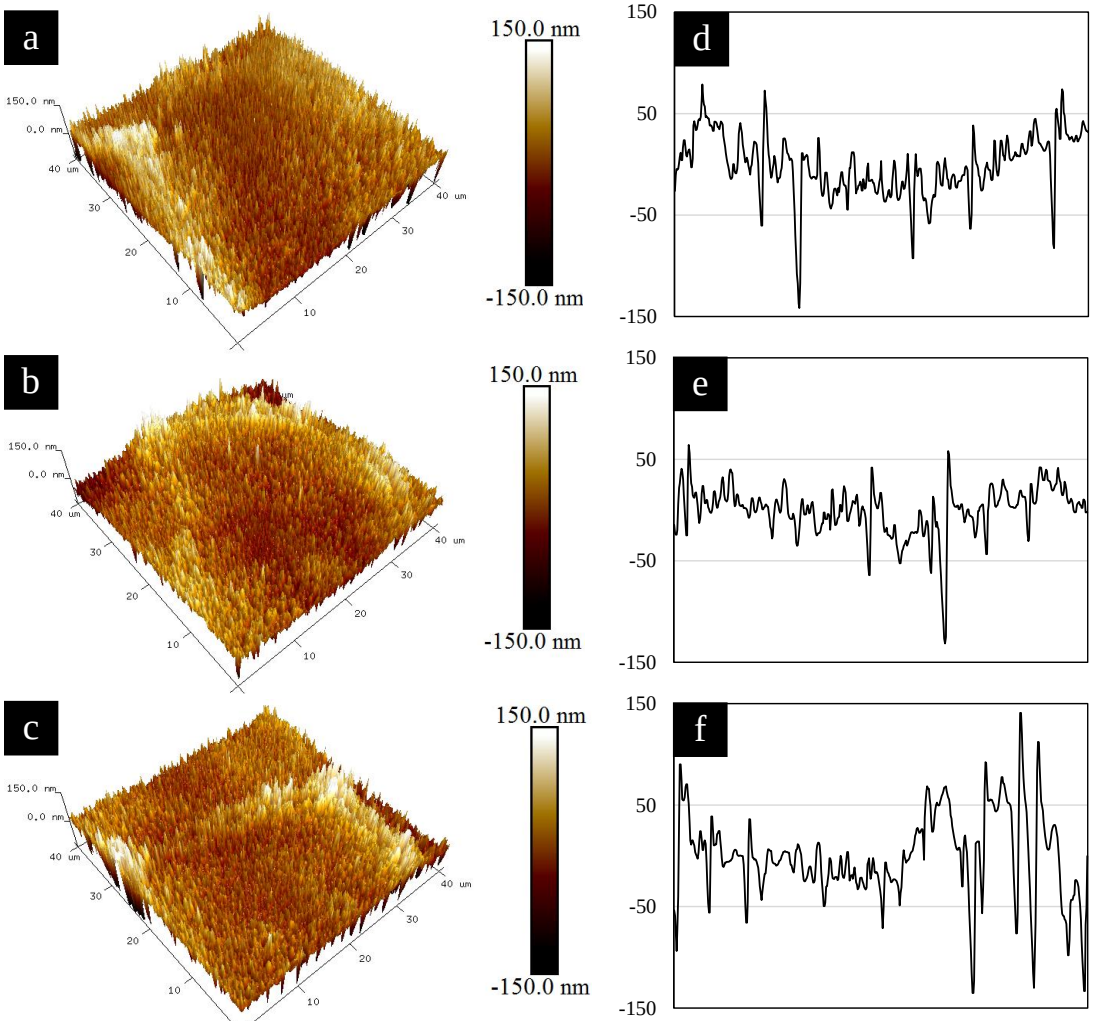

Figure 5.7 40 µm x 40 µm 3D pseudo-colour AFM images at (a) edge, (b) centre and (c) off centre areas of a spin coated 25PS75PMMA_750_air thin film surface (colour scale ± 150 nm) with corresponding line profiles generated from x-y midpoint.

The nature and distribution of the surface features observed here are similar to those for the 25PS75PMMA_air sample. However, addition of the +750 50µm PS

microspheres/ml seems to create more “jagged” features with FWHM values of <1 μm and height profiles spanning -125 nm valleys to 140 nm peaks. The AFM derived roughness for this surface indicate average R_a and R_q values of 25.20 ± 3.20 nm and 34.90 ± 2.70 nm, respectively.

XPS spectra for the 25PS75PMMA_750_air surface are provided in Figure 5.8. As before, charge correction was applied by setting the C-C aliphatic peak to 285.0 eV. Peaks are present at 284.74, 285.42, 286.65 and 288.90 eV, relating to C-H hydrocarbon, C-C-O beta-shifted carbon, C-O methoxy group and O-C=O carbonyl bond, respectively. Analysis of the O 1s region indicated a doublet made up of two peaks at 532.09 and 533.67 eV, corresponding to O=C carbonyl and O-C methoxy group oxygen.

The contributions to the C 1s spectral components are similar to those for the 25PS75PMMA_air substrate (Figure 5.3) and again correspond in position and relative intensity to those expected for PMMA.

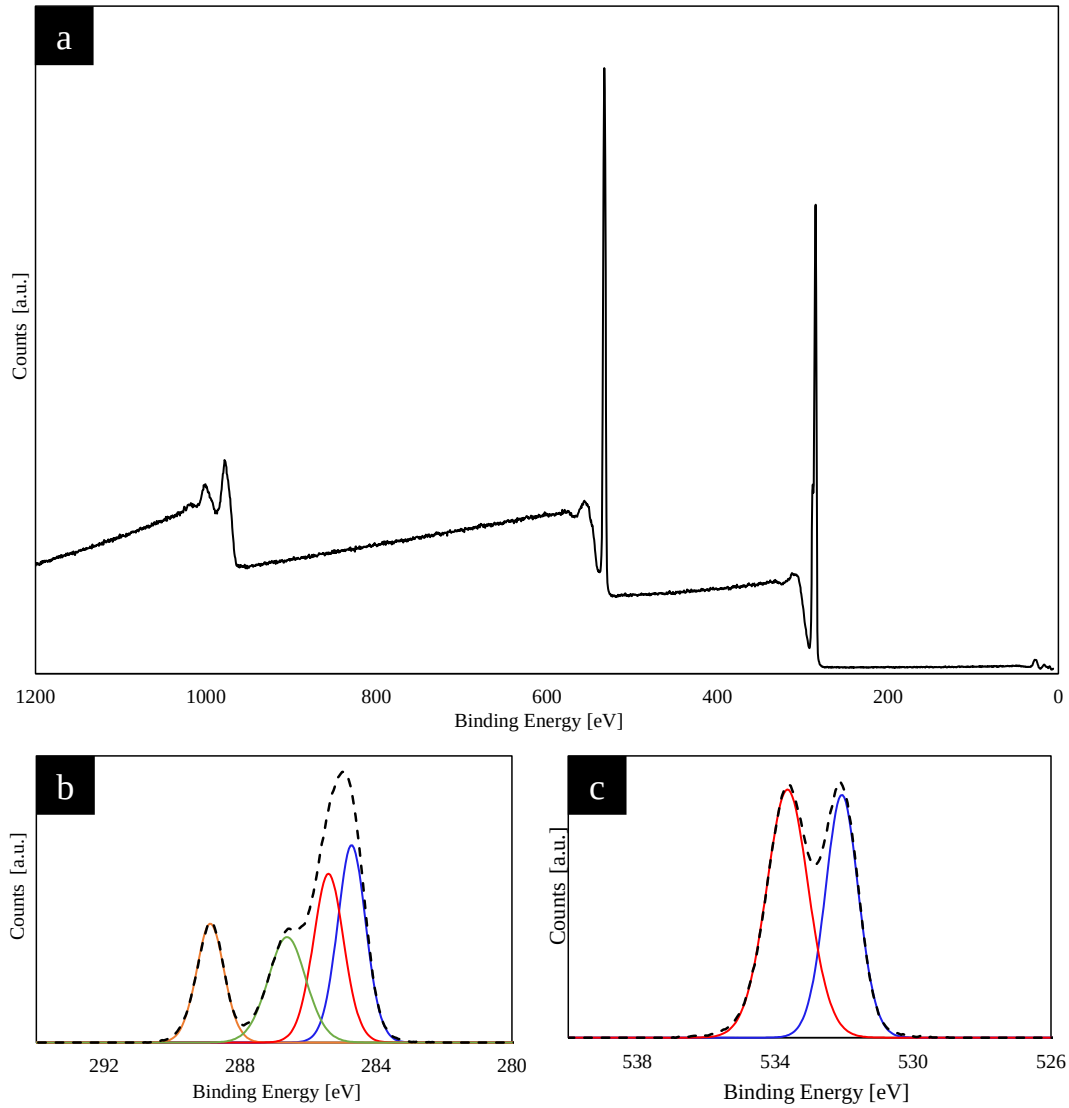

Figure 5.8 XPS spectra for spin coated 25PS75PMMA_750_air surfaces on glass substrates: (a) WESS, (b) C 1s spectra and (c) O 1s plots.

Quantitative data for this surface are provided in Table 5.4 and indicate the average % atomic concentrations for C 1s and O 1s to be 76.07 ± 0.27% and 23.93 ± 0.27%, respectively. Hence, the chemistry of the 25PS75PMMA thin film surface formed by spin coating in air does not appear to change significantly with the introduction of PS microspheres, which agrees with previous findings.

Table 5.4 XPS derived % atomic concentration data for peak fitted C 1s and O 1s contributions in 25PS75PMMA_750_air sample.

Spot	C-H (%)	C-C (%)	C-O (%)	C=O (%)	O=C (%)	O-C (%)	% C 1s	% O 1s
1	30.51	22.14	29.07	18.27	43.61	56.39	75.77	24.23
2	34.98	23.21	23.82	18.00	44.03	55.97	76.17	23.83
3	37.23	21.71	23.10	17.36	44.97	55.03	76.28	23.72
Average	34.24	22.35	25.53	17.88	44.20	55.80	76.07	23.93
Standard Deviation	3.42	0.77	3.07	0.47	0.70	0.70	0.27	0.27

5.5 Biological Assessment of 25PS75PMMA_750_air Surfaces

Platelet function analysis was carried out on five replicate 25PS75PMMA_750_air substrates using blood from Healthy Donor 1, with relevant sample profile information at the of DPFA shown in Table 5.5.

Table 5.5 Blood profile for Healthy Donor 1 consisting of platelet count and additional platelet indices used for 25PS75PMMA_750_air DPFA measurements.

Name	**Donor1_181023**	**HCT**	**38.9%**
Age	24	**PLT**	$260x10^3/\mu L$
Blood Type	O	**MPV**	9.4fL
Gender	Female	**P-LCR**	17.6%

Figure 5.9 provides the final frame fluorescence images (120/120) from the time lapse sequence for five replicates of the 25PS75PMMA_750_air surface. The amount of platelet interaction here is significantly higher than that observed for the previous

25PS75PMMA_air samples. Platelets are seen to cover much of the field of view and there are clear indications of the formation of 3D thrombi.

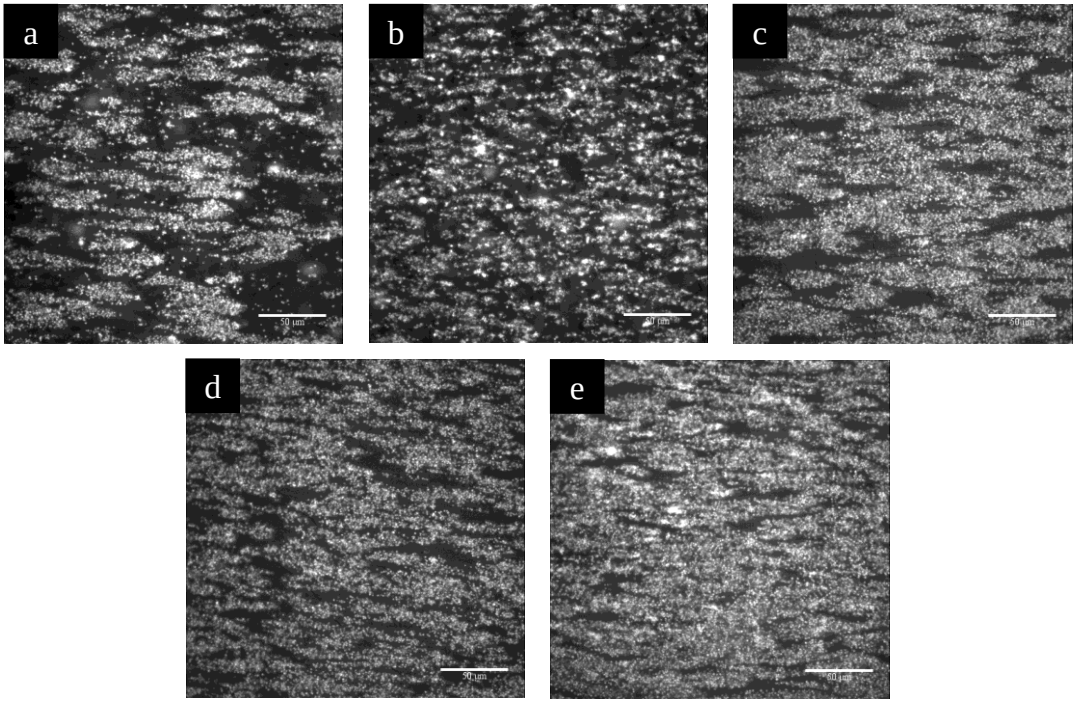

Figure 5.9 Fluorescence micrographs of whole blood DIOC6 labelled platelets in frame 120/120 for each of 5 replicates (a) to (e) of the spin coated 25PS75PMMA_750_air surface. Scale bar 50 µm.

The calculated percentage surface coverage values for these samples are provided in Table 5.6 and indicate an average coverage of 40.20 ± 13.30% which is almost twice that observed for the 25PS75PMMA_air. The standard deviation is notably higher for the 25PS75PMMA_750_air surface than was the case in the previous datasets which confirms greater variability in the amount of platelet adhesion from sample to sample.

Table 5.6 Average % surface coverage values (n=5) and standard deviation for 25PS75PMMA_750_air surfaces.

Sample	% Coverage	Average	Standard Deviation
1	27.70	40.20	13.30
2	26.90		
3	48.40		
4	39.80		
5	57.9		

5.6 Dynamic Evaluation of Platelet Behaviour

As in Chapter 4, platelet dynamics were further assessed on spin coated substrates created under normal ambient conditions by application of the autologous platelet algorithm, which employs an additional 1000-frame stack prior to the time lapse with the results obtained shown in Table 5.7.

Table 5.7 Dynamic platelet parameter values and blood indices data derived from application of the autologous platelet algorithm analysis for Donor 1 blood on ambient spin coated surface (n=5).

Dynamic Parameters	25PS75PMMA_air	25PS75PMMA_750_air
Ntracks	168 ± 44	474 ± 331
Fraction of Stably Adhered	0.75 ± 0.03	0.78 ± 0.05
Mean Translocating Distance (µm)	2.22 ± 0.31	2.13 ± 0.38
Mean Translocating Velocity (µm/s)	1.44 ± 1.06	1.21 ± 0.64
Platelet Adhesion Rate ($x10^3$ s^{-1})	0.69 ± 0.15	1.65 ± 1.27
Platelet Detachment Rate (s^{-1})	1.30 ± 1.89	2.20 ± 1.33
Fraction Platelets Sticking	0.47 ± 0.18	0.49 ± 0.09
Platelet Indices*		
Platelet Count ($x10^3$/µl)	224	260
Haematocrit (%)	31.2	38.9
vWF (IU/ml)	47.6	47.6

** No standard deviation values are reported for the platelet indices due to a single blood sample having been used for this analysis to eliminate a potential source error.*

Ntracks for 25PS75PMMA_750_air appears to be more than double that for 25PS75PMMA_air. However, a large standard deviation (±331) is noted in these measurements which makes it difficult to confirm that this is a real difference. A direct comparison of the four main dynamic parameters obtained for platelets on the 25PS75PMMA_air and 25PS75PMMA_750_air spin coated substrates are provided

in Figure 5.10, with statistical analysis carried out using a standard t-test. All parameters showed no significant difference with the addition of 50 µm microspheres.

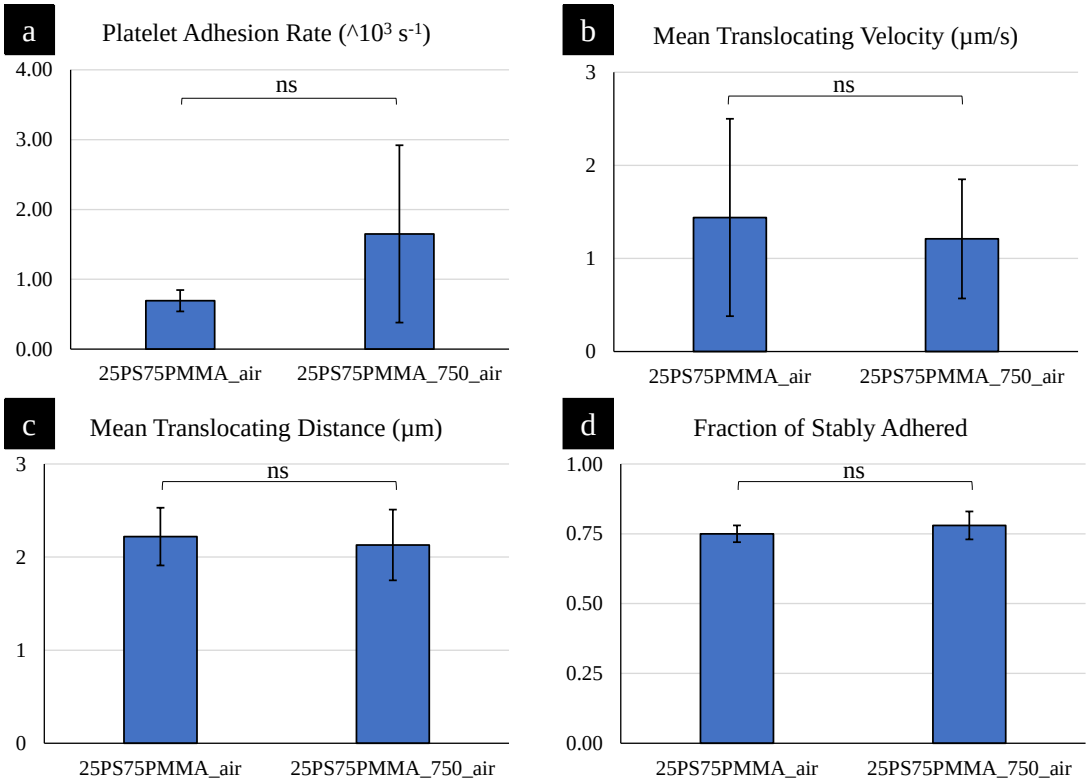

Figure 5.10 Graphical representation of four dynamic parameters, complete with statistical difference. P value = 0.05.

Relative assessment of thin films spun in a positive pressure, nitrogen environment, is provided in Chapter 4 (Figure 4.18).

5.7 Multiple Donor Study on 25PS75PMMA_750_air Substrates

As the main objective for this research is to create a synthetic DPFA substrate that can be used universally to specifically test vWF entrapment and subsequent platelet interactions thereon, a subsequent study was carried out using blood from multiple donors on the 25PS75PMMA_750_air sample. Table 5.8 lists blood profile and

additional platelet indices information for each of the six additional healthy donors (Donor 2 to Donor 7).

Table 5.8 Blood index information for all donors used within the universality study.

Donor	**Age**	**Gender**	**Blood Type**	**PLT ($x10^3/\mu l$)**	**HCT (%)**	**MPV (fL)**	**P-LCR (%)**
2	24	Female	O	266	44.1	11.5	37.0
3	29	Female*	B	152	37.3	14.9	68.8
4	27	Female	AB	285	42.5	10.6	27.7
5	30	Female	O	231	43.8	11.3	35.9
6	28	Female	B	257	38.1	11.9	39.4
7	49	Female	A	190	38.9	10.2	25.9

Figure 5.11 shows the final frame (120/120) fluorescence images for platelets from the six additional healthy donors (2 to 7) in triplicate, on the 25PS75PMMA_750_air spin coated thin films.

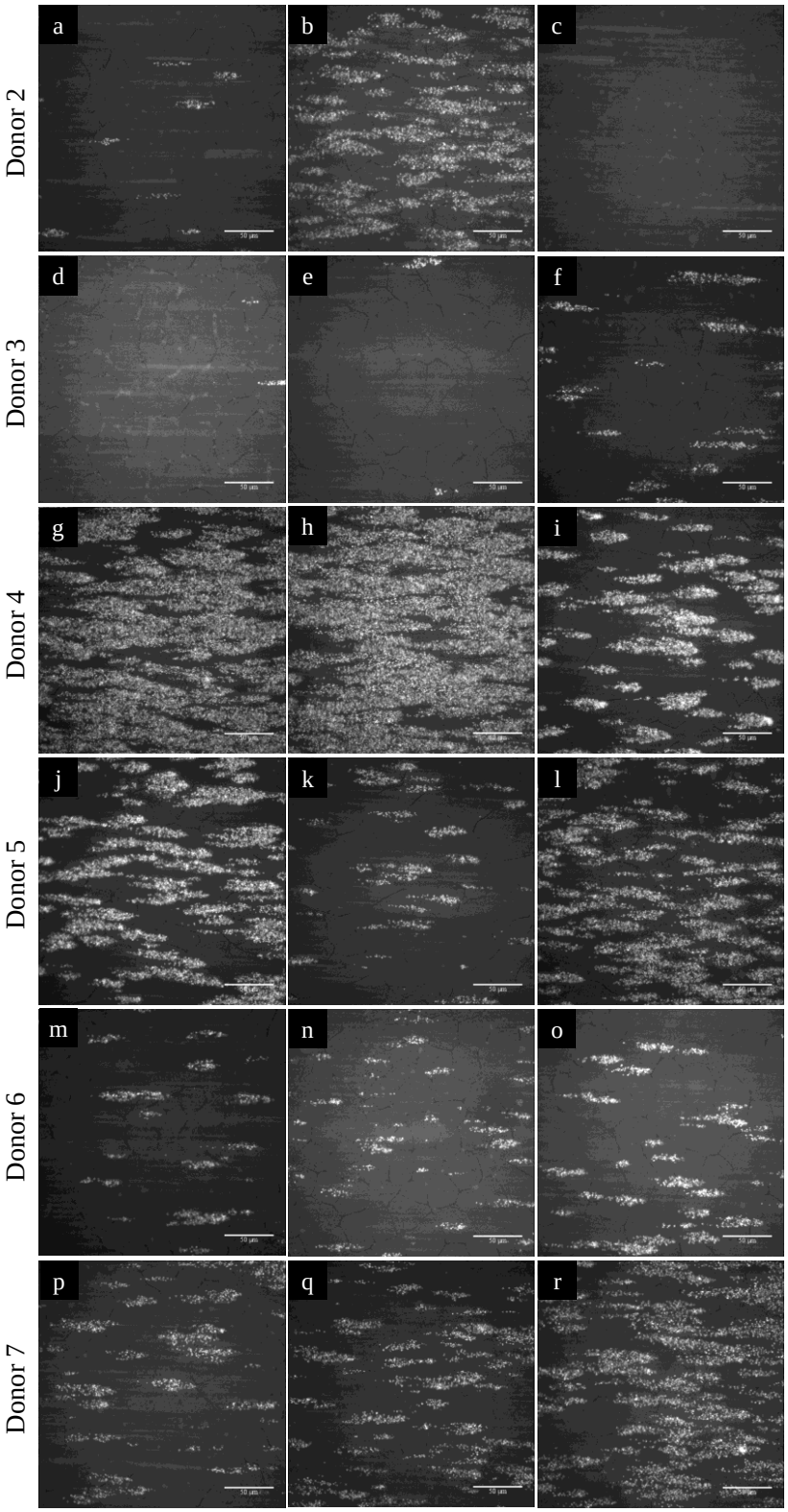

Figure 5.11 Fluorescence micrographs of whole blood DIOC6 labelled platelets from each of six additional healthy donors (Donor to Donor 7) in frame 120/120 for each of 3 replicates of the spin coated 25PS75PMMA_750_air surface. Scale bar 50 µm.

Clearly, visual inspection of these images indicates a significant variation in platelet adhesion both within donor sample sets and across different donors.

Table 5.9 provides the quantification data for the surface coverage which confirms the visually observed differences.

Table 5.9 Average % surface coverage values (n=3) and standard deviation for 25PS75PMMA_750_air spin coated surface in response to multiple healthy donors (Donor 2 to Donor 7).

Donor	Sample	% Coverage	Average	Standard Deviation
2	1	0.60	5.30	8.60
	2	15.26		
	3	0.10		
3	1	1.41	1.40	1.10
	2	0.37		
	3	2.48		
4	1	45.68	43.60	20.70
	2	63.14		
	3	21.90		
5	1	28.63	19.1	13.40
	2	3.76		
	3	25.03		
6	1	2.50	3.90	2.30
	2	2.75		
	3	6.59		
7	1	3.59	9.70	5.90
	2	9.96		
	3	15.40		

In order to better understand and rationalise these results, a vWF enzyme-linked immunosorbent assay (ELISA) test was employed to determine the protein concentration for each individual donor with the results provided in Table 5.10.

Table 5.10 vWF concentration (international units per millilitre - IU/ml) for each healthy donor blood, measured via ELISA.

Donor	**vWF Concentration (IU/ml)**
1	0.49
2	0.36
3	1.62
4	0.73
5	0.48
6	0.75
7	0.56

5.8 Discussion

The goal of the work reported in this chapter was to investigate the influence that changing the gaseous environment and pressure has on the surface topography and chemistry of substrates created by spin coating of PS/PMMA solutions. Specifically, deposition of the polymer demixed thin films has been carried out in air under ambient atmospheric pressure conditions (25PS75PMMA_air), as opposed to employing a positive pressure nitrogen to purge the chamber during spin coating (25PS75PMMA), with all other parameters being kept constant.

The surfaces created in air have been characterised by Optical Microscopy, AFM, XPS and the data obtained compared to that acquired for those produced using the positive pressure nitrogen purge conditions. The ability of these substrates to bind platelets has been measured using the DPFA technique and the resulting data also compared to that recorded for 25PS75PMMA surfaces. As indicated previously, surface bound and uncoiled vWF is required to enable platelet adhesion and aggregation *in vivo*. Therefore, the synthetic polymer demixed surface properties created here need to support the entrapment of vWF and its subsequent uncoiling to expose binding sites in a way that leads to platelet adherence thereon.

Microscopical optical analysis of the 25PS75PMMA_air thin films found that they have similar distribution patterns of PS within PMMA as was observed for 25PS75PMMA, with both striations and honeycomb structures present. However, these patterns are now noticeably more well-defined and regular in respect of the respective features. As indicated previously, this fragmentation of the PS component within the thin film surface is due to instability that occurs during the solvent evaporation gradient that is caused by the centrifugal force exerted on the solution during spinning. The positive pressure induced by the nitrogen purge condition has

been reported to influence the rate of solvent evaporation[153], in a manner that allows the polymer blend to reach thermodynamic equilibrium more readily than is the case at atmospheric pressure in air. Hence, removal of this positive pressure condition when created the 25PS75PMMA_air samples, is deemed to be responsible for the more defined structural features seen here. In this regard, it is assumed that the rate of evaporation in air and in a positive pressure of nitrogen is not sufficiently different to make a significant contribution to the attendant distribution of PS in PMMA after spin coating.

AFM images and associated line profile data indicate that the topography of the 25PS75PMMA_air thin films is different to that for the corresponding 25PS75PMMA samples. Visually, the features seem to be somewhat chaotic with many sharp protrusions ranging from -100 nm to +75 nm. The corresponding FWHM values for these features are in the range 500 nm to 1 μm, with the exception of surface shown in Figure 5.1 (e) which has a pronounced area of larger sized features which is believed to be due to an unusual agglomeration of the demixed polymer system. A review of the relevant literature indicates a lack of research into polymer demixed surface features created by spin coating under ambient atmospheric pressure air conditions. From a first principles perspective, the creation of these sharp, closely packed surface protrusions are a result of the slightly faster evaporation of the chloroform solvent that occurs due to the absence of the positive pressure provided by the nitrogen purge.

XPS analysis confirmed that the 25PS75PMMA_air substrates have a PMMA only surface chemistry which is similar to that of the 25PS75PMMA thin films (Figure 4.5) and are also consistent with the C 1s and O 1s features present in a surface that has been spin coated from 100% PMMA in chloroform (Table 4.1) with only a slight

increase in the C-O component observed. This latter effect may be due to a slight difference in the orientation of the PMMA structure close to the uppermost region of the film surface that is caused during spin coating in air at ambient pressure that is then observed due to the surface specificity of the XPS technique[152].

Platelet function on a set of five replicates of the 25PS75PMMA_air substrate was analysed using the DPFA device with blood from Healthy Donor 1 and all showed positive interactions. Platelet surface coverage increased to 17.3% from an average value of 13.8% obtained from 25PS75PMMA with the standard deviation remaining the same at 6.8%. Analysis of platelet interactions across the video frame time lapse, indicates that adhesion occurs in a linear fashion which is consistent with behaviour seen previously[151] and supports the theory that the surface supports entrapment of vWF followed by its uncoiling to expose platelet binding sites[108]. This suggests that it is the topography formed during spin coating in air at ambient atmospheric pressure that provides an environment that enables the adsorption of vWF, followed by its uncoiling and the subsequent binding of platelets from flowing whole blood under arterial shear. It is acknowledged that changes in the donor blood profile and platelet indices may play a role in the response observed and hence it is important that these factors are considered at the point of analysis rather than being assumed from historical measurements. In the case of the 25PS75PMMA_air samples, there is an increase in platelets (up 4%), MPV (up 5%) and P-LCR (up 3.9%), whilst the HCT levels drop by 13%. Chen *et al.*[128] have reported that platelet adhesion to vWF is dependent on both the blood HCT levels and flow rate. As the flow rate for the DPFA measurements has been kept fixed throughout, the only significant consideration here is the HCT level which is still this within the normal range. As such, from the results obtained

here it would seem that any effect on platelet binding due to a reduction in HCT is counteracted by increases in the number of platelets, MPV and P-LCR.

As reported in Chapter 4, the 25PS75PMMA_750 substrate has a more regular surface (50 nm feature height, 1 μm FWHM) than the corresponding 25PS75PMMA (100 nm – 1 μnm feature height, FWHM ~ 2 – 4 μm) surface and this serves to increase the scale of the platelet interactions thereon[108]. Hence, the effects of adding 750 PS microspheres/ml to the 25PS75PMMA solution on the spin coated surface created in air at atmospheric pressure was evaluated.

Microscopical optical analysis of the 25PS75PMMA_750_air substrates show patterns of PS distribution in PMMA that are consistent with the previous 25PS75PMMA_air surfaces, suggesting that at the micron scale, no changes are observed within polymer distribution. AFM analysis of the resulting topographical features indicates peak heights ranging from ± 150 nm with FWHM values between 100 nm and 1 μm, which are then now higher and narrower than those recorded for the 25PS75PMMA_air surfaces. The surface roughness has also increased slightly (Ra = 25.2 ± 3.2 nm and Rq = 34.9 ± 2.7 nm).

XPS analysis of the 25PS75PMMA_750_air substrate is again consistent with a PMMA only chemistry on the uppermost surface. The small changes noted within relative contributions of the peak fitted components are attributed here to moderate changes in the polymer chain orientation within depth of analysis.

Platelet function analysis of the 25PS75PMMA_750_air substrate within the DPFA device using whole blood from Healthy Donor 1 indicates a significant increase in surface coverage (40.20 ± 13.30%), when compared to the results for all of the previously studied spin coated surfaces. As before, the blood count profile at the point

of analysis was used for the subsequent interpretation of results with all metrics found to lie within the healthy range. A relatively high degree of variation was seen across the five samples studies (as per the SD value), which is a challenge for the potential use of this surface as a synthetic sensor substrate in the DPFA device. Some of this variation can is negated by using the same donor blood for both sample sets with some changes in the blood factors noted at the two dates of blood donation. Overall, for this surface platelet count and HCT levels both increase whilst MPV and P-LCR values decrease.

The autologous platelet algorithm used in Chapter 4 has also been applied here to further evaluate the kinetic platelet behaviour on the spin coated surfaces created in air under ambient conditions. Relying on visual analysis of the fluorescent images alone, suggests that the 25PS75PMMA_750_air substrate (Figure 5.9) outperforms the 25PS75PMMA_air surface (Figure 5.4) in terms of platelet interactions thereon. By extension, this suggests that this surface is capable of greater vWF entrapment over the same timescale. However, statistical analysis of the tracking data reveals that there is no significant difference between the behaviour of platelets on these surfaces across any of the four parameters examined. Whereas, the adhesion rate data seems to increase for the substrate augmented by +750 50 µm PS microspheres, closer inspection of these data indicate a large standard deviation which limits any further interpretation in this regard.

Direct comparison with substrates spin coated in the presence of a positive pressure of nitrogen, showed a similar trend whereby the augmented 25PS75PMMA_750 substrate (Figure 5.9) shows a higher level of platelet interaction than that seen on the 25PS75PMMA_air surface (Figure 5.4) using optical analysis only. Evaluation of dynamic parameters using the algorithm, showed similar values

for each of the parameters measured (Table 5.7) with no significant difference seen between the data obtained for the two nitrogen-spun surfaces. This suggests that, using this analytical approach, there appears to be no influence on platelet function from introduction of the PS microspheres (and the resulting effects of the surface topography). Surfaces created using both ambient air conditions and a positive pressure nitrogen environment, facilitate similar dynamic platelet function which indicates that at a dynamic level, neither the gas nor the pressure conditions influence platelet behaviour on these surfaces. Therefore, in the interests of achieving a suitable synthetic surface for use in the assay device, the sample with the most abundant platelet coverage was chosen to progress these studies beyond testing with Donor 1 blood.

Blood from an additional six healthy donors (Donors 2 to 7) was used to extend the platelet function studies on the 25PS75PMMA_750_air substrate, the complete blood count profile of which generally fall within the healthy range[3]. In general, there was a positive platelet response to the 25PS75PMMA_750_air surface for all donor bloods. Donor 2 shows an average surface coverage of 5.30 ± 8.60%. The relatively high standard deviation here can be explained by looking at the optical micrographs (Figure 5.11) wherein replicate (b) shows significantly higher levels of platelet interaction than the other surfaces. Analysis of blood indices revealed a P-LCR value of 37.0% which is higher than the healthy range (15 – 35%). However, as the two main platelet activation markers are MPV and PLT, it can be assumed that this has a minimal effect on platelet adhesion.

Donor 3, a blood type B individual, shows noticeably less platelet interaction (1.40 ± 1.10%). A more considered review of the six donors indicated that Donor 3 is pregnant and appears to have levels of HCT and PLT which fall at the lower end of

the normal range and also has higher MPV and P-LCR readings. Haemodilution is a normal physiological change that is linked to pregnancy, in that there is an increase in circulating plasma and therefore a decrease in blood count levels[154,155]. Previous studies have shown that a decreased platelet count reduces dynamic platelet interaction with vWF[10]. These authors showed that when levels of HCT were artificially reduced by 50% (representative of haemodilution), an attendant reduction in platelet adhesion was observed. Hence, this effect tends to support the findings reported here, whereby the pregnant subject shows significantly decreased surface coverage.

The highest level of platelet interaction is seen with Donor 4, a type AB individual, with average surface coverage of 43.60 ± 20.70%. This person reported the highest PLT count out of all donors but had levels that were still within the normal range. Recent results have shown that there is a significant difference between platelet function of type O and non-type O blood when measured by a DPFA device equipped with endogenous (immobilised) vWF substrates.

Donor 5 shows platelet indices which mainly lie within the healthy range, but with the P-LCR value lying slightly outside of the expected range. Surface coverage is less than half that of Donor 4, at 19.10 ± 13.40%, with a high degree of standard deviation observed. This inconsistency can be seen in Figure 5.11 (k) whereby there are significantly less platelets adhering to the surface.

Surface coverage of 3.90 ± 2.30% was recorded for another type B individual, Donor 6. Visually, the micrographs look the most repeatable observed in this study (Figure 5.11 (m-o)) and result in a low standard deviation. For this donor, elevated levels of P-LCR are seen, while all other markers are normal.

Donor 7 is the only type A subject tested and shows an average surface coverage of 9.70 ± 5.90%, which was mid-ranking in terms of relative platelet interaction. All platelet markers are within the healthy range and so the platelet interactions are deemed to be reliable.

In total, blood samples from three different type O donors were investigated using the 25PS75PMMA_750_air substrate (Donors 1, 2 and 5). However, the surface coverage values observed would seem to show no significant trend in platelet interactions with 120/120 image coverage ranging between 5.30 and 19.10%. This variation cannot be attributed to blood platelet indices only and so the vWF concentration for each donor was measured directly using an immunosorbent assay (ELISA). Normal human plasma vWF concentration has been reported to range between 0.30 and 1.57 IU/ml[156]. vWF levels are known to be influenced by blood (ABO) group with a decrease of ~25% seen in type O subjects. Gender is another factor of note, with vWF levels being higher in females. All donors within the study reported here show normal vWF levels, except Donor 3, who is known to be pregnant and reported an elevated level of vWF (1.62 IU/ml). Increase in vWF has been widely reported in pregnancy, with the greatest increase in the third trimester[157]. Overall, both the vWF ELISA and complete blood count show no results which would be considered to effect platelet interaction significantly. Hence, the variation that exists both within single blood samples and across donors with the same blood group, this remains a challenge as currently it is not possible to carry out the dynamic analysis on the multiple donor datasets.

In summary, these findings suggest that the change from a nitrogen positive pressure environment to an ambient air pressure condition during spin coating of the polymer demixed PS/PMMA solutions does not affect the ability of the attendant

surface to entrap vWF from flowing blood and thereby still facilitates platelet function testing thereon. Whereas, visual (120/120 image) analysis of these substrates show increased levels of platelet adhesion of platelets from Donor 1 (type O) blood, compared to that for surfaces created using positive pressure nitrogen purge environment when spin coating, issues with reproducibility still remain. An algorithm-based analysis shows that platelets behave similarly across both types of surfaces, with no statistically significant differences in adhesion, mean translocating velocity or distance observed. Further analysis across a cohort of ABO donor subjects shows that, polymer demixed films created by spin coating in air at ambient pressure facilitates platelet testing of all blood types. However, as before, significant variation in the datasets is again a limitation within the current study with sources of variance existing in the use of whole blood and the nature of the spin coated topography.

6. Platelet Interactions on Nanoscale Embossed Poly (methyl methacrylate) Surfaces

6.1 Introduction

As indicated throughout this work, a significant limitation of fabricating a synthetic platelet function sensor surface by spin coating is the lack of reproducibility that the technique introduces. Whereas, steps have been taken here to increase the reproducibility[108] of the nanoscale surface features created, the random nature of the polymer demixed solution distribution on the surface due to centrifugal force remains dominant[158].

An alternative method for fabrication of uniform surface features is hot embossing[159–161] whereby a master stamp, with a machined negative pattern to that required is pressed into a sheet of materials under pressure, at a set temperature. Resulting topography is then a mirror of the template stamp. A range of common plastic devices are fabricated using this technique, and results indicate excellent reproducibility for applications within microfluidics and semiconductors[160,162]. Popular plastics used include polystyrene (PS), poly (methyl methacrylate) (PMMA) and polyvinyl chloride (PVC).

Hot embossing of PMMA was therefore utilised here to produce a surface topography with nanoscale features similar to those observed for spin coated polymer demixed surfaces. The stamp used here was similar to that created in a previous study[14] but modified with a nickel coating to enhance its strength and durability during hot embossing which was a major limitation of the original pristine silicon wafer version.

As before, PMMA sheets were subjected to the hot embossing process using the nickel coated stamp to produce two channels with differing patterns of nanoscale

features. Substrates were characterisation by Atomic Force Microscopy (AFM), X-ray Photoelectron Spectroscopy (XPS) and Water Contact Angle (WCA) to measure feature size, surface chemistry and wettability, respectively. The substrates produced were tested using the Dynamic Platelet Function Assay (DPFA) system to analyse the haematological response.

6.2 Properties of Poly (methyl methacrylate) Pre- and Post-Embossing

The dimensions of the features in the two channels of the hot embossed poly (methyl methacrylate) (PMMA) substrates are provided in Table 6.1. Whereas, feature height was kept constant at 50 nm in each, the interspacing was varied between 500 nm and 1 µm, producing channels ‘a’ and ‘b’, respectively.

Table 6.1 Specification for the features created within channels 'a' and 'b' using the hot embossing master stamp.

Channel Name	Feature Height	Base Width (nm)	Apex Width (nm)	Interspacing (nm)
a	50	500	100	500
b	50	500	100	1000

Figure 6.1 displays 3D pseudo-colour AFM plots of 10 µm x 10 µm regions and corresponding line profiles for the pristine PMMA material with expected sporadic roughening caused by processing of this standard sheet material.

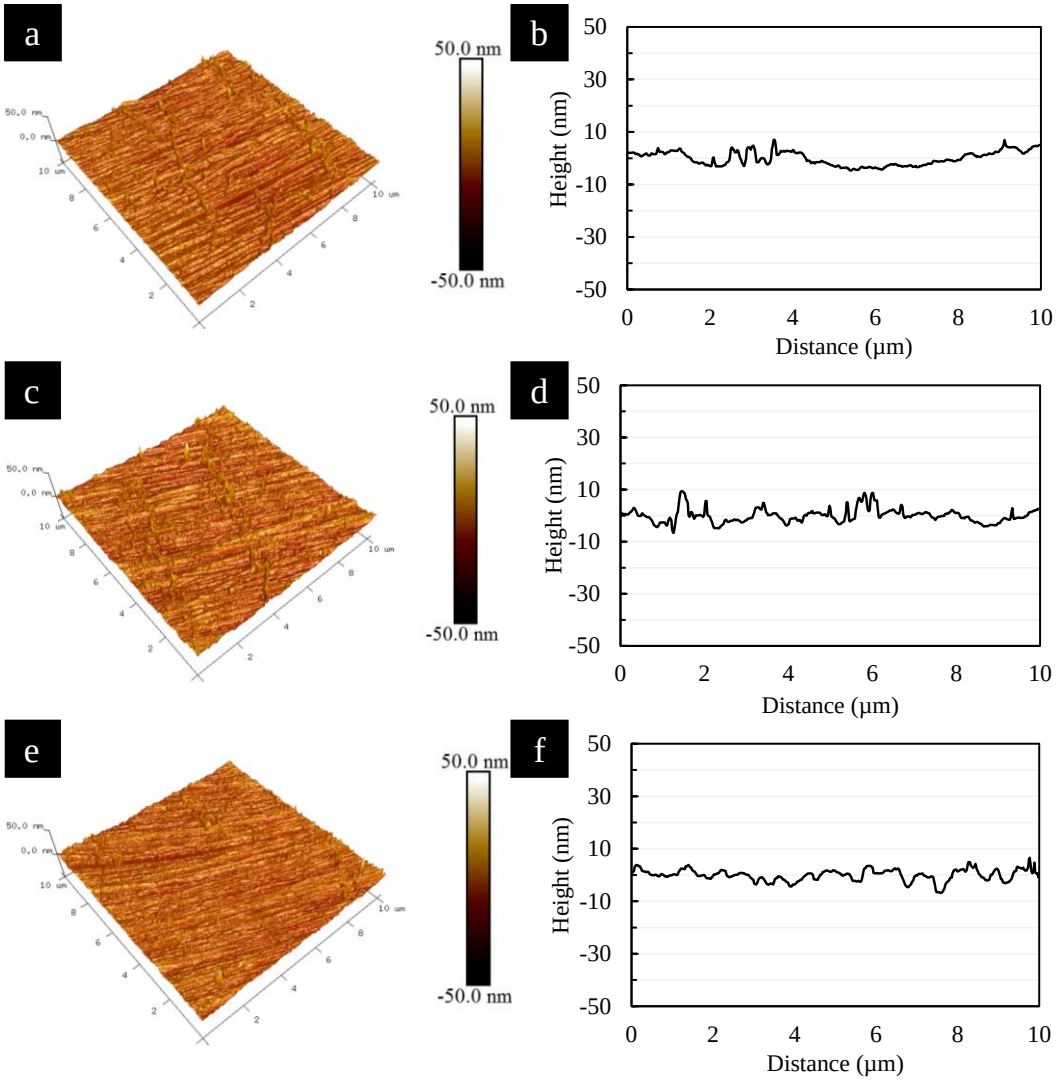

Figure 6.1 10 µm x 10 µm 3D AFM images of (a) edge, (b) centre and (c) off centre areas of pristine (pre-embossed) PMMA sheet, (colour scale ± 50 nm) with corresponding line profiles generated from the x-y midpoint.

Figure 6.1 shows a topography consisting of small irregularities on the substrate surface ranging up to ± 10 µm. Corresponding surface roughness values, R_a and R_q, are 1.8 ± 0.2 nm and 2.4 ± 0.2 nm, respectively.

A typical XPS wide energy survey scan (WESS) and associated high resolution C 1s and O 1s plots for pristine PMMA are provided in Figure 6.2, which are indicative of the expected surface chemistry.

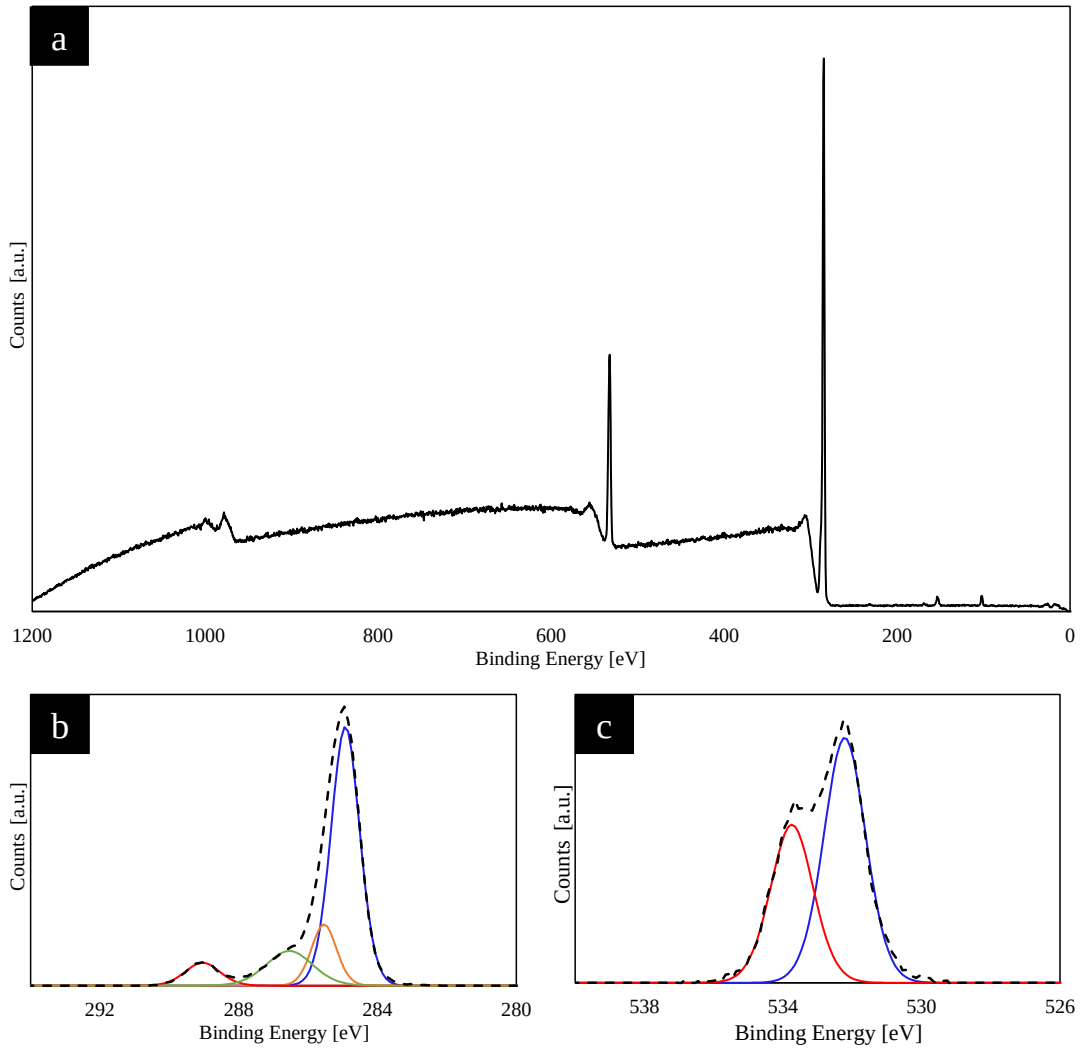

Figure 6.2 XPS spectra for pristine (pre-embossed) PMMA: (a) WESS, (b) C 1s spectra and (c) O 1s.

Charge correction was applied as standard through calibration of the aliphatic carbon to 285.0 eV. Four peaks are observed at 284.93, 285.84, 286.54 and 289.04 eV, relating to C-H hydrocarbon, C-C-O beta-shifted carbon, C-O methoxy group and O-C=O carbonyl bond, respectively. C-H and beta-shifted carbon peaks within the aliphatic peak have been identified separately for completeness. Analysis of the O 1s region indicated a doublet consisting two peaks at 532.21 and 533.74 eV, corresponding to O=C carbonyl and O-C methoxy group oxygen. Quantification of

the % atomic concentration is shown in Table 6.2, compared with post-embossed surfaces.

Figure 6.3 shows 10 µm x 10 µm 3D pseudo-colour AFM plots for three areas of channel ‘a’ embossed surfaces with corresponding line profiles taken from the x-y centre point.

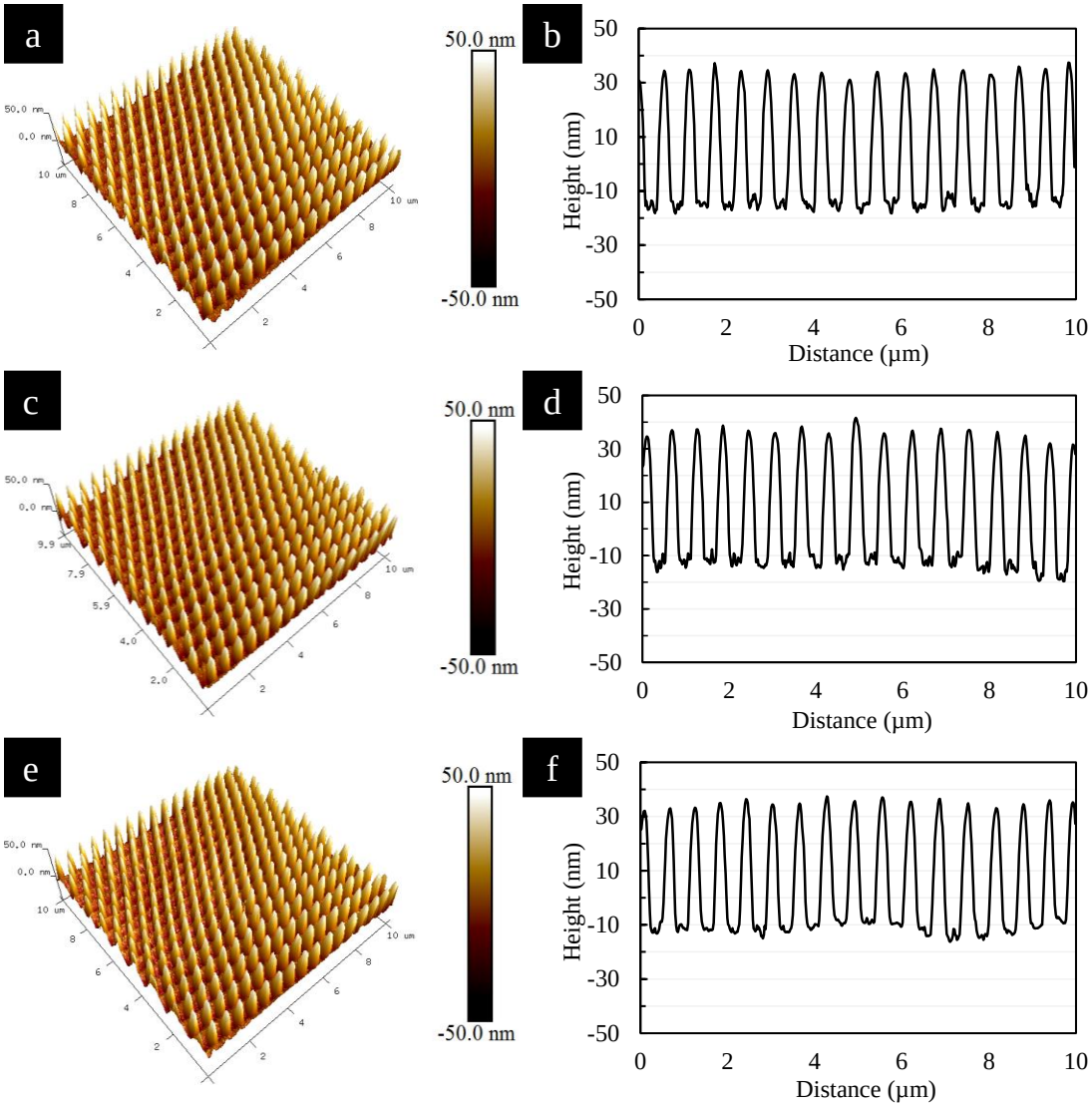

Figure 6.3 10 µm x 10 µm 3D AFM images at (a) edge, (b) centre and (c) off centre areas of channel ‘a’ embossed surfaces, (colour scale ± 50 nm) with corresponding line profiles of the generated from x-y midpoint.

The highly ordered features observed here indicate clearly that the hot embossing technique has been effective in producing a reproducible topography with feature heights of approximately 40 nm compared to the optimum 50 nm that the stamp was designed to deliver. The full width-at half maximum values are approximately 250 nm with again a high level of consistency. Surface roughness parameters R_a and R_q were measured as 9.8 ± 0.5 nm and 12.9 ± 0.6 nm, respectively. Post-embossing, surface roughness increases by a factor of 5. At the base of the features, small nano-scale protrusions can be seen, and this may be indicative of constrictions of softened PMMA as it solidifies within gaps between the stamp and backing wafer.

The WESS and high-resolution C 1s and O 1s XPS spectra for the channel ‘a’ surface are displayed in Figure 6.4.

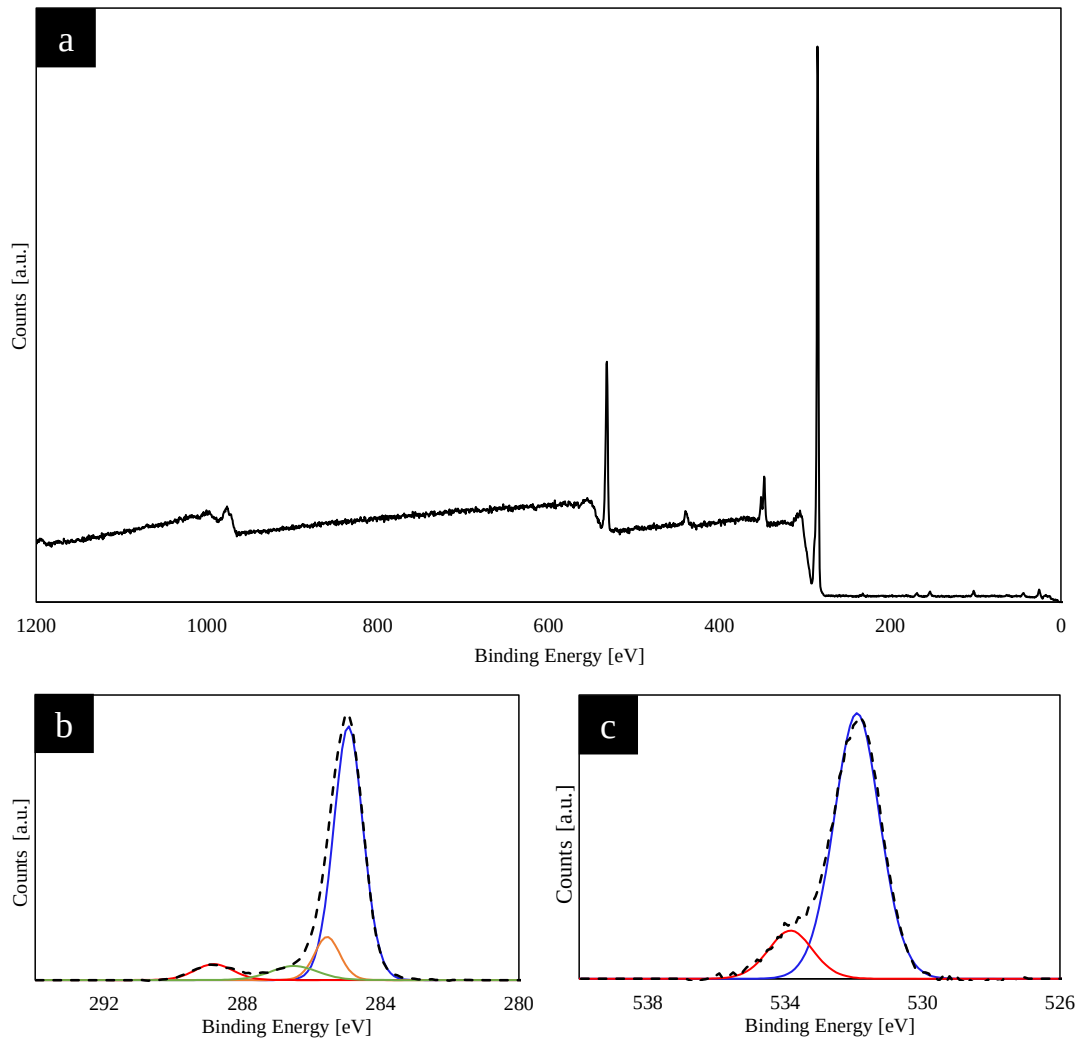

Figure 6.4 XPS spectra for channel 'a' of embossed PMMA: (a) WESS, (b) C 1s spectra and (c) O 1s plots.

Once again, the spectral components indicative of PMMA are present but the relative contributions of four peaks has changed significantly. Analysis of the C 1s spectra shows peak contributions at 284.93, 285.55, 286.50 and 288.83 eV, corresponding to C-H hydrocarbon, C-C-O beta-shifted carbon, C-O methoxy group and O-C=O carbonyl bonds, respectively. C-H and beta-shifted carbon peaks within the aliphatic peak have been identified separately for completeness. Within the O 1s region a doublet consisting of two peaks at 531.91 and 533.84 eV, is present, corresponding to O=C carbonyl and O-C methoxy group oxygen. Both oxygen components are still

present, however the carbonyl peak has increased significantly to 83.7% and the remaining 18.3% representative of O-C bond. Full quantification data is detailed in Table 6.2.

The corresponding 3D AFM images and midpoint x-y line profiles for the channel ‘b’ embossed surface are shown in Figure 6.5.

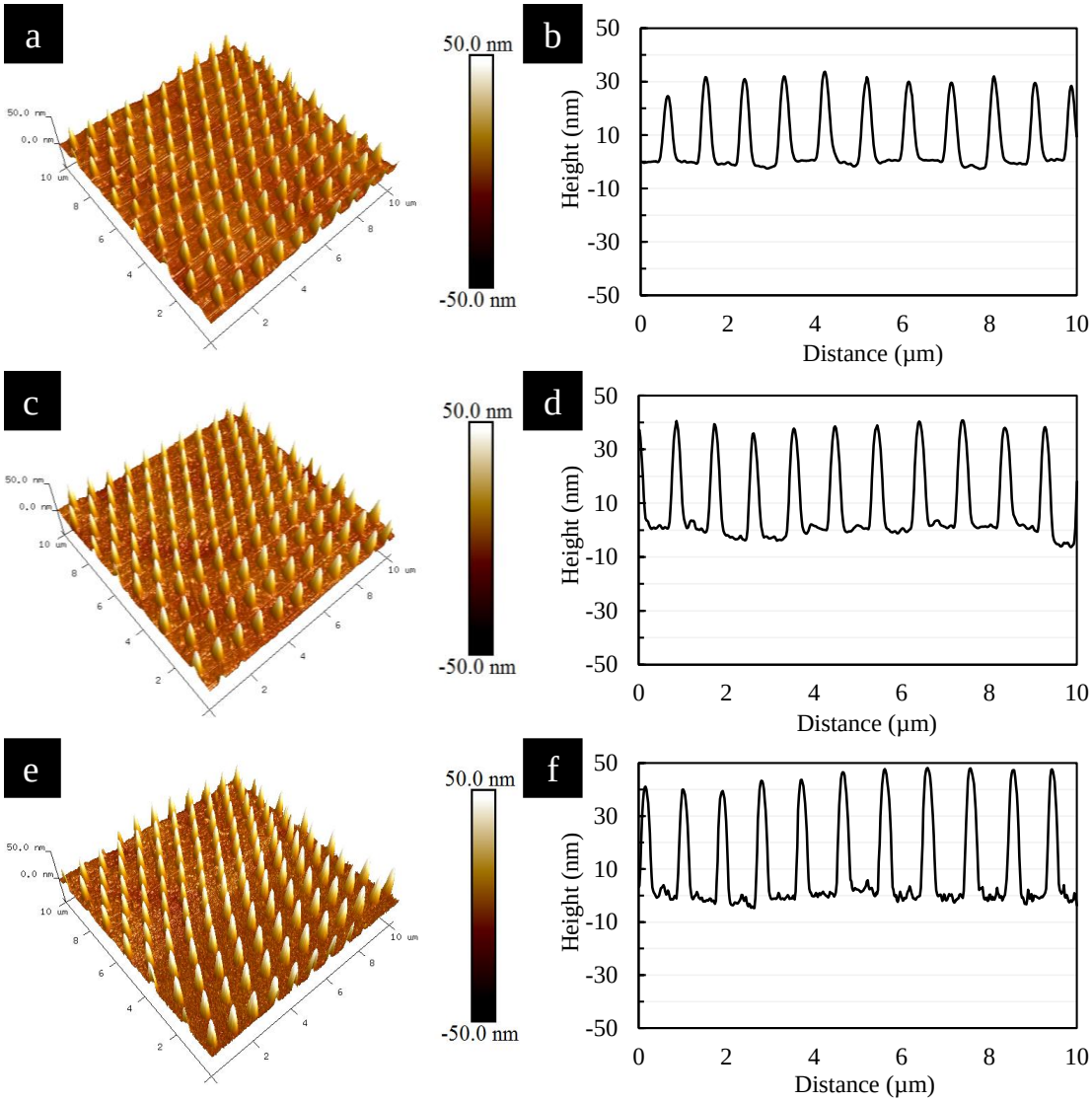

Figure 6.5 10 µm x 10 µm 3D images at (a) edge, (b) centre and (c) off centre areas of channel ‘b’ embossed surfaces, (colour scale ± 50 nm) with corresponding line profiles of the generated from x-y midpoint.

The line profile data in this case shows the features to again be very regular and sharp. The maximum average feature height is approximately 45 nm and FWHM values are 250 nm. The surface roughness parameters are R_a = 4.9 ± 0.5 nm and R_q = 8.1 ± 1.1 nm, respectively.

The WESS and high-resolution C 1s and O 1s scans for channel ‘b’ are displayed in Figure 6. 6 and are very similar to those seen for channel ‘a’.

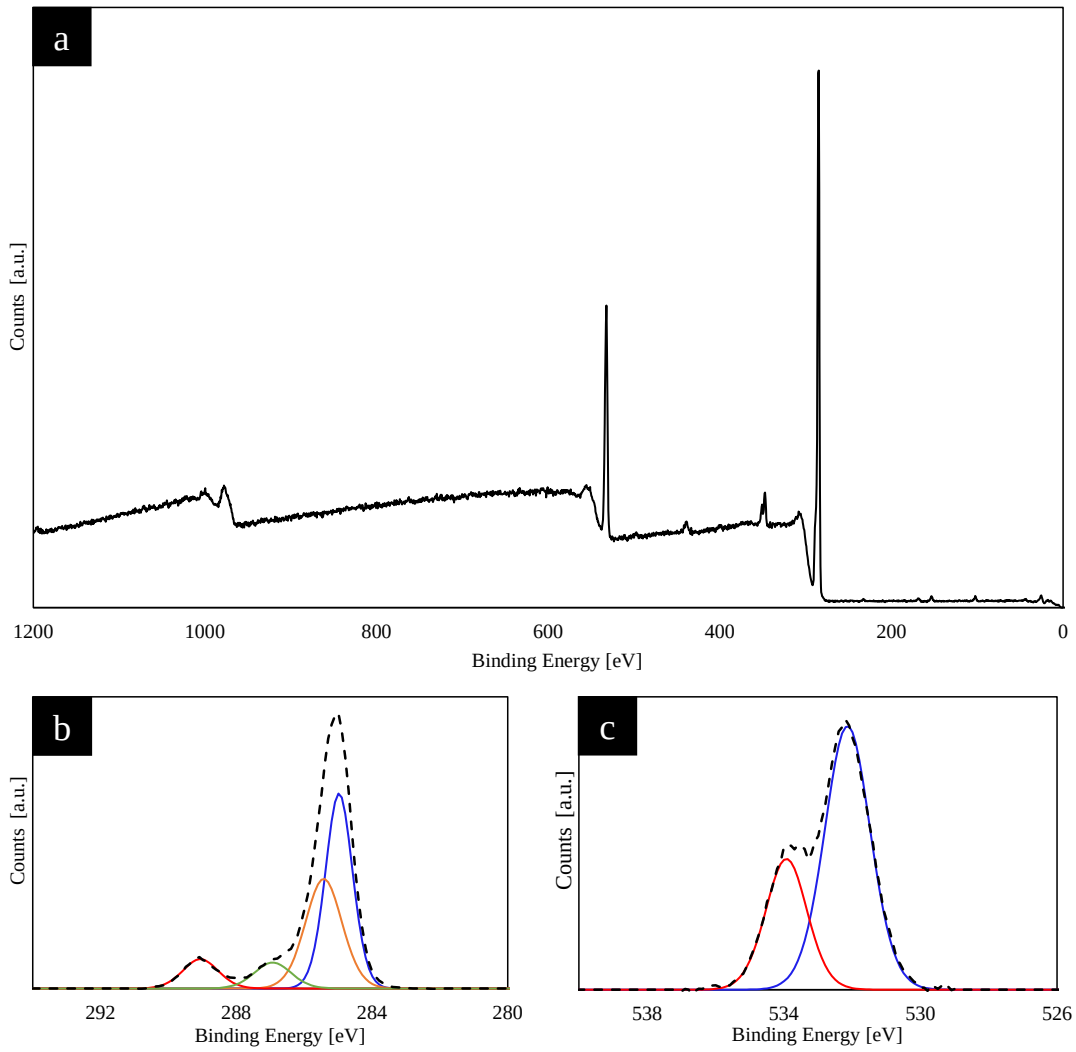

Figure 6. 6 XPS spectra for channel ‘b’ embossed PMMA: (a) WESS, (b) C 1s spectra and (c) O 1s plots.

Charge correction was applied to 285.0 eV once more, where carbon peaks were identified at 284.97, 285.42, 286.93 and 289.06 eV, representative of C-H hydrocarbon, C-C-O beta-shifted carbon, C-O methoxy group and O-C=O carbonyl bonds, respectively. C-H and beta-shifted carbon peaks within the aliphatic peak have been identified separately for completeness. Analysis of the O 1s region indicated a doublet consisting two peaks at 532.13 and 533.92 eV, corresponding to O=C carbonyl and O-C methoxy group oxygens. Atomic concentration (%) within these surfaces shows a higher % O 1s at 15.0 ± 0.64%. Full quantification data is detailed in Table 6.2.

Table 6.2 XPS derived % atomic concentration data for peak fitted C 1s and O 1s contributions for pre-embossed PMMA, channel 'a' and 'b' substrates.

	Sample	C-H (%)	C-C (%)	C-O (%)	C=O (%)	O=C (%)	O-C (%)	% C1s	% O1s
Pre-Embossed	**1**	65.18	13.52	14.26	7.05	60.38	39.62	87.25	12.75
	2	66.24	11.24	15.20	7.31	57.78	42.22	86.85	13.15
	3	65.91	9.32	16.46	8.31	60.42	39.58	84.99	15.01
	Average	65.78	11.36	15.31	7.56	59.53	40.47	86.36	13.64
	St. Dev.	0.54	2.10	1.10	0.67	1.51	1.51	1.21	1.21
Channel 'a'	**1**	76.04	11.16	6.65	6.15	85.16	14.84	89.43	10.57
	2	65.45	22.66	5.70	6.19	84.35	15.65	89.41	10.59
	3	57.51	29.59	6.20	6.70	81.68	18.32	88.73	11.27
	Average	66.33	21.14	6.18	6.35	83.73	16.27	89.19	10.81
	St. Dev.	9.30	9.31	0.48	0.31	1.82	1.82	0.40	0.40
Channel 'b'	**1**	46.69	35.51	8.50	9.30	68.97	31.03	85.55	14.45
	2	52.16	27.95	11.31	8.38	68.53	34.47	85.16	14.84
	3	63.83	11.42	14.83	9.90	64.33	35.67	84.30	15.70
	Average	54.23	24.96	11.55	9.19	67.28	33.72	85.00	15.00
	St. Dev.	8.75	12.32	3.17	0.77	2.56	2.41	0.64	0.64

Water contact angle (WCA) measurements were obtained to evaluate the wettability of the embossed surfaces as reported in Table 6.3.

Table 6.3 WCA values for pristine (pre-embossed) PMMA, and embossed channel 'a' and channel 'b' surfaces.

Substrate	Sample #	Left (θ)	Right (θ)	Average (θ)	St Dev (θ)
Pre-Embossed	1-1	86.58	86.73	88.02	2.97
	1-2	83.56	78.50		
	1-3	86.17	86.44		
	2-1	92.72	92.20		
	2-2	92.32	89.53		
	2-3	87.34	87.86		
	3-1	85.67	85.63		
	3-2	88.99	88.81		
	3-3	94.07	91.21		
Channel 'a'	1-1	78.70	77.41	74.80	2.64
	1-2	76.06	75.72		
	1-3	77.44	78.88		
	2-1	74.63	75.16		
	2-2	68.87	68.81		
	2-3	74.80	70.24		
	3-1	74.96	74.74		
	3-2	78.75	77.08		
	3-3	72.07	72.10		
Channel 'b'	1-1	76.63	76.03	70.63	0.88
	1-2	69.31	69.50		
	1-3	69.39	68.28		
	2-1	71.92	72.65		
	2-2	67.43	67.17		
	2-3	69.79	69.58		
	3-1	71.56	71.64		
	3-2	71.43	70.99		
	3-3	69.29	68.69		

6.3 Biological Assessment of Embossed PMMA Substrates

The hot embossed substrate channels were tested in the DPFA system, with regard to platelet function thereon. Unfortunately, due to the thickness of the PMMA sheet used, the microscope was unable to adequately focus on the channel ‘a’ and ‘b’ areas and so, it was not possible to carry out the study with any degree of accuracy. Figure 6.7 shows a micrograph which highlights the difficulties faced in focusing properly on the surface. Whereas, there are indications of some platelets on or traversing the surface, the image quality is insufficient for any meaningful analysis.

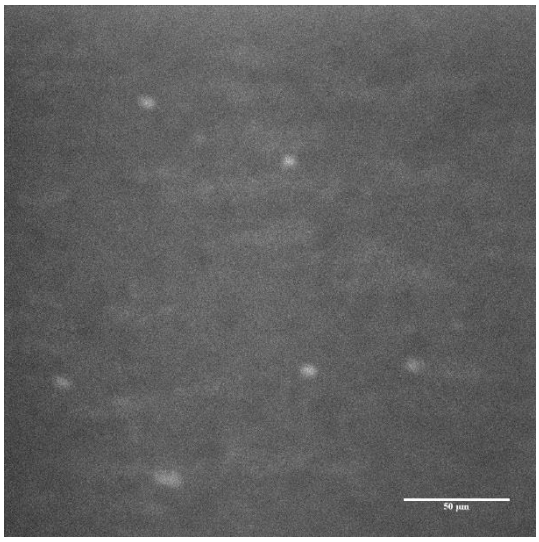

Figure 6.7 Optical micrograph at a random time after blood has contacted the embossed channel ‘a’ surface indicating difficulties focusing on the platelets. Scale bar 50 µm.

Standard DPFA protocol uses a x20 objective lens in an inverted microscope and this changed to a x10 lens to try to sharpen the focus on platelets that may be adhered to the channel. A typical micrograph at this resolution is shown in Figure 6.8 and although this image is slightly improved with respect to showing platelet interaction on channel ‘a’ it is still not of the quality needed to carry out any form of analysis.

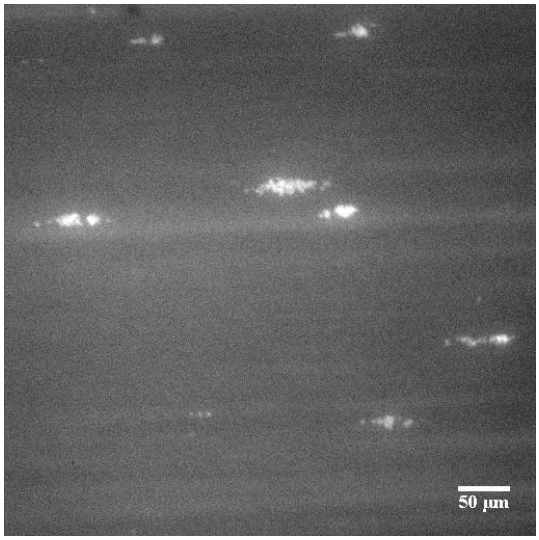

Figure 6.8 Optical micrograph taken using a x10 objective, showing a slightly increased level of focus on platelets within the channel. Scale bar 50µm.

Unfortunately, further work was not possible in this area due to associated access restrictions to the DPFA system.

6.4 Discussion

The main goal of the work reported within this chapter, was to employ hot embossing to create nanoscale features on PMMA sheets that represent those seen on the PS/PMMA spin coated polymer demixed surfaces. This involved the updating of a previously created stamp (die) with a nickel coated surface to enhance its robustness and prevent breakage during operation (which occurred with the original silicon version). The stamp involved has two channels; the difference in which is the feature spacing[14]. The fabrication process allows for creation of substrates with embossed channels that can be tested within the DPFA system. Based on the previous work, it was apparent that the polymer chemistry should remain constant, while a uniform nanotopography is produced for subsequent vWF entrapment and platelet adhesion thereon.

The PMMA sheet used here was characterised to allow for a baseline profile of physical and chemical properties, prior to embossing. Physical analysis of the topography using AFM shows it to have a predominantly flat surface, with R_a and R_q surface roughness values of 1.8 ± 0.2 nm and 2.4 ± 0.2 nm, respectively. The chemical profile for the pristine PMMA sheet was determined by XPS and indicates a surface chemistry consistent with PMMA, with the presence of the four expected carbon environments and oxygen doublet. However, when compared to the spin coated PMMA used previously in this work, it appears that the chemistry is not identical. Table 6.4 summaries the quantitative data obtained from the two types of PMMA.

Table 6.4 Comparison of the quantitative data obtained by deconvolution of the C 1s and O 1s regions for spin coated 100PMMA and pre-embossed PMMA sheets.

Sample Type	C-H (%)	C-C (%)	C-O (%)	C=O (%)	O=C (%)	O-C (%)	% C1s	% O1s
PMMA_ solvent cast	38.28	18.60	28.97	14.15	42.12	57.87	75.98	24.02
PMMA Pre-embossed Sheet	65.78	11.36	15.31	7.56	59.53	40.47	86.36	13.64

Atomic concentration of C 1s increases by 10% for the pristine PMMA sheet, compared with the solvent cast PMMA surface. Specifically, the hydrocarbon C-H bond contribution increases by 27.5%, with all other peaks showing a decrease by approximately 50%. O 1s concentration therefore decreases by the same 10%, as the compound contains only carbon and oxygen. Deconvolution of the O 1s doublet shows a 17% increase in the carbonyl O=C bond for the pristine PMMA sheet, with the resultant decrease in methoxy oxygen (O-C). The characteristic contributions for carbon environments within the C 1s XPS spectra for the pre-embossed PMMA sheet are different than those expected[127]. This is thought to be as a result of polymer processing that is used to create the sheet form material. In this regard, it is deemed that the extrusion process causes changes to very uppermost surface chemistry that is evident due to the small depth of analysis of the technique. This results in a significant increase in the aliphatic component in the C 1s envelope for the sheet which them suggests that deoxygenation has occurred. Comparison against the spin coated control surface, shows that chemical profiles are not identical, and therefore should be considered as a factor which could influence platelet interaction.

Channel ‘a’ created by embossing PMMA result in the required highly regulated arrays of features with average height between 35 nm and 50 nm, for a stamp designed to fabricate 50 nm islands. Previous work completed using a stamp of similar design but without a nickel coating, reported inconsistencies with island heights and this was linked to air pockets becoming trapped between the stamp and PMMA substrate, causing incomplete transfer of features[14].

XPS analysis of the PMMA surface chemistry post-embossing revealed a tangible degree of deoxygenation. Quantitative analysis of % atomic concentration shows a C 1s contribution of 89.2 ± 0.4% and an O 1s concentration of 10.8 ± 0.4%, for channel ‘a’. Comparison of deconvoluted C 1s components, between pristine PMMA and channel ‘a’ substrates, show an increase of approximately 10% for beta-shifted carbon, a decrease of 9.1% in the C-O component, meanwhile hydrocarbon and carbonyl components remained of a similar magnitude. O 1s components change via an increase of 24% from O=C carbonyl and a decrease of same, in O-C bonding concentration. These changes in surface chemistry may cause a source of variation in biological response[163,164] which need to be considered when haematological analysis of these surfaces is carried out.

In the case of embossed PMMA channel ‘b’ the feature density has decreased as expected, due to the greater interspacing. The average island feature height is in the range 32 nm to 45 nm. This variability may be due to the fact that one of the vacuums used during embossing this features reported a faulty vacuum which may have affected the pressure between the stamp and PMMA sheet[165]. The irregular protrusions noted as occurring between the island features are less prominent here with surface roughness parameters of R_a and R_q 4.9 ± 0.5 nm and 8.1 ± 1.1 nm, respectively. It is assumed that this is mainly due to the greater space between features which dissipates

air more effectively during polymer surface cooling. However, the problem with the vacuum uniformity during embossing noted above cannot be ruled out as a contributory factor.

XPS analysis of channel ‘b’ shows % atomic concentrations of 85.00 ± 0.64% and 15.00 ± 0.64% for C 1s and O 1s, respectively. Compared to channel ‘a’ C 1s shows a decrease of 4.2%. Specifically, this is shown by a 10% fall in C-H hydrocarbon peak contribution. Methoxy group carbon contribution doubles to 11.6%, similar to that of pristine PMMA. The remaining carbon environments increase by approximately 3%. O 1s spectra shows increase of O-C component to 33.72%, nearly double that of channel ‘a’, whilst O=C contribution decreases by 15%, approximately. It is unlikely that the differences between the XPS quantification data for channel ‘b’ and channel ‘a’ are due to the spacing variation and are more likely to be due to the unintentional change in the vacuum conditions during embossing.

WCA was employed here to compare the wettability of the PMMA channels with that of the pristine (pre-embossed) surface and indicates a decrease in contact angle for the embossed regions. WCA was employed to qualitatively determine surface energetics and identify substrates are hydrophilic or hydrophobic; no quantitative studies have been undertaken. A decrease of 14˚ is observed between pre-embossed PMMA and the channel ‘a’ region. Published literature suggests that as surface roughness increases, contact angle decreases for hydrophilic surfaces[166]. However, for the channel ‘b’ surfaces, even though the surface roughness decreases by 4.9 nm, the contact angle still falls by 4.17˚. Reasons for this may be due to the changes in surface chemistry or surface roughness, however, can also be totally reliant on differences in polymer bonds at the uppermost surface[167]. However, the values obtained show that all substrates are hydrophilic as their contact angle is < 90˚[168]. It

has been reported that even homopolymers such as poly vinyl chloride (PVC) and PMMA, have heterogenous surfaces whereby the low energy polymer and the high energy component may be provided by contaminant groups resulting from the "*incorporation of initiator fragments at the ends of the polymer chains during the polymerisation process*"[169].

Unfortunately, it was not possible to carry out DPFA haematological analysis on the embossed PMMA nanoscale features created due to problems with focusing the objective lens due to the thickness of the PMMA. Although there may be some platelets on the images obtained, the quality does not allow any form of meaningful analysis to be carried out. Attempts to view the embossed channels more clearly using a x10 objective were made but did not result in additional clarity as although the level of focus was somewhat improved, the micrograph images are still not adequately in focus.

Overall, the advances made here with respect to the provision of a highly reproducible embossed nanotopography suggest that these samples should be studied further but that this will require significant adjustments to the DPFA measurement system that are outside the scope of the current study.

7. Conclusion and Recommendations for Future Study

7.1 Conclusions

The aim of this research was to create a synthetic substrate surface that is capable measuring dynamic platelet function in an environment that is close to *in vivo* physiology, such that the data generated can advance clinical diagnostic testing for conditions such as vWD. In doing so, the substrate concerned must measure the interaction of platelets with vWF in a manner that reflects the biological processes associated with haemostasis and particularly, thrombus formation.

The starting point for the work is the creation of nanoscale topography capable of entrapping vWF from whole blood when it is perfused over it at arterial shear flow rates and that therefore creates a surface that can then interact with the platelets from the same patient blood sample at the same flow rates. Measurement of the resulting platelet adhesion and aggregation will then form the basis of an advanced PFT. In this regard, the specification for the new test sensor surface requires it to substitute for a substrate coated with immobilised endogenous vWF in the DPFA device developed at RCSI, Dublin, Ireland. In this test regime, platelets in donor whole blood are fluorescently labelled and perfused over the (endogenous vWF) surface at a flow rate of 75 μl/min equivalent to an arterial shear rate of 1500 s^{-1}. An inverted microscope equipped with a high-resolution video camera is used to image the platelet surface interactions such that various parameters relating to their function can be determined.

Spin coating of a polystyrene (PS)/poly(methyl methacrylate) (PMMA) polymer demixed solution comprising 25%PS/75%PMMA in 3% w/v chloroform (25PS75PMMA) onto glass slides under a positive pressure (purge) of nitrogen gas has been shown by optical phase contrast microscopy to result in PS distributed within

PMMA in honeycomb-like and striation configurations. AFM analysis has shown that this condition results in the creation of a sub-micron to nanoscale topography with feature that range from nanopits of depth -70 nm to nanoislands +50 nm in height and FWHM ranging between 2 and 4 μm for larger features with nanoislands in the range ~ 100 nm to 1 μm. Features can adhere platelets from flowing blood and by association entrap vWF. By contrast, control surfaces spin coated from 100% PS and 100% PMMA solutions in chloroform showed flat topographies with nanopits of depth -10 nm for PS and nanoislands that were up to 5 nm in height for PMMA. The chemistry of this surface was found to be solely that of the PMMA component. However, the substrates produced in this way show significant levels of variability in respect to platelet response which is deemed to be due to irregularity of the surface nanopit/nanoisland features present. Hence, there is a need to improve the processing methodology by which these coatings are produced or to use an alternative means to attain a more optimal topography.

Initial studies focused on improving the regularity and reproducibility of the nanoscale topography of the 25PS75PMMA blend, under a positive pressure nitrogen purge, by introducing uniform 50 μm PS microspheres in the range of 375 to 1500 microspheres/ml. Augmentation of the stock polymer demixed solution (25PS75PMMA in chloroform) has been undertaken to disrupt the fluid dynamics during spin coating. In this way, it offers a means to modify the original distribution of PS and thereby further refine the resulting surface features. With the addition of +375 microspheres/ml the topography produced was similar to that of the original 25PS75PMMA substrates; micron features FWHM 2–3 μm overlaid with nanoscale protrusions (FWHM 100-500 nm), ranging between ±50 nm. However, adding +750 microspheres/ml produced more ordered nanoscale topography. AFM analysis of this

surface indicated nanoisland features with heights ranging from 30 to 50 nm and no discernible nanopits. Addition of +1500 microspheres/ml showed an ordered landscape, with nanoisland features of heights up to 30 nm. Chemical characterisation of all these surfaces confirmed that they were still comprised solely of PMMA with no PS contribution detected by XPS.

The response of fluorescently labelled platelets in flowing blood at arterial shear rates to these substrates was assessed using the RSCI-DPFA device and revealed a positive interaction with all substrates. However, due to the similarity in topography between 25PS75PMMA and 25PS75PMMA_375, the latter was not investigated further. As platelet interactions on these surfaces are only possible in the presence of vWF that is uncoiled to expose the required binding sites, it is apparent that protein entrapment has been achieved. The average platelet surface coverage for the refined nanoscale topography created in the presence of the PS microspheres was higher than that recorded for the original surface but showed a large standard deviation (19.08 ± 12.59% for 25PS75PMMA_750 compared to 13.9 ± 6.6% for 25PS75PMMA). Although the standard deviation associated with the average platelet coverage on the 25PS75PMMA_1500 substrate was much lower (10.88 ± 4.11%), it had the lowest amount of platelet-surface interactions at the point of measurement, and so it was decided not to progress any further with this substrate. Hence, it is asserted that the nanoisland feature size height and their distribution on the 25PS75PMMA_1500 is nonoptimal in the context of the requirements for a synthetic DPFA sensor.

An algorithm developed by RSCI researchers to interpret platelet kinetics more accurately on the immobilised vWF sensor substrate attained from the DPFA technique, was applied to the data acquired in this work. The results obtained revealed that the information pertaining to platelet dynamics from the same donor blood on the

25PS75PMMA and 25PS75PMMA_750 substrate surfaces were significantly different to those measured for the standard (endogenous immobilised vWF) sensor surface. This outcome is perhaps to be expected due to the difference in the way the vWF is presented on each type of substrate, i.e. it is present from the outset for the immobilised surface but must be acquired (entrapped) in the case of the synthetic PS/PMMA demixed coatings. However, overall there were no significant differences observed between the 25PS75PMMA and 25PS75PMMA_750 surfaces such that the changes to the topography induced by the inclusion of the microspheres in the spin coating solutions did not seem to influence platelet kinetic behaviour as determined in the same manner as that currently employed in the DPFA device.

The next stage of substrate development focused on manipulation of the topography by spin coating the 25PS75PMMA blend with and without +750 microspheres/ml in air under ambient pressure rather than under the positive pressure nitrogen (purge) used previously. The majority of previously reported studies for spin coating of polymer demixed solutions have been carried out in the presence of a positive pressure of nitrogen. However, other evidence from the literature suggests that removal of this nitrogen purge to conduct the same fabrication process in air under ambient conditions influences the attendant topography. Hence, both the 25PS75PMMA and 25PS75PMMA_750 solutions were spin coated onto glass slides under these alternative conditions. It should be noted that the spin coating parameters used were not identical in both cases as the ambient air conditions could not be attained on the original equipment and required a separate device. Physical characterisation of the surfaces produced, using AFM, revealed a significant change from that seen for the nitrogen purge spun surfaces. The features created in 25PS75PMMA_air thin films comprised from nanopits of depth -100 nm to nanoislands 70 nm in height and FWHM

ranging between 500 nm-1 µm. 25PS75PMMA_750_air substrates also demonstrated features of ±140 nm in height and FWHM <1 µm, as such they are "sharper" than those formed under nitrogen purge conditions. As before, XPS analysis showed that the chemistry of the uppermost surface of these polymer layers spin coated in air is solely that of PMMA.

Platelet response to air-spun substrates was assessed within the RCSI-DPFA system and exhibited a positive response for both 25PS75PMMA_air and 25PS75PMMA_750_air surfaces. Although differences in the physical and chemical properties of the substrates were moderate, the average platelet coverage was shown to change considerably (40.20 ± 13.30% for 25PS75PMMA_750_air compared with 17.30 ± 6.80% for 25PS75PMMA_air). Application of the RSCI autologous platelet algorithm revealed that the dynamic parameters determined for the platelets were not significantly different between air-spun and nitrogen purge spun surfaces. This suggests that whereas the platelet coverage at the point of analysis changes this is not influenced by the preceding kinetics of their interactions with the surfaces and that the values measured are not influenced by changes in surface topography. However, the dynamic characterisation of the platelets from the same donor blood showed significant differences between the entrapped autologous vWF and endogenous immobilised vWF substrate.

Notwithstanding some variation within the n=5 DPFA runs and the associated kinetic parameter measurements, the 25PS75PMMA_750_air substrate proved capable of providing for enhanced platelet surface coverage. As such, it was further tested for its ability to evoke a platelet response from multiple blood groups as the basis of a clinical diagnostic test. Platelet function for a cohort of six healthy donors; all female, aged between 24 – 50 years old, with varying blood types, was investigated.

All blood types showed a positive platelet response with the 25PS75PMMA_750_air surface, although some variation was still present within the various sample sets. Interestingly, blood type AB donors displayed higher levels of platelet coverage (43.60 ± 20.70%) than any of the other blood groups. Unfortunately, it was not possible to use the RSCI DPFA algorithm analysis on these datasets due to a slight variation that was made during acquisition.

The final body of work undertaken here addressed fabrication of a highly reproducible nanotopography, with features similar to that formed on spin coated films that can entrap vWF in a manner that provides for subsequent platelet activity thereon. In this way, the random nature of spin coating as a variable for surface coverage deviation can be eliminated. Hot embossing of PMMA was used to produce 50 nm nanoislands in channels that align with the flow ports in the DPFA sensor. AFM characterisation of the resulting surfaces has shown that a high degree of accuracy can be attained, particularly with regard to feature spacing. Moreover, the nickel coated stamp template produced for this work was shown to be robust enough to withstand multiple sample fabrication. XPS analysis revealed that the PMMA sheets used for embossing were of a different quality to the PMMA (particles) used for spin coating. Unfortunately, it was not possible to measure platelet activity on these PMMA films, However, there is no reason to believe that they are not capable of doing so but this will require a redesign of the RCSI DPFA device which was outside the scope of the work undertaken here.

In summary, the core objectives of the thesis have been achieved as follows:

1. Successful refinement of topography by the introduction of microspheres and change of pressure conditions.

Addition of 50 µm microspheres to a 25PS75PMMA polymer demixed solution in chloroform changes the distribution of the PS particles within the PMMA matrix after spin coating. Platelet coverage increased on this surface as a result of the refinement in the attendant nanotopography. Air-spun coatings created topographies which increased the level of platelet adhesion further when compared to those created in a nitrogen purge.

2. Assessment of platelet dynamics using a novel autologous platelet algorithm.

This work went beyond the standard visual analysis of platelet coverage assessment to consider the kinetic behaviour of platelets with the same patient's vWF using a novel data analysis algorithm. Modification of an approach developed for the endogenous immobilised vWF sensor substrate has provided a means to better assess platelet kinetic behaviour on the surface topographies created on the synthetic autologous vWF surfaces. The dynamic interaction of platelets was found not to change significantly between samples fabricated under nitrogen purge and ambient air spin coating conditions for either the original or, microsphere-augmented substrates. Importantly, all the immobilised vWF substrates showed platelet activity thereon indicating that not only are they capable of entrapment of vWF but that the conformation of the adhered protein provides for its uncoiling to make available platelet binding sites. Moreover, the kinetic behaviour of the platelets in contact with the entrap and uncoiled vWF is responsive to changes in surface topography while remaining physiologically relevant.

3. Haematological analysis with a cohort of multiple ABO subjects.

In this work a polymer demixed surface augmented with PS microspheres has been investigated for the first time in regard to testing platelet activity within a group of

donors with varied blood type (ABO). Overall, the polymer demixed spin coated surfaces show a positive response for all blood groups. Apparent differences between blood group type are suggested in respect to platelet adhesion but limited to very small patient numbers.

4. Production of highly reproducible features via hot embossing.

Hot embossing of PMMA produced highly defined and repeatable nanoscale topographical features of the same dimensions as those produced by spin coating from the 25PS75PMMA solutions in chloroform. Preliminary analysis of the response of flowing blood on this surface proved positive but requires adjustments to the DPFA apparatus that were not possible to make at this time. However, this research gives reason to believe that, with the correct apparatus, these surfaces could facilitate a repeatable platelet interaction.

Overall, the outputs from this research provide new information that significantly enhances understanding of the surface features that can measure platelet interactions with vWF from a single patient blood sample. In this way, refinement of the DPFA with a surface that facilitates quantitative assessment of platelet adhesion and evaluation of dynamic kinetic behaviour, which can be used to further improve the clinical diagnostic pathway for vWD, is closer. This work offers additional insight into the role that topography plays in vWF uncoiling that leads to platelet tethering and binding in a manner that leads to thrombus formation in a way that mimics the *in vivo* situation.

In order to further advance the methodologies developed here, the limitations of the studies and how to overcome them needs to be considered:

- With respect to the dynamic evaluation method, modifications were made to a previously published algorithm, but this was after the datasets from the DPFA were collected. Some of the image stacks were prescribed in a different way from the inputs required for the dynamic algorithm and so limited the value of the analysis overall;
- There was a major limitation in applying the DPFA methodology to embossed PMMA substrates. Thickness was the main concern here and so limited any accurate, biological assessment of the surfaces. As it was not possible to re-configure the system to better accommodate these polymer substrates this is a limitation of note, and
- There was a lack of "unhealthy" vWD-diagnosed donor blood available for the DPFA studies and so it was not possible to compare the vWF entrapment for blood from these patients to that for the healthy donors and so a threshold to determine healthy levels of platelet adhesion was achieved as opposed to unhealthy limits for the assessment of the technique for vWD diagnosis.

7.2 Recommendations for future study

The results presented within this thesis have successfully answered key aspects of the research questions addressed. However, in order to develop this area further, the following aspects should be explored in future work;

1. Although it has been possible to show that the topography created by augmentation of 25PS75PMMA spin coating solutions is capable of enhanced vWF entrapment, as indicated by higher surface coverage values, data from a larger sample set is required to better understand the relationships involved.

2. Further refinement is needed of the algorithm for analysis of platelet kinetics for use with polymer demixed surfaces capable of autologous vWF entrapment. It is believed that with a pre-determined dataset, further evaluation of the efficacy and refinement of the software could be completed to aid more accurate results and in particular, address variation in the Ntracks values.
3. Work carried out to create relevant topography via hot embossing of PMMA proved that the nickel coated stamp was a significant improvement on that used in previous studies. However, as surface chemistry is known to be a contributing factor to cell/protein interactions, the differences between that of post embossing and the PS/PMMA spin coating, requires additional consideration. Moreover, as the thickness of the PMMA sheet needed for embossing makes it difficult to fit into the current DPFA device, a new configuration needs to be developed to allow this to be part of a platelet function assay.
4. In the case of all assay substrates, an increased pool of donor blood from defined types is essential to gain a better insight on the robustness of the new synthetic surfaces as a sensor for the diagnosis of vWD and associated diseases that effect vWF/platelet interactions. Increasing the cohort in a wider study, encompassing different blood groups and genders, will facilitate a truer representation of platelet adhesion characteristics associated with healthy and unhealthy blood samples on these polymer topographies. This is crucial to further develop the utility and applicability of this new sensor surface, so as to further improve on current vWF/platelet function tests.

8. References

1. Palta S, Saroa R, Palta A. Overview of the coagulation system. Indian J Anaesth. 2014 Sep;58(5):515–23.

2. Schulze H, Shivdasani RA. Mechanisms of thrombopoiesis. J Thromb Haemost. 2005;3(8):1717–24.

3. Hoffman R, Benz EJ, Silberstein LE, Heslop H, Anastasi J, Weitz J. Hematology: Basic Principles and Practice. 6th ed. Elsevier Science; 2013. 2343 p.

4. Margetic S. Inflammation and haemostasis. Biochem medica [Internet]. 2012;22(1):49–62. Available from: http://www.ncbi.nlm.nih.gov/pubmed/22384519%0Ahttp://www.pubmedcentral.nih.gov/articlerender.fcgi?artid=PMC4062321

5. Ratner BD, Hoffman AS, Schoen FJ, Lemons JE. Biomaterials Science: An Introduction to Materials in Medicine [Internet]. Elsevier Science; 2012. Available from: https://books.google.co.uk/books?id=8hBq-dLLaxwC

6. Sadler JE, Budde U, Eikenboom JCJ, Favaloro EJ, Hill FGH, Holmberg L, et al. Update on the pathophysiology and classification of von Willebrand disease: a report of the Subcommittee on von Willebrand Factor. J Thromb Haemost [Internet]. 2006 Aug 2;4(10):2103–14. Available from: https://doi.org/10.1111/j.1538-7836.2006.02146.x

7. Favaloro EJ, Pasalic L, Curnow J. Laboratory tests used to help diagnose von Willebrand disease: an update. Pathology. 2016;48(4):303–18.

8. PAPAIOANNOU T, STEFANADIS C. Vascular Wall Shear Stress: Basic Principles and Methods. Hell J Cardiol. 2005;46:9–15.

9. Provenzale I, Brouns SLN, Meijden PEJ Van Der, Swieringa F, Heemskerk JWM. Whole Blood Based Multiparameter Assessment of Thrombus Formation in Standard Microfluidic Devices to Proxy In Vivo Haemostasis and Thrombosis. 2019;

10. Cowman J, Müllers S, Dunne E, Ralph A, Ricco AJ, Malone FD, et al. Platelet

behaviour on von Willebrand Factor changes in pregnancy: Consequences of haemodilution and intrinsic changes in platelet function. Sci Rep. 2017;7(1):1–7.

11. Cowman J, Quinn N, Geoghegan S, Müllers S, Oglesby I, Byrne B, et al. Dynamic platelet function on von Willebrand factor is different in preterm neonates and full-term neonates: changes in neonatal platelet function. J Thromb Haemost. 2016;14(10):2027–35.

12. Lincoln B, Ricco AJ, Kent NJ, Basabe-Desmonts L, Lee LP, MacCraith BD, et al. Integrated system investigating shear-mediated platelet interactions with von Willebrand factor using microliters of whole blood. Anal Biochem [Internet]. 2010;405(2):174–83. Available from: http://dx.doi.org/10.1016/j.ab.2010.05.030

13. Roest M, Reininger A, Zwaginga JJ, King MR, Heemskerk JWM. Flow chamber-based assays to measure thrombus formation in vitro: Requirements for standardization. J Thromb Haemost. 2011;9(11):2322–4.

14. Bishop D, Meenan BJ. Bespoke Nanotopography for the Selective Capture of vWF from Whole Blood at Arterial Shear: A Potential Diagnostic Platflorm. Ulster University; 2016.

15. Dunne E, Kenny D. Why is Blood Group a Risk Marker for Myocardial Infarction? Royal College of Surgeons in Ireland; 2016.

16. Tyona MD. A theoritical study on spin coating technique. Adv Mater Res [Internet]. 2013 Dec 25;2(4):195–208. Available from: http://koreascience.or.kr/journal/view.jsp?kj=TPTPLG&py=2013&vnc=v2n4&sp=195

17. Heemskerk JWM, Sakariassen KS, Zwaginga JJ, Brass LF, Jackson SP, Farndale RW. Collagen surfaces to measure thrombus formation under flow: Possibilities for standardization. J Thromb Haemost. 2011;9(4):856–8.

18. Boretos JW, Eden M, (U.S.) NI of H. Contemporary Biomaterials: Material and Host Response, Clinical Applications, New Technology, and Legal Aspects [Internet]. Noyes Data; 1984. Available from:

https://books.google.co.uk/books?id=2c5pAAAAMAAJ

19. Le X, Poinern GEJ, Ali N, Berry CM, Fawcett D. Engineering a biocompatible scaffold with either micrometre or nanometre scale surface topography for promoting protein adsorption and cellular response. Int J Biomater. 2013;2013.

20. Kasemo B. Biological surface science. 2002;500:656–77.

21. Rechendorff K, Hovgaard MB, Foss M, Zhdanov VP, Besenbacher F. Enhancement of Protein Adsorption Induced by Surface Roughness. 2006;10885–8.

22. Curtis A, Wilkinson C. Nantotechniques and approaches in biotechnology. Trends Biotechnol. 2001;19(3):97–101.

23. Curtis ASG, Varde M. Control of Cell Behaviour - Topological Factors. J Natl Cancer Inst. 1964;33:15–26.

24. Clark P, Dow JAT. Wilkinson CD Cell guidance by ultrafine topography in vitro Cell guidance by ultrafine topography in vitro. 1991;(June).

25. Hardin J, Bertoni G, Kleinsmith LJ. Becker's World of the Cell [Internet]. Pearson; 2014. Available from: https://books.google.co.uk/books?id=GkS-oAEACAAJ

26. Curtis AS, Wilkinson CD. Reactions of cells to topography. J Biomater Sci Polym Ed. 1998;9(12):1313–29.

27. Fitton JH, Dalton BA, Beumer G, Johnson G, Griesser HJ, Steele JG. Surface topography can interfere with epithelial tissue migration. J Biomed Mater Res. 1998 Nov;42(2):245–57.

28. Dalby MJ, Riehle MO, Johnstone H, Affrossman S, Curtis ASG. In Vitro Reaction of Endothelial Cells to Polymer Demixed Nanotopography. Biomaterials. 2002;23:2945.

29. Lord MS, Foss M, Besenbacher F. Influence of Nanoscale Surface Topography on Protein Adsorption and Cellular Response. Nano Today. 2010;5:66.

30. Christenson EM, Anseth KS, Beucken JJJP Van Den, Chan CK, Ercan B, Jansen JA, et al. Nanobiomaterial Applications in Orthopedics.

2007;(January):11–22.

31. Vogler EA. Interfacial chemistry in biomaterials science. In: Wettability. New York, NY, USA; 1993. p. 184–250.

32. Anselme K, Davidson P, Popa AM, Giazzon M, Liley M, Ploux L. The interaction of cells and bacteria with surfaces structured at the nanometre scale. Acta Biomater [Internet]. 2010;6(10):3824–46. Available from: http://dx.doi.org/10.1016/j.actbio.2010.04.001

33. Blood Basics - American Society of Hematology [Internet]. [cited 2020 Jan 28]. Available from: https://www.hematology.org/Patients/Basics/

34. White JG. Chapter 7 - Platelet Structure. In: Michelson AD, editor. Platelets (Third Edition) [Internet]. Third Edit. Academic Press; 2013. p. 117–44. Available from: http://www.sciencedirect.com/science/article/pii/B9780123878373000079

35. Andrews RK, Berndt MC. Platelet physiology and thrombosis. Thromb Res. 2004;114(5–6):447–53.

36. Chung I, Lip GYH. Platelets and heart failure. Eur Heart J [Internet]. 2006 Oct 6;27(22):2623–31. Available from: https://doi.org/10.1093/eurheartj/ehl305

37. van der Meijden PEJ, Heemskerk JWM. Platelet biology and functions: new concepts and clinical perspectives. Nat Rev Cardiol [Internet]. 2019;16(3):166–79. Available from: https://doi.org/10.1038/s41569-018-0110-0

38. Fuchs B, Budde U, Schulz A, Kessler CM, Fisseau C, Kannicht C. Flow-based measurements of von Willebrand factor (VWF) function: Binding to collagen and platelet adhesion under physiological shear rate. Thromb Res [Internet]. 2010;125(3):239–45. Available from: http://dx.doi.org/10.1016/j.thromres.2009.08.020

39. Ajjan R, Grant PJ. Coagulation and atherothrombotic disease. Atherosclerosis. 2006;186(2):240–59.

40. Ranucci M, Laddomada T, Ranucci M, Baryshnikova E. Blood viscosity during coagulation at different shear rates. Physiol Rep [Internet]. 2014 Jul 3;2(7):e12065. Available from:

https://www.ncbi.nlm.nih.gov/pubmed/24994896

41. Putnam F. The Structure of the Plasma Proteins. In: The Plasma Proteins V4: Structure, Function and Genetic Control. Elsevier; 2012. p. 42–146.

42. Qiu Y, Ciciliano J, Myers DR, Tran R, Lam WA. Platelets and physics: How platelets "feel" and respond to their mechanical microenvironment. Blood Rev [Internet]. 2015;29(6):377–86. Available from: http://dx.doi.org/10.1016/j.blre.2015.05.002

43. Colman RW. Hemostasis and Thrombosis: Basic Principles and Clinical Practice [Internet]. Lippincott Williams & Wilkins; 2006. Available from: https://books.google.co.uk/books?id=Tz1V8BS5f-YC

44. Savage B, Saldívar E, Ruggeri ZM. Initiation of platelet adhesion by arrest onto fibrinogen or translocation on von Willebrand factor. Cell. 1996;84(2):289–97.

45. Savage B, Almus-Jacobs F, Ruggeri ZM. Specific synergy of multiple substrate-receptor interactions in platelet thrombus formation under flow. Cell. 1998;94(5):657–66.

46. Ikeda Y, Handa M, Kawano K, Kamata T, Murata M, Araki Y, et al. The Role of von Willebrand Factor and Fibrinogen in Platelet Aggregation under Varying Shear Stress. 1991;87(April):1234–40.

47. Valentijn KM, Sadler JE, Valentijn JA, Voorberg J, Eikenboom J. Functional architecture of Weibel-Palade bodies. Blood [Internet]. 2011/01/25. 2011 May 12;117(19):5033–43. Available from: https://www.ncbi.nlm.nih.gov/pubmed/21266719

48. Kanaji S, Fahs SA, Shi Q, Haberichter SL, Montgomery RR. Contribution of platelet vs. endothelial VWF to platelet adhesion and hemostasis. J Thromb Haemost [Internet]. 2012 Aug;10(8):1646–52. Available from: https://www.ncbi.nlm.nih.gov/pubmed/22642380

49. Spiel AO, Gilbert JC, Jilma B. Von Willebrand Factor in Cardiovascular Disease. Circulation [Internet]. 2008 Mar 18;117(11):1449–59. Available from: https://www.ahajournals.org/doi/10.1161/CIRCULATIONAHA.107.722827

50. Zhou Y-F, Eng ET, Zhu J, Lu C, Walz T, Springer TA. Sequence and structure

relationships within von Willebrand factor. Blood [Internet]. 2012 Jul 12;120(2):449–58. Available from: https://www.ncbi.nlm.nih.gov/pubmed/22490677

51. Ganderton T, Berndt MC, Chesterman CN, Hogg PJ. Hypothesis for control of von Willebrand factor multimer size by intra-molecular thiol-disulphide exchange. J Thromb Haemost. 2007;5(1):204–6.

52. Li Y, Choi H, Zhou Z, Nolasco L, Pownall HJ, Voorberg J, et al. Covalent regulation of ULVWF string formation and elongation on endothelial cells under flow conditions. J Thromb Haemost. 2008 Jul;6(7):1135–43.

53. Jenkins PV, O'Donnell JS. ABO blood group determines plasma von Willebrand factor levels: A biologic function after all? Transfusion. 2006;46(10):1836–44.

54. Ruggeri ZM. Platelet adhesion under flow. Microcirculation [Internet]. 2009 Jan;16(1):58–83. Available from: https://www.ncbi.nlm.nih.gov/pubmed/19191170

55. Aponte-Santamaría C, Huck V, Posch S, Bronowska AK, Grässle S, Brehm MA, et al. Force-sensitive autoinhibition of the von Willebrand factor is mediated by interdomain interactions. Biophys J [Internet]. 2015 May 5;108(9):2312–21. Available from: https://www.ncbi.nlm.nih.gov/pubmed/25954888

56. Yago T, Lou J, Wu T, Yang J, Miner JJ, Coburn L, et al. Platelet glycoprotein Ibalpha forms catch bonds with human WT vWF but not with type 2B von Willebrand disease vWF. J Clin Invest [Internet]. 2008/08/21. 2008 Sep 2;118(9):3195–207. Available from: https://www.ncbi.nlm.nih.gov/pubmed/18725999

57. Franchini M, Favaloro EJ, Targher G, Lippi G. ABO blood group, hypercoagulability, and cardiovascular and cancer risk. Crit Rev Clin Lab Sci [Internet]. 2012 Aug 1;49(4):137–49. Available from: https://doi.org/10.3109/10408363.2012.708647

58. Sarode R, Goldstein J, Sussman II, Nagel RL, Tsai HM. Role of A and B blood

group, antigens in the expression of adhesive activity of von Willebrand factor. Br J Haematol. 2000;109(4):857–64.

59. Dunne E, Qi QM, Shaqfeh ES, O'Sullivan JM, Schoen I, Ricco AJ, et al. Blood group alters platelet binding kinetics to von Willebrand factor and consequently platelet function. Blood. 2019;133(12):1371–7.

60. Cattaneo M, Hayward CPM, Moffat KA, Pugliano MT, Liu Y, Michelson AD. Results of a worldwide survey on the assessment of platelet function by light transmission aggregometry: a report from the platelet physiology subcommittee of the SSC of the ISTH. J Thromb Haemost. 2009 Jun;7(6):1029.

61. Bharati KP, Prashanth UR. Von Willebrand disease: an overview. Indian J Pharm Sci [Internet]. 2011 Jan;73(1):7–16. Available from: https://www.ncbi.nlm.nih.gov/pubmed/22131616

62. Federici AB. Current and emerging approaches for assessing von Willebrand disease in 2016. Int J Lab Hematol. 2016;38:41–9.

63. Rodeghiero F, Castaman G, Dini E. Epidemiological investigation of the prevalence of von Willebrands disease. Blood [Internet]. 1987 Feb 1;69(2):454 LP – 459. Available from: http://www.bloodjournal.org/content/69/2/454.abstract

64. James PD, Lillicrap D. von Willebrand disease: Clinical and laboratory lessons learned from the large von Willebrand disease studies. Am J Hematol. 2012;87(SUPPL. 1):4–11.

65. Kawecki C, Lenting PJ, Denis C V. von Willebrand factor and inflammation. J Thromb Haemost [Internet]. 2017 Jul 1;15(7):1285–94. Available from: https://doi.org/10.1111/jth.13696

66. Roberts JC, Flood VH. Laboratory diagnosis of von Willebrand disease. Int J Lab Hematol [Internet]. 2015 May;37 Suppl 1(Suppl 1):11–7. Available from: https://www.ncbi.nlm.nih.gov/pubmed/25976955

67. Diagnosis T. The Diagnosis, treatment and management of von Willebrand Disease. US Dep Heal Hum Serv [Internet]. 2007;1–111. Available from: http://reddog.rmu.edu:2179/guidelines/vwd/vwd.pdf

68. Lind BSE. The bleeding time does not predict surgical bleeding. 1991;77(12):2547–52.

69. BORN GVR. Aggregation of Blood Platelets by Adenosine Diphosphate and its Reversal. Nature [Internet]. 1962;194(4832):927–9. Available from: https://doi.org/10.1038/194927b0

70. Platelet aggregation: Part II Some results from a new method of study. J Clin Pathol [Internet]. 1962 Sep;15(5):452–5. Available from: https://www.ncbi.nlm.nih.gov/pubmed/16810986

71. Ingerman-Wojenski C, Smith JB, Silver MJ. Evaluation of electrical aggregometry: comparison with optical aggregometry, secretion of ATP, and accumulation of radiolabeled platelets. J Lab Clin Med. 1983 Jan;101(1):44–52.

72. Paniccia R, Priora R, Liotta AA, Abbate R. Platelet function tests: a comparative review. Vasc Health Risk Manag. 2015;11:133–48.

73. Harle CC. Point-of-Care Platelet Function Testing. 2007;247–51.

74. Hussein HM, Emiru T, Georgiadis AL, Qureshi AI. Assessment of platelet inhibition by point-of-care testing in neuroendovascular procedures. Am J Neuroradiol. 2013;34(4):700–6.

75. Kitchen S, Jennings I, Woods TAL, Kitchen DP, Walker ID, Preston FE. Laboratory tests for measurement of von Willebrand factor show poor agreement among different centers: results from the United Kingdom National External Quality Assessment Scheme for Blood Coagulation. Semin Thromb Hemost. 2006 Jul;32(5):492–8.

76. Castaman G, Tosetto A, Cappelletti A, Goodeve A, Federici AB, Batlle J, et al. Validation of a rapid test (VWF-LIA) for the quantitative determination of von Willebrand factor antigen in type 1 von Willebrand disease diagnosis within the European multicenter study MCMDM-1VWD. Thromb Res. 2010 Sep;126(3):227–31.

77. Sakariassen KS, Turitto VT, Baumgartner HR. Recollections of the development of flow devices for studying mechanisms of hemostasis and

thrombosis in flowing whole blood. J Thromb Haemost. 2004 Oct;2(10):1681–90.

78. Favaloro EJ. Can blood flow assays help to identify clinically relevant differences in von Willebrand factor functionality in von Willebrand disease types 1-3? [2]. J Thromb Haemost. 2008;6(3):545–6.

79. Garcia-Cordero JL, Ricco AJ. Lab-on-a-Chip (General Philosophy) BT - Encyclopedia of Microfluidics and Nanofluidics. In: Li D, editor. Boston, MA: Springer US; 2008. p. 962–9. Available from: https://doi.org/10.1007/978-0-387-48998-8_780

80. Daw R, Finkelstein J. Lab on a chip. Nature [Internet]. 2006 Jul 26;442:367. Available from: https://doi.org/10.1038/442367a

81. Harrison P, Mumford A. Screening tests of platelet function: update on their appropriate uses for diagnostic testing. Semin Thromb Hemost. 2009 Mar;35(2):150–7.

82. Jackson SP. The growing complexity of platelet aggregation. Blood. 2007 Jun;109(12):5087–95.

83. Xu LC, Bauer JW, Siedlecki CA. Proteins, platelets, and blood coagulation at biomaterial interfaces. Colloids Surfaces B Biointerfaces. 2014;124(717):49–68.

84. Zwaginga J, Sakariassen K, King M, Diacovo T, Grabowski E, Nash G, et al. Can blood flow assays help to identify clinically relevant differences in von Willebrand factor functionality in von Willebrand disease types 1-3? J Thromb Haemost. 2007;5:2547–9.

85. De Gaetano G, Cerletti C. Platelet adhesion and aggregation and fibrin formation in flowing blood: A historical contribution by Giulio Bizzozero. Platelets. 2002;13(2):85–9.

86. Baumgartner HR, Muggli R, Tschopp TB, Turitto VT. Platelet Adhesion, Release and Aggregation in Flowing Blood: Effects of Surface Properties and Platelet Function. Thromb Haemost. 1976;35(01):124–38.

87. Hansen RR, Wufsus AR, Barton ST, Onasoga AA, Johnson-Paben RM, Neeves

KB. High content evaluation of shear dependent platelet function in a microfluidic flow assay. Ann Biomed Eng. 2013 Feb;41(2):250–62.

88. Sakariassen KS, Aarts PA, de Groot PG, Houdijk WP, Sixma JJ. A perfusion chamber developed to investigate platelet interaction in flowing blood with human vessel wall cells, their extracellular matrix, and purified components. J Lab Clin Med. 1983 Oct;102(4):522–35.

89. Usami S, Chen H-H, Zhao Y, Chien S, Skalak R. Design and construction of a linear shear stress flow chamber. Ann Biomed Eng [Internet]. 1993 Jan;21(1):77–83. Available from: http://link.springer.com/10.1007/BF02368167

90. Barstad RM, Roald HE, Cui Y, Turitto VT, Sakariassen KS. A perfusion chamber developed to investigate thrombus formation and shear profiles in flowing native human blood at the apex of well-defined stenoses. Arterioscler Thromb a J Vasc Biol [Internet]. 1994 Dec;14(12):1984–91. Available from: http://www.ncbi.nlm.nih.gov/pubmed/7981189

91. Sakariassen KS, Orning L, Turitto VT. The impact of blood shear rate on arterial thrombus formation. Futur Sci OA [Internet]. 2015 Nov 1;1(4):FSO30–FSO30. Available from: https://www.ncbi.nlm.nih.gov/pubmed/28031903

92. Coelho NM, Gonzalez-Garcia C, Salmeron-Sanchez M, Altankov G. Arrangement of type IV collagen on NH(2) and COOH functionalized surfaces. Biotechnol Bioeng. 2011 Dec;108(12):3009–18.

93. Witos J, Saint-Guirons J, Meinander K, D'Ulivo L, Riekkola M-L. Collagen I and III and their decorin modified surfaces studied by atomic force microscopy and the elucidation of their affinity toward positive apolipoprotein B-100 residue by quartz crystal microbalance. Analyst. 2011 Sep;136(18):3777–82.

94. HAYWARD CPM, HARRISON P, CATTANEO M, ORTEL TL, RAO AK. Platelet function analyzer (PFA)-100R closure time in the evaluation of platelet disorders and platelet function. J Thromb Haemost [Internet]. 2006 Feb;4(2):312–9. Available from: http://doi.wiley.com/10.1111/j.1538-7836.2006.01771.x

95. Kundu SK, Heilmann EJ, Sio R, Garcia C, Davidson RM, Ostgaard RA. Description of an in vitro platelet function analyzer--PFA-100. Semin Thromb Hemost [Internet]. 1995;21 Suppl 2:106–12. Available from: http://www.ncbi.nlm.nih.gov/pubmed/7660150

96. Dean JA, Blanchette VS, Carcao MD, Stain AM, Sparling CR, Siekmann J, et al. von Willebrand disease in a pediatric-based population--comparison of type 1 diagnostic criteria and use of the PFA-100 and a von Willebrand factor/collagen-binding assay. Thromb Haemost. 2000 Sep;84(3):401–9.

97. Schoeman RM, Lehmann M, Neeves KB. Flow chamber and microfluidic approaches for measuring thrombus formation in genetic bleeding disorders. Platelets. 2017;28(5):463–71.

98. Nalayanda DD, Kalukanimuttam M, Schmidtke DW. Micropatterned surfaces for controlling cell adhesion and rolling under flow. Biomed Microdevices. 2007;9(2):207–14.

99. Kent NJ, Basabe-Desmonts L, Meade G, MacCraith BD, Corcoran BG, Kenny D, et al. Microfluidic device to study arterial shear-mediated platelet-surface interactions in whole blood: Reduced sample volumes and well-characterised protein surfaces. Biomed Microdevices. 2010;12(6):987–1000.

100. Chang WC, Lee LP, Liepmann D. Biomimetic technique for adhesion-based collection and separation of cells in a microfluidic channel. Lab Chip. 2005;5(1):64–73.

101. Lu H, Koo LY, Wang WM, Lauffenburger DA, Griffith LG, Jensen KF. Microfluidic shear devices for quantitative analysis of cell adhesion. Anal Chem. 2004;76(18):5257–64.

102. Schaff UY, Xing MMQ, Lin KK, Pan N, Jeon NL, Simon SI. Vascular mimetics based on microfluidics for imaging the leukocyte-endothelial inflammatory response. Lab Chip. 2007;7(4):448–56.

103. Basabe-Desmonts L, Meade G, Kenny D. New trends in bioanalytical microdevices to assess platelet function. Expert Rev Mol Diagn [Internet]. 2010 Oct 1;10(7):869–74. Available from: https://doi.org/10.1586/erm.10.72

104. Cowman JJ. The Dynamic Platelet Function Assay (DPFA): Assessment of platelet translocation behaviour on von Willebrand Factor (VWF) in pregnancy , neonates and adults — Use Licence —. 2015;

105. Ralph A, Somers M, Cowman J, Voisin B, Hogan E, Dunne H, et al. Computational Tracking of Shear-Mediated Platelet Interactions with von Willebrand Factor. Cardiovasc Eng Technol. 2016;7(4):389–405.

106. Lazarova E, Scott Y, van den Bos A, Wantzin P, Atugonza R, Solkar S, et al. Multicentre evaluation of the new ORTHO VISION® analyser. Transfus Med. 2017;27(5):354–61.

107. Qi QM, Dunne E, Oglesby I, Schoen I, Ricco AJ, Kenny D, et al. In Vitro Measurement and Modeling of Platelet Adhesion on VWF-Coated Surfaces in Channel Flow. Biophys J [Internet]. 2019 Mar;116(6):1136–51. Available from: https://linkinghub.elsevier.com/retrieve/pii/S0006349519301110

108. Ward J, Dunne E, Bishop D, Boyd A, Kenny D, Meenan BJ. Entrapment of Autologous von Willebrand Factor on Polystyrene/Poly(methyl methacrylate) Demixed Surfaces. Polymers (Basel) [Internet]. 2017;9(12). Available from: http://www.mdpi.com/2073-4360/9/12/700

109. Minelli C, Kikuta A, Tsud N, Ball MD, Yamamoto A. A micro-fluidic study of whole blood behaviour on PMMA topographical nanostructures. J Nanobiotechnology [Internet]. 2008;6(1):3. Available from: https://doi.org/10.1186/1477-3155-6-3

110. Emslie AG, Bonner FT, Peck LG. Flow of a Viscous Liquid on a Rotating Disk. J Appl Phys [Internet]. 1958 May 1;29(5):858–62. Available from: https://doi.org/10.1063/1.1723300

111. Hall DB, Underhill P, Torkelson JM. Spin Coating. Polym Engeneering Sci. 1998;38(12):2039–45.

112. Kang B, Lee WH, Cho K. Recent Advances in Organic Transistor Printing Processes. ACS Appl Mater Interfaces [Internet]. 2013 Apr 10;5(7):2302–15. Available from: https://doi.org/10.1021/am302796z

113. Campoy-Quiles M, Ferenczi T, Agostinelli T, Etchegoin PG, Kim Y,

Anthopoulos TD, et al. Morphology evolution via self-organization and lateral and vertical diffusion in polymer:fullerene solar cell blends. Nat Mater. 2008 Feb;7(2):158–64.

114. Morgenstern I, Binder K. ''Exact'' calculations for finite Ising spin glass lattices (invited). J Appl Phys [Internet]. 1981 Mar 1;52(3):1692–6. Available from: https://doi.org/10.1063/1.329682

115. D'Sa RA, Raj J, Dickinson PJ, McCabe F, Meenan BJ. Human Fetal Osteoblast Response on Poly(Methyl Methacrylate)/Polystyrene Demixed Thin Film Blends: Surface Chemistry Vs Topography Effects. ACS Appl Mater Interfaces. 2016;8(24):14920–31.

116. Dalby MJ, Giannaras D, Riehle MO, Gadegaard N, Affrossman S, Curtis ASG. Rapid fibroblast adhesion to 27 nm high polymer demixed nano-topography. Biomaterials. 2004;

117. Dalby MJ. Cellular response to low adhesion nanotopographies. Int J Nanomedicine. 2007;2(3):373–81.

118. Walheim S, Böltau M, Mlynek J, Krausch G, Steiner U. Structure Formation via Polymer Demixing in Spin-Cast Films. Macromolecules. 1997;30:4995.

119. Tanaka K, Takahara A, Kajiyama T. Film Thickness Dependence of the Surface Structure of Immiscible Polystyrene/Poly(methyl methacrylate) Blends. Macromolecules [Internet]. 1996 Jan 1;29(9):3232–9. Available from: https://doi.org/10.1021/ma951140+

120. Reich S, Cohen Y. Phase separation of polymer blends in thin films. J Polym Sci Polym Phys Ed [Internet]. 2018 Nov 15;19(8):1255–67. Available from: https://doi.org/10.1002/pol.1981.180190809

121. Li X, Han Y, An L. Surface morphology control of immiscible polymer-blend thin films. Polymer (Guildf). 2003;44(26):8155–65.

122. Motomatsu M, Nie H-Y, Mizutani W, Tokumoto H. Local_Properties_of_Phase-Separated_Poly.pdf. J Appl Phys. 1994;33:3775–8.

123. Ton-That C, Shard A, Teare D, Bradley R. XPS and AFM Surface Studies of

Solvent-Cast PS/PMMA Blends. Polymer (Guildf). 2001;42:1121.

124. Fleming G, Aveyard J, Fothergill JL, McBride F, Raval R, D'Sa RA. Effect of Polymer Demixed Nanotopographies on Bacterial Adhesion and Biofilm Formation. Polymers (Basel) [Internet]. 2019 Nov 21;11(12):1921. Available from: https://www.mdpi.com/2073-4360/11/12/1921

125. Shenkman B, Savion N, Dardik R, Tamarin I, Varon D. Testing of platelet deposition on polystyrene surface under flow conditions by the cone and plate(let) analyzer: Role of platelet activation, fibrinogen and von Willebrand factor. Thromb Res. 2000;99(4):353–61.

126. Neeves KB, Onasoga AA, Wufsus AR. The use of microfluidics in hemostasis. Curr Opin Hematol. 2013;20(5):417–23.

127. Beamson G, Briggs D. High resolution XPS of organic polymers: The Scienta ESCA 300 database. John Wiley & Sons, Ltd; 1992. 280 p.

128. Chen H, Angerer JI, Napoleone M, Reininger AJ, Schneider SW, Wixforth A, et al. Hematocrit and flow rate regulate the adhesion of platelets to von Willebrand factor. Biomicrofluidics [Internet]. 2013 Dec 6;7(6):64113. Available from: https://www.ncbi.nlm.nih.gov/pubmed/24396547

129. Laffan MA, Lester W, O'Donnell JS, Will A, Tait RC, Goodeve A, et al. The diagnosis and management of von Willebrand disease: a United Kingdom Haemophilia Centre Doctors Organization guideline approved by the British Committee for Standards in Haematology. Br J Haematol. 2014;167(4):453–65.

130. Flood V, Gill J, Christopherson P, Wren J, Friedman K. Comparison of Type I, Type III, and Type VI Collagen Binding Assays in Diagnosis of VWD. 2013;10(7):1–18.

131. Goddard JM, Hotchkiss JH. Polymer surface modification for the attachment of bioactive compounds. Progress in Polymer Science (Oxford). 2007.

132. Branchford B, Ng C, Neeves K, Di Paola J. Microfluidic technology as an emerging clinical tool to evaluate thrombosis and hemostasis. 2016;118(24):6072–8.

133. Minelli C, Kikuta A, Yamamoto A. Blood interaction with nano-topography. Proc 2006 Int Conf Nanosci Nanotechnology, ICONN. 2006;263–6.

134. Ton-That C, Shard AG, Bradley RH. Surface feature size of spin cast PS/PMMA blends. Polymer (Guildf). 2002;43(18):4973–7.

135. Chan CM, Weng L. Surface Characterization of Polymer Blends by XPS. 2016;

136. Sprenger M, Walheim S. Hierarchic Structure Formation in Binary and Ternary Polymer Blends. INTERFACE Sci. 2003;11:225–35.

137. Haas DE, Birnie DP, Zecchino MJ, Figueroa JT. The effect of radial position and spin speed on striation spacing in spin on glass coatings. J Mater Sci Lett. 2001;20(19):1763–6.

138. Mokarian-Tabari P, Geoghegan M, Howse JR, Heriot SY, Thompson RL, Jones RAL. Quantitative evaluation of evaporation rate during spin-coating of polymer blend films: Control of film structure through defined-atmosphere solvent-casting. Eur Phys J E. 2010;33(4):283–9.

139. Fowler PD, Ruscher C, McGraw JD, Forrest JA, Dalnoki-Veress K. Controlling Marangoni-induced instabilities in spin-cast polymer films: How to prepare uniform films. Eur Phys J E. 2016;39(9):1–11.

140. Khattak M, Pu F, Curran JM, Hunt JA, D'Sa RA. Human Mesenchymal Stem Cell Response to Poly(ε-caprolactone/Poly(methyl methacrylate) Demixed Thin Films. J Mater Sci Mater Med. 2015;26:1.

141. Lim JY, Hansen JC, Siedlecki CA, Runt J, Donahue HJ. Human foetal osteoblastic cell response to polymer-demixed nanotopographic interfaces. J R Soc Interface. 2005;2(2):97–108.

142. Koh LB, Rodriguez I, Venkatraman SS. The effect of topography of polymer surfaces on platelet adhesion. Biomaterials [Internet]. 2010;31(7):1533–45. Available from: http://dx.doi.org/10.1016/j.biomaterials.2009.11.022

143. Zuyderhoff EM, Dekeyser CM, Rouxhet PG, Dupont-Gillain CC. An AFM, XPS and wettability study of the surface heterogeneity of PS/PMMA-r-PMAA demixed thin films. J Colloid Interface Sci. 2008;

144. Tanaka K, Yoon J-S, Takahara A, Kajiyama T. Ultrathinning-Induced Surface Phase Separation of Polystyrene/Poly(vinyl methyl ether) Blend Film. Macromolecules [Internet]. 1995 Feb 1;28(4):934–8. Available from: https://doi.org/10.1021/ma00108a021

145. Dekeyser CM, Biltresse S, Marchand-Brynaert J, Rouxhet PG, Dupont-Gillain CC. Submicrometer-scale heterogeneous surfaces by PS-PMMA demixing. Polymer (Guildf). 2004;45(7):2211–9.

146. Ton-That C, Shard AG, Teare DOH, Bradley RH. XPS and AFM surface studies of solvent-cast PS/PMMA blends. Polymer (Guildf). 2001;42(3):1121–9.

147. Heriot SY, Jones RAL. An interfacial instability in a transient wetting layer leads to lateral phase separation in thin spin-cast polymer-blend films. Nat Mater. 2005;4(10):782–6.

148. Dalby MJ, Riehle MO, Johnstone H, Affrossman S, Curtis ASG. In vitro reaction of endothelial cells to polymer demixed nanotopography. Biomaterials. 2002;

149. Ahn J, Son SJ, Min J. The control of cell adhesion on a PMMA polymer surface consisting of nanopillar arrays. J Biotechnol. 2013;

150. Xu L-C, Bauer JW, Siedlecki CA. Proteins, platelets, and blood coagulation at biomaterial interfaces. Colloids Surf B Biointerfaces [Internet]. 2014;124(717):49–68. Available from: http://www.ncbi.nlm.nih.gov/pubmed/25448722%0Ahttp://www.pubmedcentral.nih.gov/articlerender.fcgi?artid=PMC5001692

151. De Ceunynck K, De Meyer SF, Vanhoorelbeke K. Unwinding the von Willebrand factor strings puzzle. Blood. 2013;121(2):270–7.

152. Kettle J, Ding Z, Horie M, Smith GC. XPS analysis of the chemical degradation of PTB7 polymers for organic photovoltaics. Org Electron. 2016;39:222–8.

153. Ossila. Spin Coating: Complete Guide [Internet]. [cited 2020 Jan 31]. Available from: https://www.ossila.com/pages/spin-coating

154. Soma-Pillay P, Nelson-Piercy C, Tolppanen H, Mebazaa A. Physiological

changes in pregnancy. Cardiovasc J Afr [Internet]. 2016;27(2):89–94. Available from: https://www.ncbi.nlm.nih.gov/pubmed/27213856

155. Rodger M, Sheppard D, Gándara E, Tinmouth A. Haematological problems in obstetrics. Best Pract Res Clin Obstet Gynaecol [Internet]. 2015 Jul;29(5):671–84. Available from: https://linkinghub.elsevier.com/retrieve/pii/S1521693415000231

156. Ng C, Motto DG, Di Paola J. Diagnostic approach to von Willebrand disease. Blood [Internet]. 2015/02/23. 2015 Mar 26;125(13):2029–37. Available from: https://www.ncbi.nlm.nih.gov/pubmed/25712990

157. Castaman G. Changes of von Willebrand Factor during Pregnancy in Women with and without von Willebrand Disease. Mediterr J Hematol Infect Dis [Internet]. 2013 Jul 16;5(1):e2013052–e2013052. Available from: https://www.ncbi.nlm.nih.gov/pubmed/23936623

158. Hirasawa S, Saito Y, Nezu H, Ohashi N, Maruyama P. Analysis of drying shrinkage and flow due to surface tension of spin-coated films on topographic substrates. IEEE Trans Semicond Manuf [Internet]. 1997;10(4):438–44. Available from: http://ieeexplore.ieee.org/document/641486/

159. Becker H, Heim U. Hot embossing as a method for the fabrication of polymer high aspect ratio structures. Sensors Actuators A Phys [Internet]. 2000 May;83(1–3):130–5. Available from: https://linkinghub.elsevier.com/retrieve/pii/S092442470000296X

160. Jeon JS, Chung S, Kamm RD, Charest JL. Hot embossing for fabrication of a microfluidic 3D cell culture platform. Biomed Microdevices [Internet]. 2011 Apr;13(2):325–33. Available from: https://www.ncbi.nlm.nih.gov/pubmed/21113663

161. Brown A, Burke GA, Meenan BJ. Patterned cell culture substrates created by hot embossing of tissue culture treated polystyrene. J Mater Sci Mater Med [Internet]. 2013 Dec 31;24(12):2797–807. Available from: http://link.springer.com/10.1007/s10856-013-5011-5

162. Deshmukh SS, Goswami A. Hot Embossing of polymers – A review. Mater

Today Proc [Internet]. 2020 Jan; Available from: https://linkinghub.elsevier.com/retrieve/pii/S2214785319340787

163. Kendall M, Hodges NJ, Whitwell H, Tyrrell J, Cangul H. Nanoparticle growth and surface chemistry changes in cell-conditioned culture medium. Philos Trans R Soc B Biol Sci [Internet]. 2015 Feb 5;370(1661):20140100. Available from: https://royalsocietypublishing.org/doi/10.1098/rstb.2014.0100

164. Somorjai GA, Li Y. Impact of surface chemistry. Proc Natl Acad Sci [Internet]. 2011 Jan 18;108(3):917–24. Available from: http://www.pnas.org/cgi/doi/10.1073/pnas.1006669107

165. Guo Y, Liu G, Xiong Y, Tian Y. Study of the demolding process—implications for thermal stress, adhesion and friction control. J Micromechanics Microengineering [Internet]. 2007 Jan 1;17(1):9–19. Available from: http://stacks.iop.org/0960-1317/17/i=1/a=002?key=crossref.5ddc88a897cb7ece49f35595d6d53ad9

166. Chau TT, Bruckard WJ, Koh PTL, Nguyen AV. A review of factors that affect contact angle and implications for flotation practice. Adv Colloid Interface Sci [Internet]. 2009 Sep;150(2):106–15. Available from: https://linkinghub.elsevier.com/retrieve/pii/S0001868609000530

167. Yasuda H, Sharma AK, Yasuda T. Effect of orientation and mobility of polymer molecules at surfaces on contact angle and its hysteresis. J Polym Sci Polym Phys Ed [Internet]. 1981 Sep;19(9):1285–91. Available from: http://doi.wiley.com/10.1002/pol.1981.180190901

168. Purkait MK, Sinha MK, Mondal P, Singh R. Photoresponsive Membranes. In 2018. p. 115–44. Available from: https://linkinghub.elsevier.com/retrieve/pii/B9780128139615000048

169. Briggs D, Rance DG, Briscoe BJ. Surface Properties. Compr Polym Sci Suppl [Internet]. 1989 Jan 1 [cited 2020 Jan 15];707–32. Available from: https://www.sciencedirect.com/science/article/pii/B9780080967011000604?via%3Dihub